Electroweak Baryogenesis in Extensions of the Standard Model

Lars Fromme

July 2006

Dissertation

submitted to the
Physics Department of the Bielefeld University, Germany
for the degree of
Doctor of Natural Sciences

Electroweak Baryogenesis in Extensions of the Standard Model

presented by

Lars Fromme

July 7th, 2006

Referees: Prof. Dr. Dietrich Bödeker
Prof. Dr. Mikko Laine

Abstract

We investigate the generation of the baryon asymmetry in two extensions of the Standard Model; these are the ϕ^6 model and the two-Higgs doublet model. Analyzing the thermal potential in the presence of CP-violation, we find a strong first order phase transition for a wide range of parameters in both models. We compute the relevant bubble wall properties which then enter the transport equations. In non-supersymmetric models electroweak baryogenesis is dominated by top transport, which we treat in the WKB approximation. We calculate the CP-violating source terms starting from the Dirac equation. We show how to resolve discrepancies between this treatment and the computation in the Schwinger-Keldysh formalism. Furthermore, we keep inelastic scatterings of quarks and W bosons at a finite rate, which considerably affects the amount of the generated baryon asymmetry depending on the bubble wall velocity. In addition, we improve the transport equations by novel source terms which are generated by CP-conserving perturbations in the plasma. It turns out that their effect is relatively small. Both models under consideration predict a baryon to entropy ratio close to the observed value for a large part of the parameter space without being in conflict with constraints on electric dipole moments.

Contents

1 Introduction

One of the most fundamental results of modern particle physics is that the discovery of every particle of a particular species assures the existence of a particle of the same mass but opposite quantum numbers, the so-called anti-particle.[1] Thus, one would expect equal number densities for particles and anti-particles in the universe. However, our environment consists only of matter and observations show that anti-matter is not only rare on earth but also in the whole visible universe. We have clear evidence from the measurements of cosmic rays that our galaxy is predominantly made of matter. Although this does not exclude the possibility that the dominance of matter is only local but the universe is globally symmetric. However, in that case we would have patches of matter and anti-matter in the universe leading to annihilation effects on the boundary between the different domains. The resulting strong γ-radiation is not observed in the measurements of the γ-ray distribution. Consequently, the observable universe is matter dominated without any anti-matter dominated areas [1].
The main question to answer is how to create the matter-anti-matter asymmetry starting from symmetric initial conditions. Explaining this discrepancy is one of the great challenges of modern particle physics and cosmology. The answer is partially given by the assumption that the origin of the matter observed today is only a tiny mismatch between particles and anti-particles in the hot plasma of the early universe. Usually, the mechanism of baryon generation is called baryogenesis.
However, the creation of the asymmetry has to be in accordance with the current picture of standard cosmology. The history of the universe contains an epoch of exponential expansion, which is called inflation (see e.g. ref. [2]). Inflation is able to explain the homogeneity and flatness of the universe as well as the absence of magnetic monopoles in a natural way. But during the epoch of inflation every relic from the very early universe is diluted and therefore the matter-anti-matter asymmetry has to be created at later times.
The asymmetry between baryons and anti-baryons has recently been determined to an unprecedented accuracy by combining measurements of the cosmic microwave background [3] and large scale structure [4]. Typically, the asymmetry is defined by a convenient dimensionless quantity,

$$\eta_B \equiv \frac{n_B}{s} = (8.7 \pm 0.3) \times 10^{-11}, \tag{1.1}$$

[1] A neutral particle can be its own anti-particle.

where n_B denotes the difference between the densities of baryons and anti-baryons and s the entropy density. Both the numerator and denominator scale with a^{-3}, where a is the scale factor of the expanding universe, such that the baryon to entropy ratio η_B remains constant during the evolution of the universe as long as equilibrium conditions hold. Comparing the present number density of photons, $n_\gamma = (410.4 \pm 0.5)\ \mathrm{cm}^{-3}$ [5], with the number density of baryons, $n_B = (2.5 \pm 0.1) \times 10^{-7}\ \mathrm{cm}^{-3}$, the diminutiveness of the matter abundance in the universe becomes apparent. There are approximately only six baryons per 10^{10} photons.
In 1967 Sakharov formulated three necessary ingredients for baryogenesis, these are: baryon number (B) nonconservation, charge (C) and charge parity (CP) violation and deviation from thermal equilibrium [6]. The first condition is obvious, there must be a mechanism which violates B, since we assume the universe to be baryon symmetric in the beginning. Secondly, if C and CP were conserved, particles and anti-particles were produced with an equal rate so that a net baryon number could not be generated. Thirdly, we need deviation from equilibrium because CPT-invariance ensures vanishing baryon density in strict thermal equilibrium. If CPT is conserved particles and anti-particles have the same distribution function in equilibrium because they have an equal mass.
Many different baryogenesis scenarios have been developed during the last 40 years [7–9]. The historically first model is based on heavy particle decays in the framework of Grand Unified Theories (GUTs) [2]. Besides the GUT baryogenesis two other scenarios have been intensively studied during the last decades which are called baryogenesis through leptogenesis and electroweak baryogenesis, for reviews see e.g. [10–14]. (For the sake of completeness there are also many other and very different scenarios which have been suggested in recent years.) In this work we will focus on electroweak baryogenesis. The great attraction of this mechanism in contrast to the others is that it involves physics that is in principle testable in the near future by experiments at the next generation of accelerators. This makes this scenario falsifiable.
In the Standard Model (SM) baryon and lepton number (L) are not exactly conserved as discovered by 't Hooft [15, 16]. Consequently, all scenarios in which the baryon asymmetry is generated at high temperatures have in common the difficulty that a nonvanishing baryon number has to survive during the decrease of temperature in the expanding universe until today. The electroweak theory has a nontrivial vacuum structure, more precisely the vacua distinguish different baryon and lepton numbers. The vacua are separated by an energy barrier and tunneling events between the different vacua are anomalous processes. With increasing temperature they become more and more efficient, while nowadays these anomalous processes are strongly suppressed. The thermally induced transitions between two adjacent vacua, called sphaleron transitions, change the baryon and lepton number such that the difference $B - L$ is conserved. Since the sphalerons only couple to the left-chiral particles, additionally C is maximally broken. The anomalous baryon number violating processes are especially efficient before the electroweak phase transition

(EWPT), i.e. at temperatures above approximately 100 GeV, when the weak gauge bosons are still massless. Then the sphalerons are able to equilibrate any already existing baryon asymmetry to zero. However, under certain conditions during the phase transition associated with the electroweak symmetry breaking these processes contribute to the generation of a nonvanishing baryon number.
In the baryogenesis scenarios operating far above the electroweak scale certain processes are thrown out of equilibrium by the expansion of the universe. But at temperatures of several 100 GeV another origin of deviation from thermal equilibrium is needed since the expansion is too slow to compete against the relevant interaction time scales. For electroweak baryogenesis the only possibility to fulfill the third Sakharov criterion is provided by the phase transition when the Higgs field acquires its expectation value. It turns out that the plasma is not driven sufficiently out of equilibrium in case of a cross-over or a transition of second order. But a first order phase transition provides the required thermal instability.
The first order EWPT is triggered by a free energy barrier in the Higgs potential which separates two energetically degenerate phases at the critical temperature T_c. Around this temperature the formation of bubbles starts, and after the bubbles have reached a critical size they expand and finally percolate. At the phase boundary the expectation value of the Higgs field changes rapidly from zero in the symmetric phase to a non-zero value v_c in the broken phase inside the bubbles. During the phase transition the required departure from thermal equilibrium is provided in the vicinity of the propagating bubble walls. A baryon asymmetry is produced if the particles of the plasma interact with the wall in a CP-violating fashion. But the generated asymmetry would be washed out again if the aforementioned sphaleron processes are still fast inside the bubbles compared to the expansion rate of the universe. In fact, electroweak baryogenesis requires a very strong criterion to be satisfied: The Higgs expectation value at the critical temperature v_c must be larger than about T_c to avoid baryon number washout [17, 18]. This is the condition for this first order transition to be strong. In that case, the sphaleron transitions are strongly suppressed in the broken phase, and the generated baryon number is frozen in after the completion of the EWPT when global equilibrium is restored.
In principle, all three Sakharov conditions could be satisfied within the SM at the EWPT [19]. However, a more quantitative analysis shows that the observed baryon asymmetry cannot be explained within the SM due to the fact that there is not enough CP-violation [20–22] and the transition is not of first order. The EWPT vanishes completely if the Higgs boson has a mass larger than approximately 80 GeV as lattice simulations have shown [23–25]. The measurements of the LEP collaboration established a current experimental lower bound on the Higgs mass of 114 GeV [26]. Consequently, the SM fails to be an adequate theory for baryogenesis. To overcome these difficulties extensions to the SM are required.
In recent years electroweak baryogenesis scenarios have mostly been investigated in supersymmetric models. In these models supersymmetry breaking provides the needed new sources of CP-violation, and the strong first order phase transition can

be induced for example by a light top squark [27–30]. Alternatively, the strong EWPT can also be driven by cubic interactions of a singlet Higgs field [31–34]. However, it is also possible to generate a baryon asymmetry in non-supersymmetric models as we will demonstrate in this work.
In one feasible non-supersymmetric scenario we modify the SM Higgs self-interactions by introducing non-renormalizable operators. These operators parameterize the effects of new physics beyond some cut-off scale Λ. In order to be relevant at weak scale temperatures one should have $\Lambda \lesssim 1$ TeV. If the Higgs potential is stabilized by a dimension-six Higgs operator a strong first order phase transition can occur for Higgs masses larger than the experimental lower bound. In addition, the non-renormalizable interactions provide new sources of CP-breaking to fuel baryogenesis.
The second model we will focus on is the so-called two-Higgs doublet model (2HDM), where the SM is augmented by an additional second Higgs doublet. Then the Higgs sector contains two extra neutral and two extra charged Higgs particles. If these extra states couple sufficiently strong, their thermal loop corrections can induce the needed strong first order phase transition. Furthermore, we can include explicit CP-violation in the Higgs potential by a complex mass term which mixes the two Higgs doublets.
Knowing in both models the parameter settings that fulfill Sakharov's conditions we use the semiclassical approximation to determine the baryon asymmetry. Typically, the electroweak baryogenesis mechanism is described by a set of transport equations including CP-violating source terms. The interactions of the particles in the hot plasma with the phase boundary during the EWPT induce CP-violating shifts in the dispersion relations of the moving particles. Since we are dealing with thick bubble walls, these dispersion relations can be determined in the standard WKB approximation, which corresponds to an expansion in gradients of the bubble wall profile. The resulting semiclassical forces act differently on particles and anti-particles leading to CP-violating sources in the transport equations. So a non-zero left-handed quark density can be created in front of the moving bubble wall. The weak sphalerons then partly transform this left-handed quark density into a baryon asymmetry.
We investigate three improvements of the semiclassical approximation. Firstly, we compute the dispersion relations in the usual way by solving the one-particle Dirac equation in a special frame to first order in gradients in the CP-violating bubble wall background. But then these relations are boosted to a general Lorentz frame leading to a result which is in accordance with the dispersion relations derived in the Schwinger-Keldysh formalism [35, 36]. This demonstrates that the full Schwinger-Keldysh result can be obtained in a much simpler way. Secondly, in the transport equations we include a finite rate for processes $bW \leftrightarrow tX$ (where X denotes a gauge boson), which previously was set to equilibrium. This allows us to study the top and bottom quarks seperately. And thirdly, we discuss novel source terms generated by CP-conserving perturbations in the plasma. Altogether, we study the influence of several parameters on the amount of baryon asymmetry.

2 Ingredients for Electroweak Baryogenesis

2.1 Baryon Number Violation

For a successful baryogenesis scenario a mechanism which violates baryon number is needed. In 1976 't Hooft was the first who realized that the SM predicts nonconservation of baryonic charge through nonperturbative effects [15, 16]. These quantum corrections give rise to baryon number violating processes which are completely negligible at low energies because they are strongly suppressed. However, at very high temperatures comparable with the electroweak scale these effects may be fast enough to play a significant role [19]. As we will see, the B-changing processes might be efficient in the early universe and produce an excess of baryons over anti-baryons.
We know from experiments that baryon and lepton numbers are good quantum numbers at present day temperatures. The Standard Model Lagrangian has a global $U(1)_B$ and $U(1)_L$ symmetry. Classically, baryonic and leptonic currents are conserved due to Noether's theorem:

$$\partial_\mu j_B^\mu = \partial_\mu \sum_q \frac{1}{3}\bar{q}\gamma^\mu q = 0, \tag{2.1}$$

$$\partial_\mu j_L^\mu = \partial_\mu \sum_l \bar{l}\gamma^\mu l = 0, \tag{2.2}$$

where q stands for the quark fields, $q = u, d, c, s, t, b$, and l for the lepton fields, $l = e, \mu, \tau, \nu_e, \nu_\mu, \nu_\tau$. Hence, the associated charges B and L are time-independent. At quantum level this conservation is spoiled by corrections through the quantum chiral anomaly (Adler-Bell-Jackiw anomaly) [37, 38]. Instead of equations (2.1) and (2.2) one gets (see e.g. ref. [7])

$$\partial_\mu j_B^\mu = \partial_\mu j_L^\mu = \frac{n_F}{32\pi^2}\left(-g^2 W^a_{\mu\nu}\widetilde{W}^{a\mu\nu} + g'^2 B_{\mu\nu}\widetilde{B}^{\mu\nu}\right), \tag{2.3}$$

where n_F is the number of families, g and g' are the gauge couplings, and $W^a_{\mu\nu}$ and $B_{\mu\nu}$ are the field strength tensors for $SU(2)_L$ and $U(1)_Y$, respectively. The tilde denotes the dual tensor, i.e. $\widetilde{W}^{a\mu\nu} = \epsilon^{\mu\nu\alpha\beta}W^a_{\alpha\beta}/2$ and $\widetilde{B}^{\mu\nu} = \epsilon^{\mu\nu\alpha\beta}B_{\alpha\beta}/2$.

Because of equation (2.3) the difference between baryonic and leptonic charge, $B-L$, is strictly conserved even at the quantum level. Thus, only $B+L$ may be violated at high temperatures. The r.h.s. of equation (2.3) can be expressed by total derivatives of vector operators such that

$$\partial_\mu j_B^\mu = \partial_\mu j_L^\mu = \frac{n_F}{32\pi^2}\left(-g^2\partial_\mu K^\mu + g'^2\partial_\mu k^\mu\right) \tag{2.4}$$

with

$$K^\mu = \epsilon^{\mu\nu\alpha\beta}\left(W^a_{\nu\alpha}W^a_\beta - \frac{g}{3}\epsilon_{abc}W^a_\nu W^b_\alpha W^c_\beta\right), \tag{2.5}$$

$$k^\mu = \epsilon^{\mu\nu\alpha\beta}B_{\nu\alpha}B_\beta, \tag{2.6}$$

where W^a_μ and B_μ are the gauge fields of $SU(2)_L$ and $U(1)_Y$, respectively. Now we want to integrate equation (2.4) over space-time. Usually, total derivatives are unobservable; they disappear through integrating by parts. This is true for the terms proportional to the field strengths $W^a_{\mu\nu}$ and $B_{\mu\nu}$ since they should vanish at infinity. Thus, the abelian part k^μ does not contribute. However, W_μ does not necessarily vanish at infinity. Considering the change in baryon number from some arbitrary initial time t_i to some final time t_f we are finally left with[1]

$$\int d^3x dt \partial_\mu K^\mu = N_{CS}(t_f) - N_{CS}(t_i) \equiv \Delta N_{CS}, \tag{2.7}$$

where

$$N_{CS}(t) = \frac{g^2}{32\pi^2}\int d^3x \epsilon^{ijk}\left(W^a_{ij}W^a_k - \frac{g}{3}\epsilon_{abc}W^a_i W^b_j W^c_k\right) \tag{2.8}$$

is the so-called Chern-Simons number, which is not a gauge invariant quantity in so-called large gauge transformations, but the change ΔN_{CS} is. N_{CS} characterizes the nontrivial topology of the gauge field configurations. The nonabelian gauge theory of weak interactions has an infinite number of ground states whose vacuum field configurations have different topological charges. The different vacua are separated by an energy barrier as indicated in figure 2.1.
Integrating also the l.h.s. of equation (2.4) yields the final result

$$\Delta B = \Delta L = n_F \Delta N_{CS}. \tag{2.9}$$

Each transition from one vacuum to an adjacent one creates nine left-handed quarks (right-handed anti-quarks), three color states for each generation, and three left-handed leptons (right-handed anti-leptons), one per generation.
At zero temperature the transition between two vacuum configurations corresponds to a tunneling process, which is strongly suppressed by a factor $e^{-4\pi/\alpha_w} \sim 10^{-164}$ [15, 16], where $\alpha_w = g^2/4\pi$ is the weak coupling constant. Thus, the probability for barrier penetration is vanishingly small. At non-zero temperature the situation

[1] We have chosen the temporal gauge $W^a_0 = 0$.

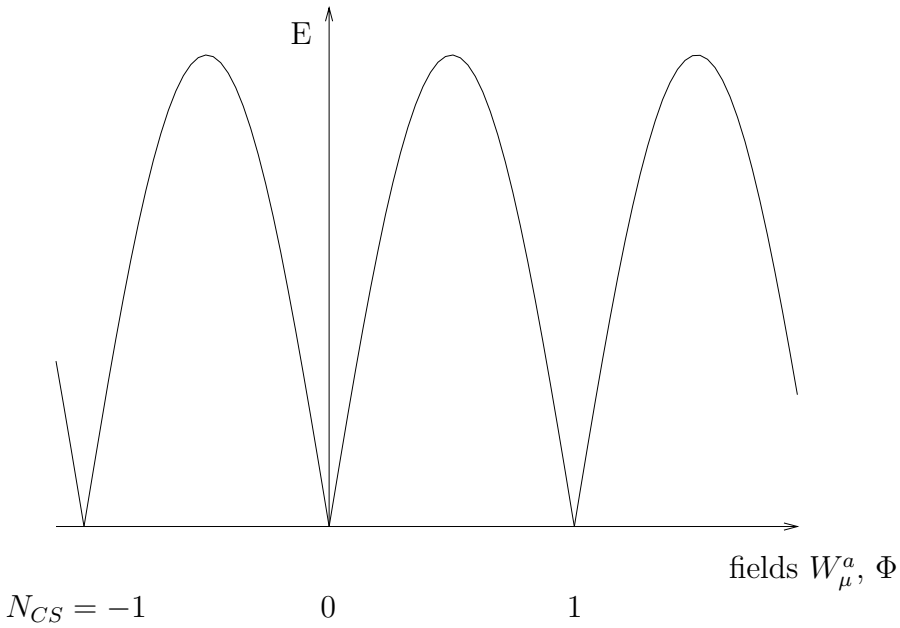

Figure 2.1: The periodic vacuum structure of static gauge and Higgs field configurations W^a_μ, Φ.

is somewhat different. The transition between two vacua differing by a unit of topological charge can be achieved by a classical motion over the barrier. Take again a look at figure 2.1. The field configuration of $N_{CS} = 1/2 + i$ (where i is an integer) refers to the so-called sphaleron, which is a saddle point solution to the classical equations of motion [39, 40]. This special field configuration corresponds to the lowest energy point on the ridge of the barrier between two degenerate minima. There the height of the barrier is given by the sphaleron energy

$$E_{ws}(T) = \frac{4\pi v_T}{g} f(\lambda/g), \tag{2.10}$$

where v_T is the expectation value of the Higgs field at the temperature T. For the SM the parameter f ranges from $f(0) \simeq 1.6$ to $f(\infty) \simeq 2.7$ depending on the Higgs self-coupling λ. At zero temperature we have $v_0 \equiv v = 246$ GeV and $E_{ws}(0) \simeq 8-13$ TeV.
In the broken phase the probability for barrier overcoming can be calculated using the semiclassical approximation. Detailed investigations led to the sphaleron rate [18, 41]

$$\hat{\Gamma}_{ws} = \kappa \left(\frac{m_W(T)}{\alpha_w T} \right)^3 m_W^4(T) e^{-E_{ws}(T)/T}, \tag{2.11}$$

where κ is a dimensionless constant and m_W the mass of the W boson.
In the symmetric phase the expectation value of the Higgs field is zero, and so the

sphaleron processes are not exponentially suppressed above T_c. There is no classical saddle point, and therefore the calculation of the transition rate is very difficult. Instead of going into the details of the complicated calculation we only present an estimate from dimensional grounds. Because there is only one relevant length scale $R \sim (g^2T)^{-1}$ and time scale $t \sim (g^4 \log(1/g)T)^{-1}$ in the symmetric phase we expect $\hat{\Gamma}_{ws} \sim (tR^3)^{-1} \sim g^{10} \log(1/g)T^4$ [42–44]. The recent numerical result is [45–49]

$$\hat{\Gamma}_{ws} \simeq 25\ \alpha_W^5 T^4 \simeq 1.0 \times 10^{-6} T^4. \tag{2.12}$$

By comparing with the expansion rate of the universe we find that the sphaleron processes are in thermal equilibrium for temperatures $T_c \sim 100$ GeV $< T \lesssim 10^{12}$ GeV. Accordingly, any excess of baryon number generated above the electroweak phase transition temperature is equilibrated to zero. For that reason a baryogenesis mechanism operating at higher temperatures has to violate also $B - L$.

2.2 The Phase Transition

2.2.1 Strength of the Phase Transition

In general, a phase transition occurs in a thermodynamic system, if the free energy density is a non-analytic function of its parameters [50, 51]. Usually, phase transitions can be characterized by an order parameter which is a thermodynamic quantity that undergoes a sudden change at the critical temperature T_c at which the particular transition occurs. If the order parameter has a discontinuity, the transition is called first order. Then two different phases coexist at T_c. In a so-called second order transition the change of the order parameter is continuous at T_c. Physically there is only one phase (no coexistence) that goes through a singularity at T_c. It is also possible that properties of the system change rapidly without an occurance of a phase transition. The corresponding continuous process is called cross-over.
The electroweak phase transition is associated with the electroweak symmetry breaking. In the SM the EWPT is not really a phase transition but a cross-over [23–25]. However, under certain conditions a real phase transition can occur in extensions of the SM. In that case, the expectation value of the Higgs field plays the role of the order parameter. In the so-called symmetric phase it is zero (or small) while in the broken phase it receives a non-zero value v_c. For successful baryogenesis the required deviation from thermal equilibrium is only possible if the transition is first order. In that case, there are two energetically degenerate phases which are separated by an energy barrier at the critical temperature T_c. If the system cools down further, nucleation of bubbles of the broken phase in the sea of the symmetric phase is in principle possible. The bubbles have to have a critical size, so that their volume

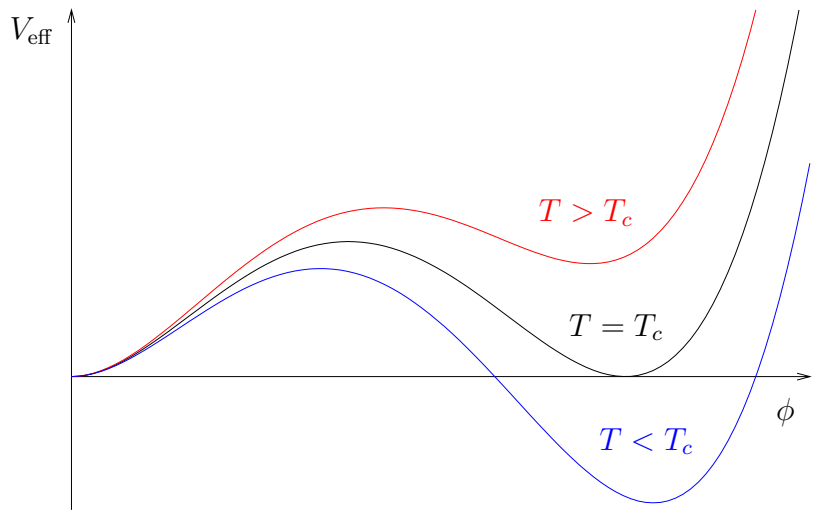

Figure 2.2: The effective potential as a function of ϕ for three different temperatures. Above T_c the minimum at $\phi = 0$ is the global one, while below T_c this is true for the minimum at $\phi \neq 0$. At the critical temperature both minima are degenerate.

energy is large enough to overcome the competing surface tension. However, the likelihood of bubble nucleation is exponentially small close to T_c. Therefore, within the finite amount of time allowed by the expansion of the universe, nucleation happens only once the universe arrives at some particular temperature below T_c, called T_n (nucleation temperature), where the likelihood has grown sufficiently large [52]. Then the bubbles expand and finally percolate so that the whole space is filled with the broken phase after the transition is completed. During this process the plasma is thrown out of equilibrium only locally in the vicinity of the bubble walls, where the order parameter changes rapidly.
In the effective potential description which will be introduced in the next section this behavior of the system at the phase transition can be described as is indicated in figure 2.2. For very high temperatures the global minimum of the potential is located at $\phi = 0$. Close to the critical temperature a second local minimum at $\phi \neq 0$ arises. At T_c both minima, i.e. $\phi = 0$ and $\phi_c \equiv v_c$, become degenerate displaying the coexistence of the two phases. The minima are separated by a bump and the transition starts by thermal tunneling.[2] Below T_c the minimum at $\phi \neq 0$ becomes the global one.
For the generation of a non-vanishing baryon number in our present-day universe a further condition has to be satisfied. We have seen that the sphaleron rate in the broken phase (2.11) depends on the Higgs expectation value. There the baryon number violating processes have to be practically switched off, otherwise any asym-

[2]This is no tunneling process in a quantum mechanical sense. The transition from the symmetric to the broken minimum is caused by thermal fluctuations.

metry would be equilibrated to zero again. Only if we avoid this washout in the broken phase is the generated baryon number frozen in until today after the phase transition is completed. Shaposhnikov has shown that the sphaleron effects are suppressed sufficiently if the requirement

$$\xi \equiv \frac{v_c}{T_c} \gtrsim 1 \tag{2.13}$$

holds [17, 18]. A phase transition that fulfills this condition is usually called a strong first order one. As we will see, this special condition is met in both models under consideration.

2.2.2 The Effective Potential

To compute an expectation value of a field at the classical level, one has to minimize the potential energy. In quantum field theory this classical value can be modified by perturbative loop corrections. The potential that includes all quantum corrections is called effective potential. To lowest order in perturbation theory V_{eff} is in agreement with the classical potential energy. Possibly, the higher order corrections need renormalization to remove the infinities occurring [53].
Consider a quantum field theory described by a scalar field φ with a Lagrange density $\mathcal{L}[\varphi]$. In the path-integral representation the vacuum persistence amplitude in presence of an external source J is defined by

$$Z[J] = e^{iW[J]} = \int \mathcal{D}\varphi \exp\left(i \int d^4x (\mathcal{L}[\varphi] + J\varphi)\right), \tag{2.14}$$

where $W[J]$ is the so-called connected generating functional [54, 55]. The effective action is obtained from $W[J]$ by a Legendre transform

$$\Gamma[\phi_{\text{cl}}] = W[J] - \int d^4x \phi_{\text{cl}}(x) J(x). \tag{2.15}$$

Here we introduced the classical field ϕ_{cl} which is defined by the functional derivative of $W[J]$ with respect to $J(x)$

$$\phi_{\text{cl}}(x) = \frac{\delta W[J]}{\delta J(x)}. \tag{2.16}$$

$\Gamma[\phi_{\text{cl}}]$ is the generating functional of one-particle-irreducible (1PI) correlation functions, and ϕ_{cl} is the expectation value of the field φ we started with in presence of the source J. From equation (2.15) follows

$$\frac{\delta}{\delta \phi_{\text{cl}}(x)} \Gamma[\phi_{\text{cl}}] = -J(x), \tag{2.17}$$

and accordingly the effective action satisfies

$$\frac{\delta}{\delta\phi_{\rm cl}(x)}\Gamma[\phi_{\rm cl}] = 0 \tag{2.18}$$

in absence of the external source. The solutions of (2.18) are the values of $\langle\varphi\rangle$ we are looking for. Assuming invariance of the possible vacuum states under translations and Lorentz transformations, each corresponding solution $\phi_{\rm cl}$ is a constant. After removing an overall factor of space-time volume from $\Gamma[\phi_{\rm cl}]$, we are left with the effective potential which is defined via

$$\Gamma[\phi_{\rm cl}] = -\int d^4x V_{\rm eff}[\phi_{\rm cl}]. \tag{2.19}$$

Then the condition (2.18) reduces to the more easily manageable equation

$$\frac{\partial}{\partial\phi_{\rm cl}}V_{\rm eff}(\phi_{\rm cl}) = 0. \tag{2.20}$$

In practice $V_{\rm eff}$ cannot be determined exactly. In the following we will use the loop-expansion to first order. The zero-loop contribution is simply given by the classical potential while the one-loop corrections can be computed as the sum of all 1PI diagrams containing a singe loop with zero external momenta. (For a nice review see e.g. ref. [56].) To simplify the notation we will omit the index "cl" from the field $\phi_{\rm cl}$ in the following.
In case of the SM, the Higgs potential for the $SU(2)$ doublet Φ reads

$$V(\Phi) = -\mu^2\Phi^\dagger\Phi + \lambda(\Phi^\dagger\Phi)^2. \tag{2.21}$$

With

$$\Phi = \begin{pmatrix} \phi^+ \\ \phi^0 \end{pmatrix} = \frac{1}{\sqrt{2}}\begin{pmatrix} \chi_1 + i\chi_2 \\ \phi + h + i\chi_3 \end{pmatrix}, \tag{2.22}$$

where h denotes the Higgs and χ_j $(j = 1, 2, 3)$ the three Goldstone bosons, the tree-level potential in terms of the field ϕ is given by

$$V_0(\phi) = -\frac{\mu^2}{2}\phi^2 + \frac{\lambda}{4}\phi^4. \tag{2.23}$$

The minimum of V_0 at $\phi_{\rm min} = v = \sqrt{\mu^2/\lambda}$ corresponds to the expectation value of the neutral component of the Higgs doublet at $\langle\phi^0\rangle = v/\sqrt{2}$. ($v$ is fixed by experimental results to 246 GeV.) The tree-level field dependent masses of the Higgs and the Goldstone bosons are

$$\begin{aligned} m_h^2(\phi) &= 3\lambda\phi^2 - \mu^2, \\ m_\chi^2(\phi) &= \lambda\phi^2 - \mu^2. \end{aligned} \tag{2.24}$$

Obviously, the Goldstone bosons become massless for $\phi = v$. At this stage we can concentrate on the $W^\pm$ and Z bosons as well as the top quark since only these particles give a significant contribution to the one-loop effective potential. Their tree-level masses are given by

$$\begin{aligned} m_W^2(\phi) &= \frac{g^2}{4}\phi^2, \\ m_Z^2(\phi) &= \frac{g^2+g'^2}{4}\phi^2, \\ m_t^2(\phi) &= \frac{y_t^2}{2}\phi^2, \end{aligned} \tag{2.25}$$

where y_t is the top quark Yukawa coupling.
For zero temperature the contribution to the effective potential to one-loop order is [57]

$$V_1(\phi) = \sum_i \pm \frac{n_i}{64\pi^2}\, m_i^4(\phi) \ln \frac{m_i^2(\phi)}{Q^2}. \tag{2.26}$$

The + and − signs refer to the bosons and fermions, respectively. n_i counts the degrees of freedom, in particular

$$n_h = 1, \quad n_\chi = 3, \quad n_W = 6, \quad n_Z = 3, \quad n_t = 12, \tag{2.27}$$

and Q is the renormalization scale (in a particular scheme).
In addition, the effective potential is modified at finite temperature by interactions with the hot plasma. The temperature dependent one-loop contribution takes the form [58]

$$\begin{aligned} V_1^T(\phi) \quad = \quad & \sum_B \frac{n_B T^4}{2\pi^2} \int_0^\infty dx\, x^2 \ln\left[1 - \exp\left(-\sqrt{x^2 + \frac{m_B^2(\phi)}{T^2}}\right)\right] \\ - \quad & \sum_F \frac{n_F T^4}{2\pi^2} \int_0^\infty dx\, x^2 \ln\left[1 + \exp\left(-\sqrt{x^2 + \frac{m_F^2(\phi)}{T^2}}\right)\right], \end{aligned} \tag{2.28}$$

where the indices B and F denote the boson and fermion circulating in the loop, respectively. Instead of the numerical evaluation of these integrals, simpler approximations can be used in case of very high and low temperatures [58, 59]. For more details see appendix A.
Finally, the one-loop effective potential is obtained from the sum

$$V_{\text{eff}}(\phi) = V_0(\phi) + V_1(\phi) + V_1^T(\phi). \tag{2.29}$$

Starting with this function, it is possible to compute the relevant properties of the phase transition.

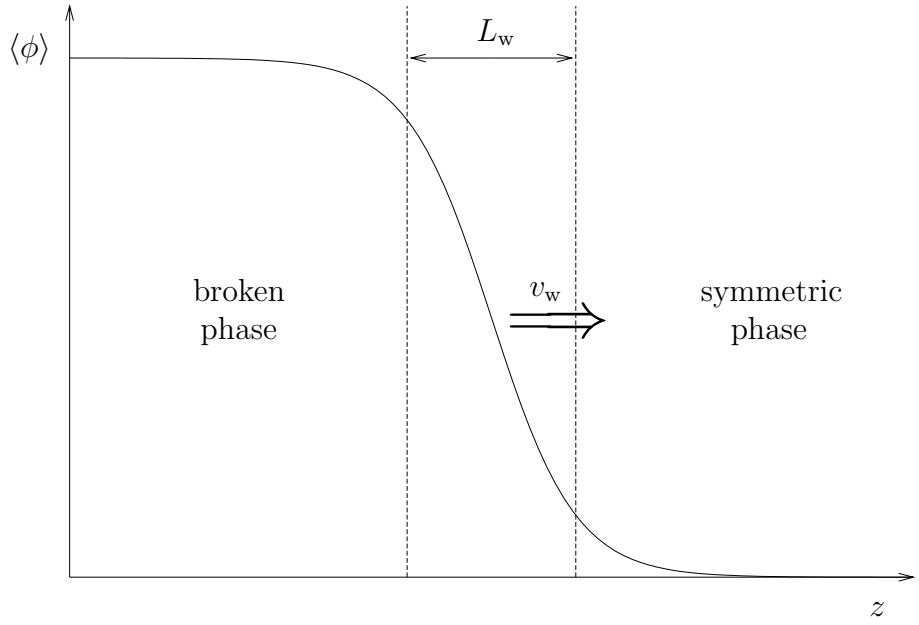

Figure 2.3: The shape of the phase boundary.

2.2.3 Bubble Characteristics

In this section we want to present the determination of the strength of a phase transition, and we give a rough estimate for the wall thickness L_w and comment on the wall velocity v_w. All these quantities will enter the following computation of the baryon asymmetry.
To determine the non-zero expectation value v_c and the critical temperature T_c, the two conditions

$$\left.\frac{\partial}{\partial\phi}V_{\text{eff}}(\phi,T_c)\right|_{\phi=v_c}=0 \qquad \text{and} \qquad V_{\text{eff}}(v_c,T_c)=0 \tag{2.30}$$

have to be fulfilled. In a particular model the strength of the phase transition has to be computed numerically for every given set of parameters.
Figure 2.3 schematically shows the shape of the phase boundary, and also L_w and v_w are indicated. The question is: what do we mean by these properties and how do we estimate them? First of all, we have to make some fundamental remarks. As already mentioned, the two minima of V_{eff} acquire the same depth at T_c. The tunneling, accompanied by the formation of bubbles, starts somewhat later at the temperature T_n. As shown by Linde [60–62], the thermal tunneling probability per unit volume and unit time at high temperatures is

$$P \simeq A(T)e^{-S_3/T} \tag{2.31}$$

with the prefactor $A(T)$ being of order $\mathcal{O}(T^4)$. The tunneling rate is exponentially suppressed by the three-dimensional Euclidean action of the spherically symmetric static field configuration $\phi(r)$,

$$S_3[\phi] = 4\pi \int_0^\infty dr\, r^2 \left[\frac{1}{2} \left(\frac{d\phi(r)}{dr} \right)^2 + V_{\text{eff}}(\phi(r), T) \right]. \tag{2.32}$$

The phase transition starts if the nucleation probability per horizon volume becomes of order unity, which translates into the condition

$$\frac{S_3(T_n)}{T_n} \sim 130 - 140 \tag{2.33}$$

for the energy of the critical bubble [59, 63].
The $O(3)$-symmetric field configuration $\phi(r)$ has to satisfy the Euclidean equation of motion

$$\frac{d^2\phi(r)}{dr^2} + \frac{2}{r}\frac{d\phi(r)}{dr} = \frac{\partial}{\partial\phi} V_{\text{eff}}(\phi, T), \tag{2.34}$$

with the boundary conditions

$$\left.\frac{d\phi(r)}{dr}\right|_{r=0} = 0 \qquad \text{and} \qquad \phi(r \to \infty) = \phi_{\text{sym}} = 0. \tag{2.35}$$

In case of tunneling between two almost degenerate minima of the potential, i.e. with an energy difference ΔV small compared to the height of the barrier, the equation (2.34) can be simplified further. The radius of the bubble is then much larger than the thickness of the wall L_{w}, and the term $d\phi/dr$ in (2.34) can be neglected. Replacing r by z, the field equation reads

$$\frac{d^2\phi(z)}{dz^2} = \frac{\partial}{\partial\phi} V_{\text{eff}}(\phi, T), \tag{2.36}$$

with the boundary conditions

$$\phi(z \to -\infty) = \phi_{\text{brk}} = v_c \qquad \text{and} \qquad \phi(z \to \infty) = \phi_{\text{sym}} = 0. \tag{2.37}$$

Now the solution is a planar domain wall with translational invariance perpendicular to the z-direction.
In general, the non-linear differential equation (2.36) has to be solved numerically. However, it is possible to find an analytic solution for a toy model which is very similar to our given situation. Consider an effective potential at T_c of the form

$$V_{\text{eff}}(\varphi) = \frac{\lambda}{4}\varphi^2(\varphi - u)^2. \tag{2.38}$$

This potential has two degenerate minima at $\varphi = 0$ and $\varphi = u$ separated by a barrier of the height

$$V_b = V\left(\varphi = \frac{u}{2}\right) = \frac{\lambda}{64}u^4. \tag{2.39}$$

In this case, the solution of (2.36) is given by

$$\varphi(z) = \frac{u}{2}\left(1 - \tanh\frac{z}{L}\right), \tag{2.40}$$

where the wall thickness L reads

$$L^2 = \frac{8}{\lambda u^2} = \frac{u^2}{8V_b}. \tag{2.41}$$

We have shown that also for more complicated effective potentials than (2.38) this kink solution fits the wall profile quite well [64]. In more realistic scenarios the top of the barrier is not exactly located at $\phi = v_c/2$, and V_b cannot be determined analytically any longer. Nevertheless, we define the wall thickness L_w again by

$$L_\mathrm{w} = \sqrt{\frac{v_c^2}{8V_b}}, \tag{2.42}$$

where the height V_b of the barrier of the respective potential has to be calculated numerically. In both models under consideration the bubble profile can approximately be described by the kink

$$\phi(z) = \frac{v_c}{2}\left(1 - \tanh\frac{z}{L_\mathrm{w}}\right). \tag{2.43}$$

The computation of another bubble property, the wall velocity v_w, is very complex. Once a critical bubble is nucleated it will expand. On one hand the expansion is accelerated by the internal pressure, but on the other hand it is slowed down by plasma friction. The wall propagates with a constant velocity when the forces are balanced and a stationary situation is reached. For a strong first order phase transition, with ξ being close to one, we obtain a wall velocity of order unity if we take into account only the friction related to the infrared gauge field modes [65]

$$v_\mathrm{w} = \frac{32\pi L_\mathrm{w}\Delta V}{11g^2T^3\left[\ln(m_W L_\mathrm{w}) + \mathcal{O}(1)\right]}. \tag{2.44}$$

Here ΔV denotes the potential difference at the nucleation temperature T_n. The order unity correction in the denominator is induced by friction of other particles in the plasma, in particular the top quark [66]. This friction will slow down the wall considerably, because the other term in the denominator, $\ln(m_W L_\mathrm{w})$, is of order unity too. In addition, v_w is also reduced by the latent heat of the nucleating bubbles. Altogether, it is only possible to give rough estimates with large uncertainties, and for large wall velocities even the estimate (2.44) breaks down. The only thing one can definitely say is, that in case of a stronger phase transition, the movement of the wall is faster. Because of all these uncertainties we decided to treat v_w as a free parameter in the following computation of the baryon asymmetry.

2.3 CP-Violation

The CP-transformation is a combination of the charge conjugation C, which interchanges particles and anti-particles by conjugation of all internal quantum numbers, and parity P, under which the space-coordinates change the sign, i.e. $\mathbf{x} \to -\mathbf{x}$. If CP were an exact symmetry, no baryon asymmetry generation would be possible.
In the SM the only source of CP-violation is a complex phase occurring in the Cabibbo-Kobayashi-Maskawa (CKM) mixing matrix. The flavor eigenstates differ from the mass eigenstates and the CKM matrix relates these two bases. However, this CP-breaking mechanism is too weak to fuel baryogenesis [20–22]. In extensions of the SM, additional sources of CP-violation usually arise through a richer set of Yukawa and Higgs self-interactions. These additional interactions lead to complex fermion masses in case of both models under consideration, as we will see in the following chapters. So let us first make some general remarks about the consequences of a complex fermion mass M.
Consider the Lagrange density of a non-interacting fermion

$$\mathcal{L} = \bar{\Psi}\left(i\gamma_\mu\partial^\mu - P_L M - P_R M^*\right)\Psi = \bar{\Psi}\left(i\gamma_\mu\partial^\mu - \Re(M) - i\Im(M)\gamma^5\right)\Psi \tag{2.45}$$

with the left- and right-handed projection operators

$$P_L = \frac{1}{2}\left(1-\gamma^5\right) \qquad \text{and} \qquad P_R = \frac{1}{2}\left(1+\gamma^5\right). \tag{2.46}$$

It is well known that the action of a non-interacting fermion with a real mass is invariant under CP. Thus, we only have to look at the behavior of the term $i\bar{\Psi}\gamma^5\Psi$. For charge conjugation

$$\Psi \to \Psi^c = C\bar{\Psi}^T = C\gamma^0\Psi^* \qquad \text{with} \qquad C\gamma_\mu C^{-1} = -\gamma_\mu^T \tag{2.47}$$

we have

$$\begin{aligned} i\bar{\Psi}^c\gamma^5\Psi^c &= i\left(C\gamma^0\Psi^*\right)^\dagger\gamma^0\gamma^5 C\gamma^0\Psi^* \\ &= i\Psi^T\gamma^0 C^{-1}\gamma^0 C C^{-1}\gamma^5 C\gamma^0\Psi^* \\ &= -i\Psi^T\gamma^{5T}\gamma^0\Psi^* \\ &= i\bar{\Psi}\gamma^5\Psi. \end{aligned} \tag{2.48}$$

Here we used the identities

$$C^{-1}\gamma^0 C = -\gamma^0 \qquad \text{and} \qquad C^{-1}\gamma^5 C = -\gamma^{5T}. \tag{2.49}$$

Under parity

$$\Psi \to \Psi^p = \gamma^0\Psi \tag{2.50}$$

we obtain

$$\begin{aligned} i\bar{\Psi}^p\gamma^5\Psi^p &= i\left(\gamma^0\Psi\right)^\dagger\gamma^0\gamma^5\gamma^0\Psi \\ &= i\Psi^\dagger\gamma^5\gamma^0\Psi \\ &= -i\bar{\Psi}\gamma^5\Psi. \end{aligned} \tag{2.51}$$

Accordingly, $i\bar{\Psi}\Im(M)\gamma^5\Psi$ in equation (2.45) is C-conserving but P-violating.
For each model, the new sources of CP-violation are restricted by measurements of the electric dipole moments (EDMs). The strongest constraints are given by the upper limit of the electron EDM [67] and the neutron EDM [68],

$$|d_e| \leq 1.6 \times 10^{-27} e \text{ cm}, \tag{2.52}$$

$$|d_n| \leq 3.0 \times 10^{-26} e \text{ cm}, \tag{2.53}$$

at 90% confidence level. We will discuss these constraints in more detail in the following chapters after the ϕ^6 model and the 2HDM have been introduced.

3 The ϕ^6 Model

It is well known that the SM fails to account for an electroweak baryogenesis scenario. As demonstrated in section 2.2.1, a first order phase transition is triggered by a barrier in the effective Higgs potential. In case of the SM, this barrier can be provided by a cubic term in the potential coming from the one-loop thermal corrections of the weak gauge bosons. But this does not suffice to give rise to a strong first order phase transition. A promising idea for an extended setting is to add non-renormalizable operators. If the stability of the Higgs potential is restored by a ϕ^6 interaction, the barrier can also be generated from a negative quartic term, which will no longer destabilize the potential. This yields a strong first order phase transition, sufficient to drive baryogenesis in a large part of the parameter space [69–74]. Another advantage of non-renormalizable interactions is that we easily get an extra mechanism for CP-breaking to fuel baryogenesis, in addition to the usual breaking via the CKM matrix [75, 76].
Non-renormalizable operators parameterize the effects of new physics beyond some cut-off scale Λ. This new dynamics could be an ordinary quantum field theory like an extended Higgs sector, or even something more fundamental like strongly coupled gravity, if the hierarchy problem is solved by the presence of extra dimensions. We will concentrate on the lowest higher dimension operator and add a non-renormalizable ϕ^6 operator to the SM potential such that

$$V_0(\phi) = \frac{\mu^2}{2}\phi^2 + \frac{\lambda}{4}\phi^4 + \frac{1}{8\Lambda}\phi^6. \tag{3.1}$$

3.1 EWPT in the ϕ^6 Model

At zero temperature we include the one-loop correction from the top quark

$$V_{\text{eff}}(\phi, 0) = V_0(\phi) + V_1(\phi) = V_0(\phi) - \frac{3y_t^4}{64\pi^2}\phi^4 \ln\left(\frac{y_t^2\phi^2}{2Q^2}\right), \tag{3.2}$$

using the same notation as in section 2.2.2. With the two conditions

$$\frac{\partial}{\partial\phi}V_{\text{eff}}(\phi, 0)\bigg|_{\phi=v} = 0 \qquad \text{and} \qquad \frac{\partial^2}{\partial\phi^2}V_{\text{eff}}(\phi, 0)\bigg|_{\phi=v} = m_h^2, \tag{3.3}$$

the two unknown parameters μ and λ can be expressed by the physical quantities $v = 246$ GeV and m_h^2. We obtain

$$\mu^2 = \frac{1}{2}\left[m_h^2 + \frac{3v^2}{8}\left(\frac{y_t^4}{\pi^2} - \frac{4v^2}{\Lambda^2}\right)\right], \tag{3.4}$$

$$\lambda = \frac{1}{2v^2}\left(m_h^2 - \frac{3v^4}{\Lambda^2}\right) + \frac{3y_t^4}{32\pi^2}\left[3 + 2\ln\left(\frac{y_t^2 v^2}{2Q^2}\right)\right]. \tag{3.5}$$

In the following, we treat the cut-off scale Λ and the Higgs mass m_h as the free parameters of the model. In order for the dimension-six operator to be relevant at weak scale temperatures, we assume $\Lambda \lesssim 1$ TeV. In addition, Λ should certainly be larger than a few hundred GeV to be consistent with electroweak precision data. The other parameter is only restricted from below, since the SM constraint on the Higgs mass, $m_h > 114$ GeV, also applies to the model under consideration.
At finite temperature we add the one-loop contribution $V_1^T(\phi)$ to the effective potential. In the high temperature expansion (cf. appendix A) it contains the thermal Higgs mass term

$$\frac{1}{2}\left(\frac{\lambda}{2} + \frac{3g^2}{16} + \frac{g'^2}{16} + \frac{y_t^2}{4}\right) T^2\phi^2, \tag{3.6}$$

the one-loop contributions due to the transverse gauge bosons

$$-\frac{2}{3}\left(\frac{g^3}{16\pi} + \frac{(g^2+g'^2)^{3/2}}{32\pi}\right) T\phi^3 \approx -\frac{g^3}{16\pi} T\phi^3 \tag{3.7}$$

and the one-loop top quark contribution

$$-\frac{3y_t^4}{64\pi^2}\phi^4 \ln\left(\frac{y_t^2\phi^2}{2c_F T^2}\right), \tag{3.8}$$

where $c_F \approx 13.94$ [58]. Furthermore, we add the leading one- and two-loop corrections due to the ϕ^6 interaction

$$\frac{1}{8\Lambda}\left(2T^2\phi^4 + T^4\phi^2\right). \tag{3.9}$$

Finally, the high temperature effective potential is given by

$$\begin{aligned} V_{\text{eff}}(\phi, T) = \quad & -\frac{\mu^2}{2}\phi^2 + \frac{1}{2}\left(\frac{\lambda}{2} + \frac{3g^2}{16} + \frac{g'^2}{16} + \frac{y_t^2}{4}\right) T^2\phi^2 \\ & -\frac{g^3}{16\pi} T\phi^3 + \frac{\lambda}{4}\phi^4 + \frac{3y_t^4}{64\pi^2}\phi^4 \ln\left(\frac{Q^2}{c_F T^2}\right) \\ & +\frac{1}{8\Lambda}\left(2T^2\phi^4 + T^4\phi^2\right). \end{aligned} \tag{3.10}$$

We choose $Q = 178$ GeV for the renormalization scale. Note that another choice of Q would only change the value of the Higgs self-coupling λ.

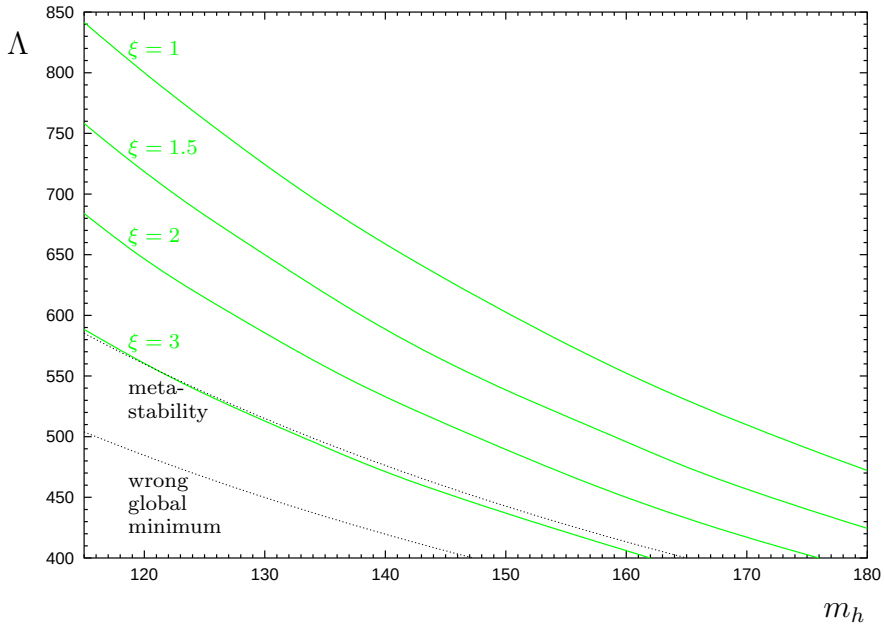

Figure 3.1: Contours of constant $\xi = v_c/T_c$ in the Λ-m_h-plane. Λ and m_h are given in units of GeV.

With the effective potential (3.10), the phase structure of this model can be computed via the conditions (2.30). In figure 3.1 the strength of the phase transition is shown as a function of the model parameters. It becomes weaker for increasing Higgs masses, and for the smallest allowed Higgs mass, $m_h = 115$ GeV, we need $\Lambda \lesssim 850$ GeV to satisfy the washout criterion (2.13). Below the lowest line which is indicated by "wrong global minimum" the symmetric vacuum is the global one for every temperature meaning the non-zero vacuum is metastable and there is no longer a phase transition. Below the "metastability" line the probability for thermal tunneling gets too small compared to the Hubble expansion rate. This means that in this region the universe remains stuck in the symmetric vacuum. We have excluded the corresponding values from the parameter space, but there remains a large part of the parameter space satisfying the necessary condition for electroweak baryogenesis. In contrast to the SM, we find a strong first order phase transition for Higgs masses up to 180 GeV.
It is possible to fulfill the washout criterion even for higher Higgs masses. In general, there is no particular bound on the ϕ^6 operator [77]. However, we restricted the cut-off scale from below, i.e. $\Lambda \gtrsim 400$ GeV, to make an expansion in powers of v/Λ reasonable. In addition, a lower cut-off scale may be problematic for this model to be in agreement with precision measurements on electroweak observables. Other dimension-six operators, such as $(\Phi^\dagger D_\mu \Phi)^2/\Lambda^2$ for example, are also expected to be present. As demonstrated in ref. [70], these operators have to be suppressed by a higher scale of about 10 TeV in order to coincide with electroweak precision

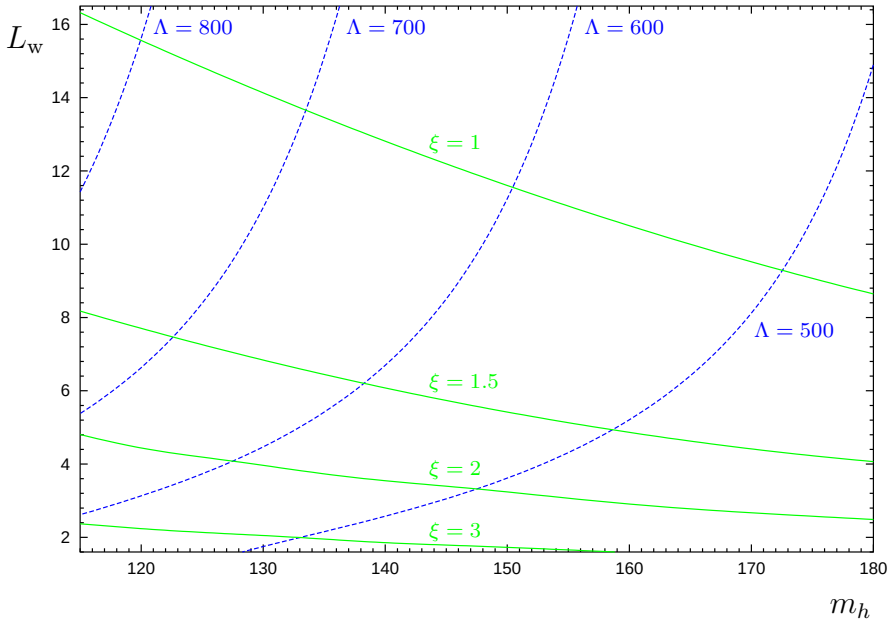

Figure 3.2: The wall thickness L_w in units of T^{-1} as a function of the Higgs mass for several fixed values of the cut-off scale. m_h and Λ are given in units of GeV.

measurements. The required fine-tuning of the couplings has to be explained by the UV completion of the model.
The various one-loop contributions to the effective potential (3.10) affect the strength of the transition in different ways. Some of them weaken it and others make the transition stronger. A detailed discussion about their particular relevance can be found in ref. [64]. Furthermore, we have checked that an additional dimension-eight term $(\Phi^\dagger\Phi)^4/\Lambda^4$ changes ξ only at the order $\mathcal{O}(v^2/\Lambda^2)$.
The wall thickness can be evaluated via equation (2.42). It varies in a wide range between 2 and $16T^{-1}$ depending on the combination of the parameters. In particular, it becomes smaller if we decrease m_h at fixed Λ. The same happens if we decrease Λ at fixed m_h. The main effect comes from the decrease of the critical temperature in both cases. In figure 3.2 this behavior is presented in dependence of the model parameters. In addition, lines of constant ξ are shown.

3.2 The Top Quark Mass in the ϕ^6 Model

Non-renormalizable operators allow for new sources of CP-violation to fuel baryogenesis [75, 76]. If gauge singlets are absent the leading operators are of dimension six. In the model under consideration the CP-violating source is generated by a

dimension-six Higgs-fermion interaction. Let us consider the Lagrangian

$$\mathcal{L}_m = \bar{\Psi}_L \left(y\Phi + \frac{x}{\Lambda^2} \left(\Phi^\dagger \Phi\right) \Phi \right) \Psi_R + h.c., \tag{3.11}$$

where y stands for the usual Yukawa couplings and x for new couplings containing complex phases relative to y. In general, these x have an unknown flavour structure. To avoid fine-tuning of the fermion masses m_f, their couplings should at most be of order $\mathcal{O}(m_f \Lambda^2/v^3)$, if the top quark coupling is of order unity. Thus, the electron coupling should not exceed $10^{-4} \times (\Lambda/\text{TeV})^2$ for example. If we bear this in mind and consider a theory without flavor mixing, we are allowed to assume that the couplings x have the same structure as the corresponding ordinary Yukawa couplings. This could also be motivated by a Froggatt-Nielsen type mechanism [78].
Since the Φ and Φ^3 terms of equation (3.11) vary differently during the EWPT, the fermion masses acquire space-dependent phases which cannot be rotated away. Let us concentrate on the top quark interactions and denote the relative phase between the two couplings y_t and x_t as $\varphi_t = \arg(y_t x_t^*)$. The Lagrangian reduces to

$$\mathcal{L}_m = \bar{t}_L M_t t_R + \bar{t}_R M_t^* t_L \tag{3.12}$$

with the complex top mass

$$M_t(z) = y_t \frac{\phi(z)}{\sqrt{2}} + i \sin(\varphi_t) |x_t| \frac{\phi^3(z)}{2\sqrt{2}\Lambda^2} \equiv m_t(z) e^{i\theta_t(z)}, \tag{3.13}$$

where y_t is chosen to be purely real, and we have ignored the real part of x_t[1]. Thus, the CP-violating phase is defined as

$$\theta_t(z) = \arctan\left(\frac{\sin(\varphi_t)|x_t|\phi^2(z)}{2y_t\Lambda^2} \right). \tag{3.14}$$

In the following we take this phase as maximal, i.e. $\sin(\varphi_t) = 1$, and we choose $|x_t| = 1$.
In ref. [76] the EDMs of the electron and the neutron in a non-standard top quark scenario are discussed. Using their formulas with our effective Yukawa coupling

$$y_t^{\text{eff}} = y_t \left(1 + \frac{i\phi^2(z)}{2y_t\Lambda^2} \right), \tag{3.15}$$

we find $d_e \simeq 0.04 \times 10^{-27} e$ cm for $m_h = 115$ GeV and $\Lambda = 1$ TeV. We only give a rough estimate for the electric dipole moment of the neutron, since its calculation contains large uncertainties. In a non-relativistic quark model we have $d_n \simeq (4d_d - d_u)/3 \simeq (m_d/m_e) d_e \simeq 0.04 \times 10^{-26} e$ cm. Therefore, both EDMs are below the current experimental bounds (2.52) and (2.53).

[1] This is a good approximation since the real part of x_t is negligible in comparison to y_t because of the Λ^2 in the denominator. Therefore, only its imaginary part is of relevance.

4 The Two Higgs Doublet Model

Of course, adding non-renormalizable operators is not the only possibility to extend the SM in a way convenient for successful baryogenesis. An alternative is to augment the Higgs sector by an additional Higgs doublet. The particle spectrum then includes three neutral and two charged Higgs particles and the general potential contains a large number of unknown parameters. One would expect that in such a model it is possible to find regions in the parameter space which allow for a strong first order phase transition. As a matter of fact, the 2HDM arranges the requirements of a sufficiently strong first order EWPT as is shown for instance in refs. [79–83] by investigating the effective potential at finite temperature. Another advantage of this model is that it allows non-standard CP-violation which is also needed for baryogenesis.

4.1 Effective Potential and Particle Spectrum

In general, the 2HDM suffers from flavor changing neutral currents (FCNCs) at tree-level. Thus, in a realistic model the couplings of the Higgs-fermion interactions have to be chosen carefully to avoid the FCNCs. The model can be classified by two different cases treating this issue, the so-called "type I" and "type II" case. In a "type I" model only one Higgs doublet couples to both, the up- and down-type quarks. In the "type II" case one Higgs field, Φ_1, couples to the down-type quarks and the other Higgs field, Φ_2, couples to the up-type quarks. Consequently, neutral flavor conservation is enforced by imposing a discrete Z_2 symmetry, such that $H_1 \to -H_1$ and $d_i^c \to \mp d_i^c$ while the other fields do not transform. Then the "$-$" case corresponds to the "type II" and the "$+$" case to the "type I" model. Howsoever, in the following the only relevant coupling will be the one of the top quark, so that we do not need to distinguish between both types.
The most general $SU(2)_L \times U(1)_Y$ invariant tree-level potential is [84, 85]

$$\begin{aligned} V_0(\Phi_1,\Phi_2) &= -\mu_1^2\Phi_1^\dagger\Phi_1 - \mu_2^2\Phi_2^\dagger\Phi_2 - \mu_3^2(e^{i\alpha}\Phi_1^\dagger\Phi_2 + \text{h.c.}) \\ &\quad + \frac{\lambda_1}{2}(\Phi_1^\dagger\Phi_1)^2 + \frac{\lambda_2}{2}(\Phi_2^\dagger\Phi_2)^2 + \lambda_3(\Phi_1^\dagger\Phi_1)(\Phi_2^\dagger\Phi_2) \\ &\quad + \lambda_4|\Phi_1^\dagger\Phi_2|^2 + \frac{\lambda_5}{2}\left((\Phi_1^\dagger\Phi_2)^2 + \text{h.c.}\right). \end{aligned} \tag{4.1}$$

Without loss of generality the couplings λ_i and μ_i can always be taken real. The mass term $\mu_3^2 e^{i\alpha}$ breaks the aforementioned Z_2 symmetry softly without violating the necessary suppression of FCNCs [86]. If this term is complex, CP-invariance is broken in the Higgs sector. Thus, the case $\alpha \neq 0$ is important for this model to be able to generate a baryon asymmetry.
The Higgs potential contains nine parameters, which are three squared masses, μ_i, five couplings, λ_i, and one phase, α. One of them can be fixed by the Z boson mass, leaving an eight-dimensional parameter space, which is still quite large. The parameters have to satisfy some constraints, because the potential has to be bounded from below. At tree-level this translates into the conditions [81]

$$\lambda_1 > 0, \quad \lambda_2 > 0, \quad \sqrt{\lambda_1 \lambda_2} + \lambda_3 > 0, \quad \sqrt{\lambda_1 \lambda_2} + \lambda_3 + \lambda_4 \pm \lambda_5 > 0. \tag{4.2}$$

To simplify the analysis we focus on the simpler case

$$\mu_1^2 = \mu_2^2 \quad \text{and} \quad \lambda_1 = \lambda_2 \tag{4.3}$$

in the following. At tree-level this implies the symmetry

$$\Phi_1 \leftrightarrow \Phi_2^\dagger. \tag{4.4}$$

Furthermore, equation (4.3) is a reasonable assumption, since it was shown in ref. [79] that setting the quadratic self-couplings equal, favors large Higgs expectation values in the broken phase. As demonstrated in section 2.1 this is required to avoid baryon number washout after the phase transition is completed.
Let us first consider the CP-conserving case $\alpha = 0$. Under the assumption that the charged Higgs mass squared is positive there exist no charge breaking minima [87]. Thus, we can restrict ourselves to the neutral fields. In the following, we will assume that this result generalizes to the one-loop level, including a small CP-violating phase. If we parameterize the neutral components of the Higgs fields such that $\Phi_1^0 = h_1$ and $\Phi_2^0 = h_2$[1] the potential reads

$$V_0(h_1, h_2) = -\mu_1^2(h_1^2 + h_2^2) - 2\mu_3^2 h_1 h_2 + \frac{\lambda_1}{2}(h_1^4 + h_2^4) + (\lambda_3 + \lambda_4 + \lambda_5) h_1^2 h_2^2. \tag{4.5}$$

The symmetry (4.4) causes the minimum to be at $\tan(\beta) \equiv \langle h_2 \rangle / \langle h_1 \rangle = 1$. With $\langle h_1 \rangle = \langle h_2 \rangle = h = 123$ GeV the extremal conditions

$$\frac{\partial}{\partial h_1} V_0 \bigg|_{h_1 = h_2 = h} = \frac{\partial}{\partial h_2} V_0 \bigg|_{h_1 = h_2 = h} = 0 \tag{4.6}$$

lead to

$$-\mu_1^2 - \mu_3^2 + (\lambda_1 + \lambda_3 + \lambda_4 + \lambda_5) h^2 = 0. \tag{4.7}$$

[1] Note that we do not introduce the usual factor $1/\sqrt{2}$ here.

Because each Higgs doublet contains four real scalar fields, the Higgs mass matrix is a 8×8 matrix. It is block diagonal, and we obtain on one hand three massless Goldstone bosons ($G^0, G^\pm$) and on the other hand five physical Higgs bosons which are two neutral and CP-even (h^0, H^0), one neutral and CP-odd (A^0) and two charged ($H^\pm$) Higgs bosons. The corresponding squared masses can be expressed by the following linear combinations of the couplings:

$$\begin{aligned} m^2_{h^0} &= 2(\lambda_1 + \lambda_3 + \lambda_4 + \lambda_5)h^2, && (4.8)\\ m^2_{H^0} &= 2\mu_3^2 - 2(-\lambda_1 + \lambda_3 + \lambda_4 + \lambda_5)h^2, && (4.9)\\ m^2_{A^0} &= 2\mu_3^2 - 4\lambda_5 h^2, && (4.10)\\ m^2_{H^\pm} &= 2\mu_3^2 - 2(\lambda_4 + \lambda_5)h^2. && (4.11) \end{aligned}$$

Via these relations the model can be parameterized in terms of the four Higgs masses and μ_3^2.
In case of non-vanishing α CP is violated by the Higgs potential. Now we use the parameterization

$$\Phi_1^0 = h_1 e^{-i\theta_1} \quad \text{and} \quad \Phi_2^0 = h_2 e^{i\theta_2} \tag{4.12}$$

of the neutral fields. Note that the potential only depends on the sum of both phases, $\theta = \theta_1 + \theta_2$, and in the minimum we can always choose the special gauge $\theta_1 = \theta_2 = \theta/2$. The potential in terms of h_1, h_2 and θ is then given by

$$\begin{aligned} V_0(h_1, h_2, \theta) &= -\mu_1^2(h_1^2 + h_2^2) - 2\mu_3^2 h_1 h_2 \cos(\theta + \alpha) + \frac{\lambda_1}{2}(h_1^4 + h_2^4) \\ &\quad + (\lambda_3 + \lambda_4 + \lambda_5 \cos(2\theta))h_1^2 h_2^2. && (4.13) \end{aligned}$$

Using the notation $\langle\theta\rangle = \vartheta$ the two extremal conditions

$$\begin{aligned} \frac{\partial}{\partial h_1} V_0 \bigg|_{h_1=h_2=h,\theta=\vartheta} &= \frac{\partial}{\partial h_2} V_0 \bigg|_{h_1=h_2=h,\theta=\vartheta} = 0 && (4.14)\\ \frac{\partial}{\partial \theta} V_0 \bigg|_{h_1=h_2=h,\theta=\vartheta} &= 0 && (4.15) \end{aligned}$$

yield

$$\begin{aligned} -\mu_1^2 - \mu_3^2 \cos(\vartheta + \alpha) + (\lambda_1 + \lambda_3 + \lambda_4 + \lambda_5 \cos(2\vartheta))h^2 &= 0 \\ \mu_3^2 \sin(\vartheta + \alpha) - \lambda_5 \sin(2\vartheta)h^2 &= 0. && (4.16) \end{aligned}$$

In the CP-violating case the corresponding squared Higgs boson masses additionally depend on ϑ via

$$\begin{aligned} m^2_{H_1} &= -\mu_1^2 + 2(\lambda_1 + \lambda_3 + \lambda_4)h^2 - \sqrt{\mu_1^4 + 4\lambda_5 \cos(2\vartheta)\mu_1^2 h^2 + 4\lambda_5^2 h^4}, && (4.17)\\ m^2_{H_2} &= -2\mu_1^2 + 4\lambda_1 h^2, && (4.18)\\ m^2_{H_3} &= -\mu_1^2 + 2(\lambda_1 + \lambda_3 + \lambda_4)h^2 + \sqrt{\mu_1^4 + 4\lambda_5 \cos(2\vartheta)\mu_1^2 h^2 + 4\lambda_5^2 h^4}, && (4.19)\\ m^2_{H^\pm} &= -2\mu_1^2 + 2(\lambda_1 + \lambda_3)h^2. && (4.20) \end{aligned}$$

Now the neutral Higgs states are mixtures with scalar and pseudoscalar content. Again these relations can be used to define the model in terms of the four Higgs masses, μ_3^2 and α.
We also take the zero temperature one-loop contribution (2.26) to the effective potential into account. In V_1, the $m_i^2 = m_i^2(\Phi_1, \Phi_2)$ are the mass eigenvalues depending on both Higgs fields. We choose $Q = 246/\sqrt{2}$ GeV for the renormalization scale and consider only the heaviest bosons, i.e. $m_i = m_{H_2}, m_{H_3}, m_{H^\pm}$, and the fermion with the largest Yukawa coupling, i.e. $m_i = m_t$. For the top quark mass we have $m_t^2 = y_t^2 \Phi_2^\dagger \Phi_2$. All other particles can be safely neglected due to their small contributions to the effective one-loop potential.
Furthermore, we add counter terms to the potential, such that the tree-level minimum and Higgs masses are preserved at the one-loop level. We renormalize the potential by introducing seven counter terms

$$\begin{aligned} V_{CT}(\Phi_1, \Phi_2) &= -\delta\mu_1^2(\Phi_1^\dagger\Phi_1 + \Phi_2^\dagger\Phi_2) - \delta\mu_3^2(e^{i\phi}\Phi_1^\dagger\Phi_2 + \text{h.c.}) \\ &\quad + \frac{\delta\lambda_1}{2}(\Phi_1^\dagger\Phi_1)^2 + \frac{\delta\lambda_2}{2}(\Phi_2^\dagger\Phi_2)^2 + \delta\lambda_3(\Phi_1^\dagger\Phi_1)(\Phi_2^\dagger\Phi_2) \\ &\quad + \delta\lambda_4|\Phi_1^\dagger\Phi_2|^2 + \frac{\delta\lambda_5}{2}\left((\Phi_1^\dagger\Phi_2)^2 + \text{h.c.}\right) \end{aligned} \tag{4.21}$$

and solving the renormalization conditions. Since the top quark couples only to Φ_2 the symmetry (4.4) no longer holds at one-loop level leading to $\delta\lambda_1 \neq \delta\lambda_2$. The renormalization conditions are evidently given by

$$\left.\frac{\partial}{\partial h_1}(V_1 + V_{CT})\right|_{h_1=h_2=h,\theta=\vartheta} = 0, \tag{4.22}$$

$$\left.\frac{\partial}{\partial h_2}(V_1 + V_{CT})\right|_{h_1=h_2=h,\theta=\vartheta} = 0, \tag{4.23}$$

$$\left.\frac{\partial}{\partial \theta}(V_1 + V_{CT})\right|_{h_1=h_2=h,\theta=\vartheta} = 0, \tag{4.24}$$

meaning that the minimum of the potential $V = V_0 + V_1 + V_{CT}$ does not change with respect to the tree-level case. Moreover, we fix the Higgs masses to their tree-level values leading to four additional conditions. We require that the eigenvalues of the mass matrix corresponding to the potential V are equal to the eigenvalues of the tree-level mass matrix. For details concerning this calculation see ref. [64].
For the finite temperature one-loop contribution to the effective potential, V_1^T, we use the low and high temperature approximations, because it is much more convenient to deal with analytic expressions than the full integral expressions of ref. [58]. Both limits as well as all technical details about the smooth interpolation between them can be found in appendix A.
Finally, the effective potential, which governs the dynamics of the phase transition, is given by the sum

$$V_{\text{eff}} = V_0 + V_1 + V_{CT} + V_1^T. \tag{4.25}$$

This quantity depends on the fields h_1, h_2 and θ and the temperature T.
We have to pay attention to some experimental constraints for the 2HDM. First of all, the lightest Higgs boson is restricted from below by the LEP bound of 114 GeV, since it is SM-like in the parameter range under consideration. Secondly, the 2HDM does not respect the custodial symmetry of the SM, and therefore large corrections to the electroweak precision observables are possible. These corrections can be approximately described in terms of self-energy contributions, the so-called "oblique" corrections. We will not discuss these here in detail, but all relevant expressions can be found in ref. [88]. One result is that in order to be consistent with the measurements, the mass splitting between the extra Higgs states should not be much larger than the W mass. Since we will set these masses equal in the following to reduce the dimension of the parameter space, the oblique corrections are automatically small. Furthermore, we know from the decay $b \to s\gamma$ that the charged Higgs boson (in the "type II" model) should be larger than about 200 GeV [89]. Other possible constraints from the muon anomalous magnetic moment [90] and from the tau decays [91] are irrelevant for values of $\tan(\beta)$ close to 1.

4.2 EWPT in the 2HDM

To make a statement about the strength of the phase transition, we first have to define the order parameter. In the 2HDM the transition between two minima of the effective potential, as described in section 2.2.1, occurs in the h_1-h_2-plane. At the critical temperature T_c the symmetric minimum is located at $\langle h_1 \rangle_T = \langle h_2 \rangle_T = 0$ and the broken one at $\langle h_1 \rangle_T = v_1 > 0$ and $\langle h_2 \rangle_T = v_2 > 0$. Of course, also in the 2HDM both minima are degenerate and separated by an energy barrier at T_c. The total non-zero Higgs expectation value is defined by $v_c = \sqrt{2}\sqrt{v_1^2 + v_2^2}$.[2]
As already mentioned, we reduce the number of parameters by focusing on the case where the heavy Higgs masses are degenerate. Thus, we take the phase α, the real parameter μ_3^2, the light Higgs mass $m_h = m_{H_1}$, and the heavy Higgs mass $m_H = m_{H_2} = m_{H_3} = m_{H^\pm}$ as input parameters. We find a strong first order phase transition for a large part of the parameter space, but for large values of the phase α (e.g. $\alpha = 0.4$) the transition can change into a "two-stage" one if the heavy Higgs mass is sufficiently small. In that case the potential develops an extra minimum. Close to the critical temperature (which is no longer well defined) the system undergoes, in the first step, a second order transition from the symmetric phase to the extra minimum followed by a first order transition to the low temperature broken phase. All parameter values at which this two-stage transition occurs have been excluded from the parameter space. Hence, the strength ξ of the phase transition is defined only in case of a pure first order one.

[2]Note, that the factor $\sqrt{2}$ is due to the normalization of the Higgs fields we use.

We describe the wall profile of the expanding bubbles filled with the broken phase by the kink ansatz (2.43) as before. It is not obvious whether this is a good approximation also in the 2HDM. To determine the profile in principle one has to solve the field equations of the Higgs fields, which can only be done numerically. One possible algorithm to solve this problem is proposed in ref. [92]. In order to achieve a strong first order transition the condition $m_H^2 \gg m_h^2$ must hold. Accordingly, the shape of the effective potential exhibits a valley, corresponding to the light Higgs field. The strong curvature of the potential in the direction corresponding to the heavy Higgs masses forces the fields to follow the valley very closely during the phase transition. In this manner the transition can be approximated by single field dynamics as before. Numerically the valley can be determined by minimizing $V_{\text{eff}}(T_c)$ with respect to h_2 and θ at fixed values of h_1 between both phases. We estimate the wall thickness L_{w} with equation (2.42), where V_b is the height of the barrier along the valley that connects the two minima of the potential.
In figures 4.1 - 4.3 lines of constant ξ and L_{w} are shown in the dependence of the Higgs masses m_h and m_H for different values of μ_3^2 and α. In general, the phase transition becomes stronger and the bubble wall thinner if we increase m_H for fixed other parameters. This leads to an upper bound on the heavy Higgs mass for two reasons. First, we require $L_{\text{w}}T \gtrsim 2$. To compute the baryon asymmetry we use the WKB approximation which will be introduced in chapter 5. Since the gradient expansion is justified only for so-called thick walls, the value of m_H is restricted from above. Secondly, there is also a constraint from perturbativity arguments. From the equations (4.17) - (4.20) we know that in this model larger Higgs masses come from larger quartic couplings. Hence, the limit of large m_H does not give rise to the decoupling of the heavy states, and perturbation theory will break down at some point. In practice, both upper bounds on m_H are similar.
As we compare figures 4.1 and 4.2 it becomes apparent that the effect of the CP-violating phase α on ξ and L_{w} is rather small. Only for small m_H are the lines of constant ξ and L_{w} shifted marginally. In principle, this behavior continues even for larger values of α. But if we increase α further the phase transition can change into a two-stage one as described above. In case of $\alpha = 0.4$ the shift of the lines above $\xi \approx 1.5$ is still marginal, but below $\xi \approx 1.3$ a pure first order transition no longer occurs.
By comparing figures 4.2 and 4.3 one gets an idea how the value of the real parameter μ_3^2 influences the situation. If we double μ_3^2, the contemplable range of m_H is moved to somewhat higher values, while its extent shrinks. This means that in case of larger values of μ_3^2 the same quartic couplings cause larger Higgs masses. But the influence of the quartic couplings on ξ is much stronger than the one of the actual value of m_H.
In addition, in all three figures a line indicating a perturbativity constraint (labeled with $\Delta = 0.5$) is plotted. Here the one-loop corrections to the quartic couplings, or in other words the size of the counter terms compared to the corresponding tree-level ones, i.e. $\Delta = \max |\delta\lambda_i/\lambda_i|$, reach 50%. Above these lines sizable corrections to our

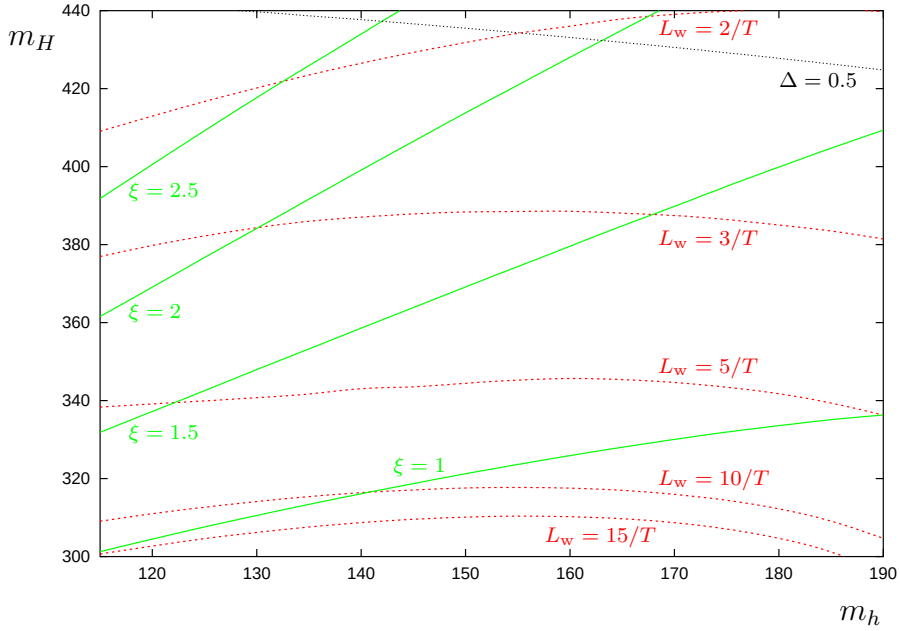

Figure 4.1: Lines of constant ξ and L_w in the m_h-m_H-plane for $\mu_3^2 = 10000$ GeV^2 and $\alpha = 0.0001$. The Higgs masses are given in units of GeV.

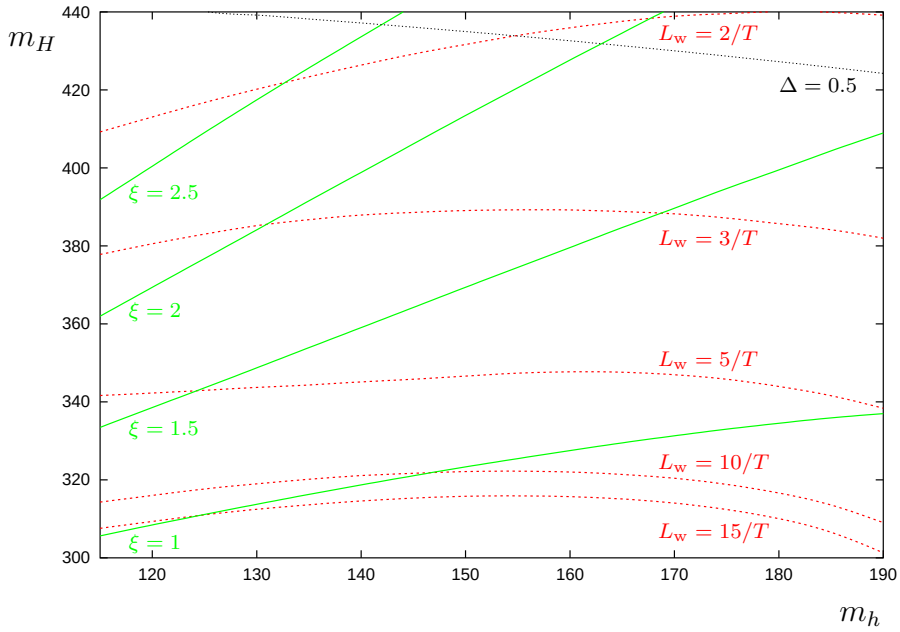

Figure 4.2: The same as in figure 4.1 for $\mu_3^2 = 10000$ GeV^2 and $\alpha = 0.2$.

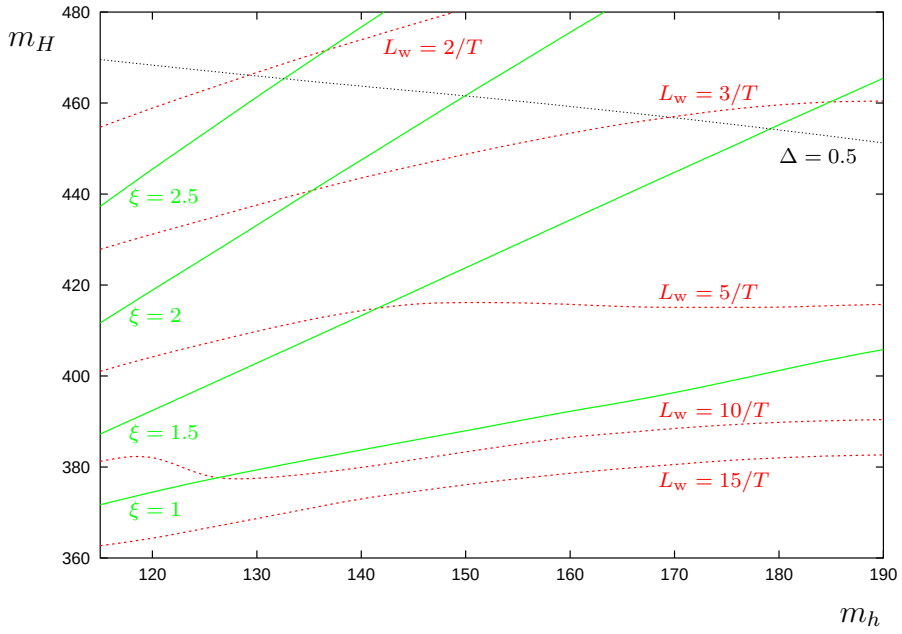

Figure 4.3: The same as in figure 4.1 for $\mu_3^2 = 20000$ GeV^2 and $\alpha = 0.2$.

results arise and perturbation theory starts to break down. But for a large region of the parameter space the higher order corrections are well under control and the requirements of electroweak baryogenesis are satisfied.

4.3 The Top Quark Mass in the 2HDM

Of course, also the CP-violating phase θ is essential for baryogenesis. During the phase transition θ changes from $\theta_{\rm sym}$ to $\theta_{\rm brk}$ and its profile is similar to a tanh-function. Therefore, it appears appropriate to approximate the θ-profile by the kink ansatz

$$\theta(z) = \theta_{\rm brk} - \frac{\Delta\theta}{2}\left(1 + \tanh\frac{z}{L_{\rm w}}\right), \tag{4.26}$$

where $\Delta\theta = \theta_{\rm brk} - \theta_{\rm sym}$. Obviously, the CP-violation in the Higgs sector entails complex fermion masses. In the following, we will consider only the top quark which couples to the Higgs doublet Φ_2 through Yukawa interactions. With our parameterization of the neutral Higgs components (4.12) the complex z-dependent top mass is given by

$$M_t(z) = y_t h_2(z)\, e^{i\theta(z)/2} = y_t \frac{h(z)}{\sqrt{2}} \sin\beta_T\, e^{i\theta(z)/2} \equiv m_t(z)\, e^{i\theta_t(z)}. \tag{4.27}$$

The angle β_T is defined via $\tan(\beta_T) = v_2/v_1$, which is less than, but rather close to one. The top Yukawa coupling y_t is chosen such that the top mass at zero temperature is 173 GeV. As we will see when we compute the baryon asymmetry, the change of M_t when the particles pass through the bubble wall is responsible for baryon number generation. In particular, the derivative of $\theta_t(z)$ enters the source terms, so that a large value of $\Delta\theta_t$ enhances the asymmetry. In case of large $\tan(\beta_T)$ the change in $\theta_2(=\theta_t)$ is suppressed such that $\Delta\theta_2 = \Delta\theta/(1+\tan^2(\beta_T))$ [93]. But for $\tan(\beta_T) \simeq 1$, as in our computation, this effect is small. We find that $\Delta\theta$ strongly depends on the Higgs masses. If one increases m_h and m_H also $\Delta\theta$ grows. Moreover, the change in θ grows almost linearly with the input phase α, whereas the influence of μ_3^2 is rather small.
Let us briefly comment on the EDMs. They are induced by scalar-pseudoscalar mixing in the neutral Higgs sector. The measure of CP-violation can be computed in terms of the imaginary parts of Higgs field renormalization constants [94]. For the electron EDM, the dominant contributions are two-loop amplitudes [95]. Using the results of ref. [96] the electron EDM is the sum of the following contributions

$$\begin{aligned} d_e/e &= (d_e/e)^{H\gamma\gamma}_{t-\text{loop}} + (d_e/e)^{HZ\gamma}_{t-\text{loop}} + (d_e/e)^{H\gamma\gamma}_{W-\text{loop}} \\ &\quad + (d_e/e)^{HZ\gamma}_{W-\text{loop}} + (d_e/e)^{H\gamma\gamma}_{G-\text{loop}} + (d_e/e)^{HZ\gamma}_{G-\text{loop}}. \end{aligned} \tag{4.28}$$

In the whole parameter space analyzed, d_e is about five to thirty times smaller than the experimental bound (2.52). Therefore, no constraint on the parameters arises due to the electron EDM.
Because of hadronic effects the computation of the neutron EDM is much more difficult. It is dominated basically by the contributions coming from the color EDMs of the constituent quarks, $\tilde{d}_u$, and $\tilde{d}_d$ [97]. Unfortunately, at present the most accurate result for this contribution has an error of about 50% [98]

$$(d_n/e)(\tilde{d}_u, \tilde{d}_d) = (1 \pm 0.5)(0.55\tilde{d}_u + 1.1\tilde{d}_d). \tag{4.29}$$

Similar to the electron EDM, there emerges no additional constraint due to the neutron EDM in the parameter regions considered. But to some extent, d_n reaches its upper bound (2.53) for small Higgs masses in case of $\alpha = 0.4$. Nevertheless, due to large uncertainties in the theoretical determination the neutron EDM does not definitely exceed the experimental limit.
In this chapter, we summarized the most important results concerning the discussion of the phase transition and the EDMs in the 2HDM. A detailed analysis of different parameter settings and single contributions to the EDMs can be found in [64, 83].

5 Baryon Asymmetry in the Semiclassical Approximation

5.1 General Idea

During a strong first order phase transition, expanding bubbles convert the symmetric phase into the broken phase. The masses and mixings of most particles of the hot plasma differ in the two phases. The phase boundary behaves like a potential on which the particles scatter. Because of the movement of the bubble wall, the plasma is driven out of equilibrium at the phase boundary. The particles then interact with the wall in a CP-violating fashion leading to different population densities for particles with different helicities in the vicinity of the wall. At this stage, the sphalerons cannot effectively generate a net baryon number, since the particle densities are thrown out of equilibrium only locally. Transport is needed to carry the particle densities into the symmetric phase, where the sphaleron processes convert the CP-asymmetry into a baryon asymmetry [99, 100]. Usually transport is described by classical Boltzmann or diffusion equations. In this classical treatment mixing between different species is neglected, and the equations describe only the dynamics of decoupled quasi-particle densities.
The general idea is to find a formalism which incorporates on one hand the microscopic quantum effects and on the other hand macroscopic physics of a classical system. CP-violation makes it unavoidable to leave classical physics and to allow for quantum effects, but it is also important to include statistical aspects for transport. The formalism we use works such that we first extract some CP-sensitive information in a quantum treatment and include this information in a classical transport equation.
More precisely, we use the WKB method to determine dispersion relations of fermions in a space-time dependent background, that is given by the Higgs expectation value. Due to the CP-violating interaction of the particles with the wall, this approach results in different dispersion relations for particles with different helicities, depending on their complex mass. These dispersion relations lead to CP-violating source terms which enter the classical Boltzmann equations. This method can be found for example in refs. [101–106]. With these equations we can compute the evolution of the particle distribution functions in the presence of the CP-violating

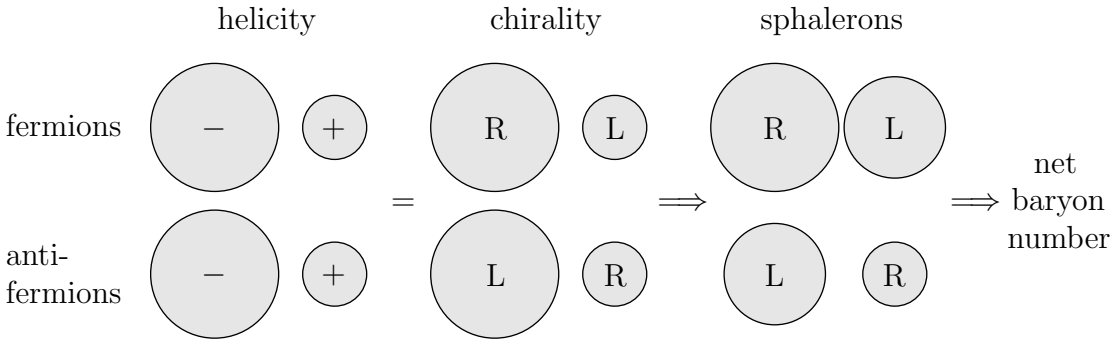

Figure 5.1: The particle-wall interactions create an excess of fermions and anti-fermions of one helicity over the other. Also the corresponding chirality population densities and the emerging net baryon number generation produced by the sphalerons in the symmetric phase are indicated.

sources and particle scattering. Hence, an excess of right-handed quarks over the corresponding anti-quarks and an equal and opposite left-handed asymmetry is created.[1] Note that in our convention handedness means chirality. The schematic figure 5.1 shows the influence of the different dispersion relations on the particle population densities in a descriptive way. The sphaleron transitions, where only left-chiral particles are involved, violate baryon number in the symmetric phase. The expanding bubble sweeps over this region, and in the broken phase these (B+L)-violating reactions are suppressed because of the high Higgs expectation value after the strong first order phase transition. As a result, a net baryon asymmetry is generated. The total amount of the produced baryon number depends strongly on the motion and shape of the phase boundary.

One can find many different approximations in the literature, which describe the CP-violating interactions between particles of the hot plasma and the moving wall, leading to CP-violating source terms in the transport equations. The main difference of the diverse methods depends on the thickness L_w of the bubble wall.

In the so-called "thin wall" limit one neglects the influence of the plasma during the scattering of the particles off the wall, since the mean free path l of the particle is much larger than L_w. In that case, the fermion or boson interacting with the wall is treated as a "free" particle. The CP-violating interaction with the bubble wall then entails different transmission and reflection coefficients for particles and their anti-particles, resulting in a charge flux into the symmetric phase (see e.g. [102, 107]). This current is inserted into classical Boltzmann equations to evaluate the evolution of the particle distributions.

In the case of a thicker wall, i.e. $L_w \sim l$, interactions with the plasma during the scattering process off the wall cannot be neglected any more. But most of the particles can be treated semiclassically since they have inverse momenta $1/p \ll L_w$ if

[1] Quarks will turn out to be more important than leptons because of the large top mass.

$L_{\mathrm{w}} \gg 1/T$ [103, 104]. In this case, one can use the WKB approximation to obtain the dispersion relations which subsequently enter the classical Boltzmann equations as described above. Altogether, this method combines particle scattering, CP-violation and transport.
In principle, whether one has to use the thick or thin wall regime depends on the particle species, because different species have different mean free paths due to their different interactions. In our models, we concentrate especially on the top quarks, which demand a thick wall treatment.
Carena *et. al.* [108–110] follow an approach which differs from ours. They intended to include also mixing effects into their analysis. This method is based on a non-equilibrium quantum field theory diagrammatic approach and is also applicable for thick walls. The CP-violating source terms entering the classical Boltzmann equations are computed using the closed time-path formalism instead of the WKB approximation. A qualitative comparison of the two different approaches can be found in ref. [111].

In the subsequent sections we follow basically the idea of Cline, Joyce and Kainulainen [104, 106]. We solve the one-particle Dirac equation to first order in gradients in the CP-violating bubble wall background, in order to derive the WKB dispersion relations. Here we use the notation of the works by Huber and Schmidt [112, 113]. But in contrast to former approaches we boost the result back to a general Lorentz frame [74]. Thus, we obtain in a much simpler way the same dispersion relations as were derived in the Schwinger-Keldysh formalism [35, 36, 114, 115]. In addition, we improve on the transport equations by keeping the scatterings with W bosons at a finite rate. Furthermore, we introduce additional source terms generated by CP-conserving perturbations in the plasma.

5.2 Dispersion Relations in the WKB Approximation

In this section we present the origin of the CP-violating source terms which enter the classical Boltzmann equations that describe particle transport during the phase transition. We use a semiclassical approximation to develop different dispersion relations for particles and anti-particles with different helicities, which later on lead to different population densities in the vicinity of the moving wall. We are only interested in the derivation of fermionic dispersion relations, because the most important particle species under consideration will be the top quark. Hence, we start with the Dirac equation.

5.2.1 The Dirac Equation

Let us neglect flavour mixing and consider a single Dirac fermion denoted by Ψ_D that couples to a Higgs doublet Φ. Since the expectation value of the Higgs changes during the phase transition, also the fermion mass becomes space-time dependent by passing through the phase boundary.
For simplicity we neglect the curvature of the wall. This is a good approximation when the bubble has grown to macroscopic size in the sense that the bubble radius is much larger than the wall width. In addition, we assume that the stationary situation is reached and the wall moves with its final constant velocity v_w. Then we can boost to the bubble wall rest frame, because the momentum components parallel to the wall are constants of motion for every particle. Denoting the coordinate perpendicular to the wall by z, the particle mass only depends on this position coordinate, i.e. $M(z) = m(z)e^{i\theta(z)}$. The varying space-dependent phase $\theta(z)$ incorporates CP-violation. Note that any constant phase θ could be absorbed by a redefinition of the field Ψ_D.
At this stage, no interactions between the particle and the plasma are taken into account. The scattering effects will be included in the following section in the collision term of the Boltzmann equation. The Dirac equation including the complex mass of the fermion reads

$$\left(i\gamma^\mu\partial_\mu - P_L M - P_R M^*\right)\Psi_D = \begin{pmatrix} -M & i\sigma^\mu\partial_\mu \\ i\bar{\sigma}^\mu\partial_\mu & -M^* \end{pmatrix}\Psi_D = 0. \tag{5.1}$$

We use the Weyl representation where the Dirac spinor consists of two Weyl spinors with opposite chirality, i.e. $\Psi_D^T = (\eta_\alpha, \bar{\chi}^{\dot{\alpha}})$ and accordingly $\bar{\Psi}_D = (\chi^\alpha, \bar{\eta}_{\dot{\alpha}})$, and the γ-matrices take the form

$$\gamma^\mu = \begin{pmatrix} 0 & \sigma^\mu \\ \bar{\sigma}^\mu & 0 \end{pmatrix}, \qquad \gamma^5 = i\gamma^0\gamma^1\gamma^2\gamma^3 = \begin{pmatrix} -1 & 0 \\ 0 & 1 \end{pmatrix}. \tag{5.2}$$

The two sets of σ-matrices σ^μ and $\bar{\sigma}^\mu$ are defined as

$$\sigma^\mu = (1, \sigma^1, \sigma^2, \sigma^3), \qquad \bar{\sigma}^\mu = (1, -\sigma^1, -\sigma^2, -\sigma^3), \tag{5.3}$$

where σ^i $(i = 1, 2, 3)$ are the Pauli matrices. The left- and right-handed projection operators are again given by equation (2.46).
We can simplify the problem by boosting to the Lorentz frame in which the momentum parallel to the wall is zero and take advantage of energy conservation. Taking the ansatz $\Psi_D = e^{-i\omega t}\xi(z)$ and multiplying equation (5.1) with γ^3 from the left,

$$\begin{pmatrix} 0 & \sigma^3 \\ \bar{\sigma}^3 & 0 \end{pmatrix}\begin{pmatrix} -M & i(\partial_0 + \sigma^3\partial_z) \\ i(\partial_0 + \bar{\sigma}^3\partial_z) & -M^* \end{pmatrix} e^{-i\omega t}\xi(z) = 0, \tag{5.4}$$

we end up with a one dimensional problem

$$i\partial_z \begin{pmatrix} \xi_1 \\ \xi_2 \\ \xi_3 \\ \xi_4 \end{pmatrix} = \begin{pmatrix} \omega & 0 & -M^* & 0 \\ 0 & -\omega & 0 & M^* \\ M & 0 & -\omega & 0 \\ 0 & -M & 0 & \omega \end{pmatrix} \begin{pmatrix} \xi_1 \\ \xi_2 \\ \xi_3 \\ \xi_4 \end{pmatrix}. \tag{5.5}$$

We can separate this into two equations [102]

$$i\partial_z \xi_\pm(z) = \pm Q(z)\xi_\pm(z), \tag{5.6}$$

because the interaction between the fermion and the wall conserves the z-component of the spin. Here $\xi_+ = (\xi_1, \xi_3)$ and $\xi_- = (\xi_2, \xi_4)$ are the $S_z = \pm\frac{1}{2}$ components of ξ, respectively. Since we consider only particles moving perpendicular to the wall, these vectors build a helicity basis. Note that ξ_+ and ξ_- both combine one component of η and one of $\bar{\chi}$ (accordingly one of χ and one of $\bar{\eta}$), i.e. states of opposite chirality. Q is the z-dependent matrix

$$Q(z) = \begin{pmatrix} \omega & -m(z)e^{-i\theta(z)} \\ m(z)e^{i\theta(z)} & -\omega \end{pmatrix}, \tag{5.7}$$

whose eigenvalues are given by $\pm\sqrt{\omega^2 - m^2}$. In principle, there is no difference between fermions and anti-fermions so far, but we have to distinguish between the two in the following.

5.2.2 Fermions

Fermions are described by the positive energy solutions, i.e. $\omega = +E$. In this case, equation (5.6) can be solved by diagonalizing the matrix via $Q = DQ_D D^{-1}$, where

$$Q_D(z) = \begin{pmatrix} \sqrt{E^2 - m^2(z)} & 0 \\ 0 & -\sqrt{E^2 - m^2(z)} \end{pmatrix}, \tag{5.8}$$

$$D(z) = \begin{pmatrix} \cosh X(z) & e^{-i\theta(z)} \sinh X(z) \\ e^{i\theta(z)} \sinh X(z) & \cosh X(z) \end{pmatrix}, \tag{5.9}$$

$$D^{-1}(z) = \begin{pmatrix} \cosh X(z) & -e^{-i\theta(z)} \sinh X(z) \\ -e^{i\theta(z)} \sinh X(z) & \cosh X(z) \end{pmatrix} \tag{5.10}$$

and switching to another local helicity basis $\tilde{\xi}_\pm = D^{-1}\xi_\pm$ [104]. Here X is defined by $\tanh X = (E - \sqrt{E^2 - m^2})/m$. This quantity arranges the mixing between the chirality and helicity states. Making use of the product rule, the Dirac equation (5.6) can be converted to

$$i\hbar\partial_z \tilde{\xi}_\pm(z) = \left(\pm Q_D(z) - D^{-1}(z) i\hbar\partial_z D(z)\right) \tilde{\xi}_\pm(z). \tag{5.11}$$

We have reintroduced $\hbar$ to be able to make an expansion in powers of this quantity. In contrast to the matrix Q_D, the correction term $D^{-1}i\hbar\partial_z D$ is not of diagonal form. Hence, the two components of $\tilde{\xi}_\pm$ are still coupled. We have

$$D^{-1}i\hbar\partial_z D = \begin{pmatrix} \hbar\theta' \sinh^2 X & \hbar e^{-i\theta}(iX' + \theta' \sinh X \cosh X) \\ \hbar e^{i\theta}(iX' - \theta' \sinh X \cosh X) & -\hbar\theta' \sinh^2 X \end{pmatrix}, \tag{5.12}$$

where $\theta' = \partial_z\theta$ and $X' = \partial_z X$. However, at this stage we can use the WKB approximation and expand equation (5.11) in powers of $\hbar$ due to the fact that $\partial_z D \sim D/L_{\rm w}$. The typical momenta of the particles are of order T and therefore $p \gg 1/L_{\rm w}$.

In the classical limit the correction term $D^{-1}i\hbar\partial_z D$ does not contribute, thus the two components of $\tilde{\xi}_\pm$ decouple. The WKB ansatz for the fermion field,

$$\begin{aligned} \tilde{\xi}_\pm^{(1)} &= \begin{pmatrix} 1 \\ 0 \end{pmatrix} \exp\left\{-\frac{i}{\hbar}\int^z p_{{\rm can},z}(z')dz'\right\}, \\ \tilde{\xi}_\pm^{(2)} &= \begin{pmatrix} 0 \\ 1 \end{pmatrix} \exp\left\{-\frac{i}{\hbar}\int^z p_{{\rm can},z}(z')dz'\right\}, \end{aligned} \tag{5.13}$$

then leads to the dispersions relations

$$\begin{aligned} p_{{\rm can},z}(E) &= +\sqrt{E^2 - m^2} \quad \text{for} \quad \tilde{\xi}_+^{(1)} \quad \text{and} \quad \tilde{\xi}_-^{(2)}, \\ p_{{\rm can},z}(E) &= -\sqrt{E^2 - m^2} \quad \text{for} \quad \tilde{\xi}_+^{(2)} \quad \text{and} \quad \tilde{\xi}_-^{(1)}. \end{aligned} \tag{5.14}$$

These are the canonical momenta of the particles as indicated by the subscript "can". Later on, we will define also the kinetic momenta so that we have to distinguish between them at this stage. Of course, the momenta $p_{{\rm can},z}$ are the eigenvalues of the matrix Q_D. Note that to order $\hbar^0$ there is no θ-dependence in the dispersion relations. This demonstrates that CP-violation is truly a quantum-mechanical phenomenon.

If we want to solve the Dirac equation (5.11) to order $\hbar$, the correction term $D^{-1}i\hbar\partial_z D$ cannot be neglected any more. Because of its non-zero off-diagonal elements the components of $\tilde{\xi}_\pm$ are now coupled. The dispersion relations $p_{{\rm can},z}(E)$ are the eigenvalues of the matrix $\pm Q_Q - D^{-1}i\hbar\partial_z D$ and can be associated with its eigenvectors in the following way:

$$\begin{aligned} p_{{\rm can},z}(E) &= +\sqrt{E^2 - m^2} - \hbar\theta' \sinh^2 X \quad \text{for} \quad \tilde{\xi}_+^{(1)}, \\ p_{{\rm can},z}(E) &= -\sqrt{E^2 - m^2} + \hbar\theta' \sinh^2 X \quad \text{for} \quad \tilde{\xi}_+^{(2)}, \\ p_{{\rm can},z}(E) &= -\sqrt{E^2 - m^2} - \hbar\theta' \sinh^2 X \quad \text{for} \quad \tilde{\xi}_-^{(1)}, \\ p_{{\rm can},z}(E) &= +\sqrt{E^2 - m^2} + \hbar\theta' \sinh^2 X \quad \text{for} \quad \tilde{\xi}_-^{(2)}. \end{aligned} \tag{5.15}$$

In this calculation, terms of order $\hbar^2$ are omitted. The corresponding eigenvectors or in other words the WKB wave functions, given by

$$\tilde{\xi}_\pm^{(1)} = \begin{pmatrix} 1 \\ \mp\frac{\hbar e^{i\theta}(iX' - \frac{1}{2}\theta' \sinh 2X)}{2\sqrt{E^2 - m^2}} \end{pmatrix} \exp\left\{-\frac{i}{\hbar}\int^z p_{{\rm can},z}(z')dz'\right\},$$

$$\tilde{\xi}^{(2)}_{\pm} = \begin{pmatrix} \pm\frac{\hbar e^{-i\theta}(iX'+\frac{1}{2}\theta'\sinh 2X)}{2\sqrt{E^2-m^2}} \\ 1 \end{pmatrix} \exp\left\{-\frac{i}{\hbar}\int^z p_{\mathrm{can},z}(z')dz'\right\}, \tag{5.16}$$

fulfill the Dirac equation (5.11) to order $\hbar$.
Take notice of the CP-violating part of the dispersion relations, $\Delta p_{\mathrm{can},z} = \hbar\theta' \sinh^2 X$. It is proportional to the derivative of the phase θ, and accordingly only a varying phase makes a contribution to CP-violation in the WKB approximation. Moreover, $\Delta p_{\mathrm{can},z}$ is proportional to $\sinh^2 X$, which makes sure that the effect of CP-violation is turned off in the limit $m \to 0$, where θ is no longer well defined.
The transformation matrix to the local helicity basis D is not unique. We used a special one in our computation. For more details see appendix B.

5.2.3 Anti-Fermions

The negative-energy solutions, i.e. $\omega = -E$, are associated with the anti-fermions. In this case, we again have to diagonalize the matrix Q from equation (5.6), but now via $Q = \bar{D}\bar{Q}_D\bar{D}^{-1}$, where $\bar{Q}_D = -Q_D$ and

$$\bar{D}(z) = \begin{pmatrix} \cosh Y(z) & e^{-i\theta(z)}\sinh Y(z) \\ e^{i\theta(z)}\sinh Y(z) & \cosh Y(z) \end{pmatrix} \tag{5.17}$$

and $\bar{D}^{-1}$ of the same form as before, but with another argument in the hyperbolic functions. The mixing between helicity and chirality is now given by Y which is defined as $\tanh Y = -m/(E+\sqrt{E^2-m^2})$. Similar to the previous section, the Dirac equation takes the form

$$i\hbar\partial_z\tilde{\bar{\xi}}_{\pm}(z) = \left(\pm\bar{Q}_D(z) - \bar{D}^{-1}(z)i\hbar\partial_z\bar{D}(z)\right)\tilde{\bar{\xi}}_{\pm}(z) \tag{5.18}$$

in the local helicity basis $\tilde{\bar{\xi}}_{\pm} = \bar{D}^{-1}\xi_{\pm}$, and we can expand equation (5.18) in powers of $\hbar$.
Using the same WKB ansatz (5.13) for the fermion field we obtain the dispersion relations

$$\begin{aligned} p_{\mathrm{can},z}(E) &= -\sqrt{E^2-m^2} \quad \text{for} \quad \tilde{\bar{\xi}}^{(1)}_{+} \quad \text{and} \quad \tilde{\bar{\xi}}^{(2)}_{-}, \\ p_{\mathrm{can},z}(E) &= +\sqrt{E^2-m^2} \quad \text{for} \quad \tilde{\bar{\xi}}^{(2)}_{+} \quad \text{and} \quad \tilde{\bar{\xi}}^{(1)}_{-} \end{aligned} \tag{5.19}$$

in the classical limit.
To order $\hbar$ we are left with the dispersion relations

$$\begin{aligned} p_{\mathrm{can},z}(E) &= -\sqrt{E^2-m^2} - \hbar\theta'\sinh^2 Y \quad \text{for} \quad \tilde{\bar{\xi}}^{(1)}_{+}, \\ p_{\mathrm{can},z}(E) &= +\sqrt{E^2-m^2} + \hbar\theta'\sinh^2 Y \quad \text{for} \quad \tilde{\bar{\xi}}^{(2)}_{+}, \\ p_{\mathrm{can},z}(E) &= +\sqrt{E^2-m^2} - \hbar\theta'\sinh^2 Y \quad \text{for} \quad \tilde{\bar{\xi}}^{(1)}_{-}, \\ p_{\mathrm{can},z}(E) &= -\sqrt{E^2-m^2} + \hbar\theta'\sinh^2 Y \quad \text{for} \quad \tilde{\bar{\xi}}^{(2)}_{-} \end{aligned} \tag{5.20}$$

as the eigenvalues to the matrix $\pm\bar{Q}_D - \bar{D}^{-1} i\hbar\partial_z \bar{D}$. Since $\sinh Y = -\sinh X$ the CP-violating part $\Delta p_{\mathrm{can},z}$ is identical to the one for fermions.
Let us make a short remark on the transformation matrices to the helicity basis D and $\bar{D}$ of the last two sections. The phase θ enters here, leading to different interactions of fermions and anti-fermions with the surrounding plasma, because the interaction eigenstates and the helicity states are not the same. This generates additional CP-violating source terms. But in the following we will not focus on this mechanism which is called "spontaneous" baryogenesis [100, 116, 117], since it is only a small effect [36].

5.3 The Semiclassical Force

Up to this point we have derived the dispersion relations for the different components of the local helicity basis vectors of fermions and their anti-particles. In the following, we are more interested in the dispersion relations written in terms of the asymptotic chirality states. Since the relevant particles under consideration are relativistic, we can approximate helicity by chirality. Using the identity

$$\sinh^2 X = \sinh^2 Y = \frac{E - \sqrt{E^2 - m^2}}{2\sqrt{E^2 - m^2}} \tag{5.21}$$

and the abbreviated form $p_0 = \mathrm{sign}(p_z)\sqrt{E^2 - m^2}$ we can summarize our results for fermions

$$\begin{aligned} p_{\mathrm{can},z}(E) &= p_0 - \theta' \frac{sE - p_0}{2p_0} \qquad \text{for} \quad L \quad (\eta), \\ p_{\mathrm{can},z}(E) &= p_0 - \theta' \frac{sE + p_0}{2p_0} \qquad \text{for} \quad R \quad (\bar{\chi}), \end{aligned} \tag{5.22}$$

and for anti-fermions

$$\begin{aligned} p_{\mathrm{can},z}(E) &= p_0 + \theta' \frac{sE + p_0}{2p_0} \qquad \text{for} \quad R \quad (\chi), \\ p_{\mathrm{can},z}(E) &= p_0 + \theta' \frac{sE - p_0}{2p_0} \qquad \text{for} \quad L \quad (\bar{\eta}). \end{aligned} \tag{5.23}$$

We have dropped the factor $\hbar$ and introduced a spin factor s which is related to the helicity λ by

$$s = \lambda\,\mathrm{sign}(p_z). \tag{5.24}$$

Table 5.1 is useful to convince oneself that the summary of the previous sections is correct. Up to now we have neglected the freedom to perform space-dependent vector-like phase redefinitions of the Dirac field, such that $\Psi_D \to e^{i\alpha(z)}\Psi_D$, which

particles				anti-particles			
spin s	sign(p_z)	helicity λ	chirality	spin s	sign(p_z)	helicity λ	chirality
$\Uparrow$	$+$	$+$	L	$\Uparrow$	$-$	$-$	L
$\Uparrow$	$-$	$-$	R	$\Uparrow$	$+$	$+$	R
$\Downarrow$	$-$	$+$	L	$\Downarrow$	$+$	$-$	L
$\Downarrow$	$+$	$-$	R	$\Downarrow$	$-$	$+$	R

Table 5.1: The relation between spin, helicity and chirality.

results in an additional gauge dependent term in the dispersion relations, $p_{\mathrm{can},z} \to p_{\mathrm{can},z} + \alpha'$. Introducing an additional sign factor c which is 1 for particles and -1 for anti-particles, we finally end up with the dispersion relations for the canonical momentum in terms of energy to first order in derivatives:

$$\begin{aligned} p_{\mathrm{can},z}(E) &= p_0 - c\theta' \frac{sE - p_0}{2p_0} + \alpha' \qquad \text{for} \quad L, \\ p_{\mathrm{can},z}(E) &= p_0 - c\theta' \frac{sE + p_0}{2p_0} + \alpha' \qquad \text{for} \quad R. \end{aligned} \tag{5.25}$$

This is in good agreement with the dispersion relations derived in ref. [106].[2] As the authors pointed out, the gauge dependence shows that $p_{\mathrm{can},z}$ is not the physical momentum of the WKB-state. All physical quantities should better be expressed in terms of the kinetic momentum rather than the canonical momentum. Then this ambiguity disappears. The velocity of the particle can be identified with the group velocity of the WKB wave-packet, $\mathbf{v}_g$, which is the derivative of the energy with respect to the canonical momentum. The physical kinetic momentum corresponds to the movement of a wave-packet along its world line and is defined as $\mathbf{p}_{\mathrm{kin}} = E\mathbf{v}_g$. To first order $p_{\mathrm{can},z}(E)$ can be inverted to

$$E(p_{\mathrm{can},z}) = \sqrt{m^2 + (p_{\mathrm{can},z} - \alpha_{CP})^2} + cs\frac{\theta'}{2}, \tag{5.26}$$

where $\alpha_{CP} = \alpha' \pm c\theta'/2$ in the left- and right-chiral sector. Remember, that we have boosted to the frame with zero momentum parallel to the wall, i.e. $p_x = p_y = 0$. In ref. [106] equation (5.26) was used to compute the semiclassical force which then was generalized to a Lorentz frame with finite $\mathbf{p}_\parallel$. But we have shown that first equation (5.26) should be boosted to the general frame and all further manipulations should be carried out later on [74]. This guarantees that the full Schwinger-Keldysh result [35, 36] is correctly reproduced.
For a generalization to non-zero $\mathbf{p}_\parallel$ we simply have to replace $E^2 \to E^2 + p_x^2 + p_y^2$. Parallel to the bubble wall we do not have to distinguish between canonical and

[2]Note that in our notation the role of L and R are exchanged because we have started with MP_L in the Dirac equation contrary to ref. [106].

kinetic momentum, i.e. $p_{\mathrm{can},x(y)} = p_{\mathrm{kin},x(y)} = p_{x(y)}$. The dispersion relation for energy (5.26) turns into

$$E(p_{\mathrm{can},z}) = \sqrt{m^2 + p_x^2 + p_y^2 + (p_{\mathrm{can},z} - \alpha_{CP})^2} + cs\frac{\theta' E_{0z}}{2E_0}, \tag{5.27}$$

where we introduced

$$E_{0z} = \sqrt{m^2 + p_z^2} \qquad \text{and} \qquad E_0 = \sqrt{m^2 + p_x^2 + p_y^2 + p_z^2} = \sqrt{m^2 + p^2}. \tag{5.28}$$

To leading order $p_{\mathrm{can},z}$ and $p_{\mathrm{kin},z}$ coincide, and consequently also E_{0z} and E_0 agree in terms of the canonical and the kinetic momentum to leading order. In the limit $E_{0z} = E_0$ we are back on the old result. For the group velocity of the WKB wave packet in z-direction we obtain

$$\begin{aligned} v_{g,z} = \left(\frac{\partial E}{\partial p_{\mathrm{can},z}}\right)_z &= \frac{p_{\mathrm{can},z} - \alpha_{CP}}{\sqrt{m^2 + p_x^2 + p_y^2 + (p_{\mathrm{can},z} - \alpha_{CP})^2}} \\ &\simeq \frac{p_{\mathrm{can},z} - \alpha_{CP}}{E} + cs\frac{\theta' p_{\mathrm{can},z}}{2E_{0z}E_0}, \end{aligned} \tag{5.29}$$

where we used equation (5.27) in the last step. Accordingly, the kinetic momentum is given by

$$p_{\mathrm{kin},z} = E v_{g,z} = (p_{\mathrm{can},z} - \alpha_{CP}) + cs\frac{\theta' p_{\mathrm{can},z}}{2E_{0z}}, \tag{5.30}$$

leading to the relation

$$(p_{\mathrm{can},z} - \alpha_{CP}) = p_{\mathrm{kin},z}\left(1 - cs\frac{\theta'}{2E_{0z}}\right) \tag{5.31}$$

between the canonic and the kinetic momentum. Inserting equation (5.31) into equations (5.27) and (5.29) yields

$$E(p_{\mathrm{kin},z}) = E_0 + cs\frac{\theta' m^2}{2E_{0z}E_0} \tag{5.32}$$

and

$$v_{g,z}(p_{\mathrm{kin},z}) = \frac{p_{\mathrm{kin},z}}{E_0} - cs\frac{\theta' m^2 p_{\mathrm{kin},z}}{2E_{0z}E_0^3}. \tag{5.33}$$

Note that the ambiguity related to α_{CP} has disappeared. To compute the force acting on the particles we follow the idea of Cline, Joyce and Kainulainen. The force is the time derivative of the kinetic momentum

$$F_z = \dot{p}_{\mathrm{kin},z} = E\dot{v}_{g,z}, \tag{5.34}$$

where we take advantage of the energy conservation along the trajectory in the wall frame. We have

$$\begin{aligned}\dot{v}_{g,z} &= \dot{z}(\partial_z v_{g,z})_{p_{\mathrm{can},z}} + \dot{p}_{\mathrm{can},z}(\partial_{p_{\mathrm{can},z}} v_{g,z})_z \\ &= v_{g,z}(\partial_z v_{g,z})_{p_{\mathrm{can},z}} - (\partial_z E)_{p_{\mathrm{can},z}}(\partial_{p_{\mathrm{can},z}} v_{g,z})_z \end{aligned} \tag{5.35}$$

with

$$\begin{aligned}(\partial_z v_{g,z})_{p_{\mathrm{can},z}} &= -\alpha'_{CP}\frac{m^2+p_x^2+p_y^2}{E_0^3} - \frac{v_{g,z}(m^2)'}{2E^2} + cs\frac{\theta''(p_x^2+p_y^2)p_{\mathrm{can},z}}{2E_{0z}E_0^3} \\ &\quad -cs\frac{\theta'(m^2)'p_{\mathrm{can},z}(E_0^2+E_{0z}^2)}{4E_{0z}^3E_0^3}, \end{aligned} \tag{5.36}$$

$$\dot{p}_{\mathrm{can},z} = \alpha'_{CP}v_{g,z} - \frac{(m^2)'}{2E} - cs\frac{\theta''E_{0z}}{2E_0} - cs\frac{\theta'(m^2)'}{4E_{0z}E_0}, \tag{5.37}$$

$$\begin{aligned}(\partial_{p_{\mathrm{can},z}} v_{g,z})_z &= \frac{1}{E} - \frac{(p_{\mathrm{can},z}-\alpha_{CP})v_{g,z}}{E^2} + cs\frac{\theta'}{2E_{0z}E_0} \\ &\quad -cs\frac{\theta'p_{\mathrm{can},z}^2(E_0^2+E_{0z}^2)}{2E_{0z}^3E_0^3}. \end{aligned} \tag{5.38}$$

Finally, the gauge-dependent terms cancel out exactly again. To linear order, the force in terms of the kinetic momentum is given by

$$F_z(p_{\mathrm{kin},z}) = -\frac{(m^2)'}{2E_0} - cs\frac{(\theta' m^2)'}{2E_{0z}E_0} + cs\frac{\theta'(m^2)'m^2}{4E_{0z}E_0^3}. \tag{5.39}$$

Thus, the resulting force contains two different parts. There is a CP-conserving part independent of c, yielding to the same deceleration of every particle. This part is of first order in derivatives. But there is also a CP-violating part opposite for particles and anti-particles, which is of second order in derivatives. Hence, particles and anti-particles experience a different force as they pass through the wall. The same is true for particles with opposite spins. As already mentioned, the relevant interactions in the theory are related to the chirality of a particle rather than its spin. Since helicity is close to chirality for relativistic particles, it is convenient to replace the spin by the helicity via equation (5.24) in the following.
The dispersion relation (5.32), the group velocity (5.33) and the semiclassical force (5.39) are in accordance with the results of ref. [35, 36]. This demonstrates that we can obtain the full Schwinger-Keldysh result for a single Dirac fermion in a much simpler way by means of the Dirac equation.
Note that the factor E_{0z} in equations (5.32), (5.33) and (5.39) emerges because we have boosted to a general frame before the relevant physical quantities were computed. In the special case when the particle momentum parallel to the wall is zero, we have $E_{0z} = E_0$, and our expressions agree with those of ref. [106]. But E_{0z} only contains roughly a third of the total energy in a relativistic scenario. Thus, the CP-violating part of the dispersion relation and the force term get enhanced by a

factor up to about three when keeping the correct factors E_{0z} in the corresponding expressions. In case of non-relativistic particles the effect is somewhat smaller. Since these factors are missing in former computations of the baryon asymmetry based on the WKB approximation, we will study the resulting enhancement of η_B by keeping the full E_{0z}-dependence.

5.4 Transport Equations

In this section we study particle interactions and transport during the phase transition. We describe particle distributions by the phase space densities $f_i(t, \mathbf{x}, \mathbf{p})$. Treating the plasma as consisting of quasiclassical particles, their time evolution is given by classical Boltzmann equations,

$$\left[\partial_t + \dot{\mathbf{x}}\partial_{\mathbf{x}} + \dot{\mathbf{p}}\partial_{\mathbf{p}}\right] f_i(t, \mathbf{x}, \mathbf{p}) = \mathcal{C}_i[f], \tag{5.40}$$

where the dot represents the time derivative. A crucial assumption made in ref. [106] is that it is the kinetic momentum that is conserved in scatterings of the WKB particles. Therefore, also the equilibrium phase space distributions should be written in terms of $\mathbf{p}_{\text{kin}}$. In the following we will drop the subscript "kin" to simplify the notation. In equation (5.40) $\dot{\mathbf{x}} = \mathbf{v}_g$ is the group velocity, and $\dot{\mathbf{p}} = \mathbf{F}$ is the semiclassical force derived in the previous section. The $\mathcal{C}_i$ are the collision terms describing the change of the phase space densities by particle interactions that drive the system back to equilibrium.
We assume a planar wall moving with constant velocity v_{w} as before. Hence, in the rest frame of the wall the distributions f_i only depend on z, $|\mathbf{p}| = p$ and p_z due to the translational invariance parallel to the wall. For each fluid of particle type i we have

$$\left[v_{g,z}\partial_z + F_z\partial_{p_z}\right] f_i(z, p, p_z) = \mathcal{C}_i[f], \tag{5.41}$$

without any explicit time dependence, as we are looking for a stationary solution. The equilibrium distribution is given by

$$f_i^{(\text{eq})}(z, p, p_z) = \frac{1}{e^{\beta\gamma_{\text{w}}(E_i + v_{\text{w}}p_z)} \pm 1}, \tag{5.42}$$

where $\beta = 1/T$ and $\gamma_{\text{w}} = 1/\sqrt{1 - v_{\text{w}}^2}$ and plus (minus) applies to fermions (bosons), respectively. We introduce perturbations around the chemical and kinetic equilibrium with the fluid-type truncation

$$f_i(z, p, p_z) = \frac{1}{e^{\beta[\gamma_{\text{w}}(E_i + v_{\text{w}}p_z) - \mu_i]} \pm 1} + \delta f_i(z, p, p_z). \tag{5.43}$$

Here the chemical potentials $\mu_i(z)$ model a local departure from the equilibrium particle density and the perturbations δf_i describe the movement of the particles in

response to the force caused by the different dispersions relations. The latter do not contribute to the particle density, i.e.

$$\int d^3p\ \delta f_i(z,p,p_z) = 0. \tag{5.44}$$

To first order in derivatives the perturbations are CP-even and equal for particles and antiparticles. But to second order they have CP-even and CP-odd parts, which we treat separately, i.e.

$$\mu_i = \mu_{i,1\mathrm{e}} + \mu_{i,2\mathrm{o}} + \mu_{i,2\mathrm{e}}, \tag{5.45}$$
$$\delta f_i = \delta f_{i,1\mathrm{e}} + \delta f_{i,2\mathrm{o}} + \delta f_{i,2\mathrm{e}}, \tag{5.46}$$

so that the perturbations to second order for particles differ from those of the anti-particles. The most important quantities are the CP-odd parts of the chemical potential perturbations, as will be discussed below. The correct combination of them yields the asymmetry in the left-handed quark density, which is one crucial ingredient to determine the baryon asymmetry.
In the end, we will get a coupled set of differential equations for all relevant particles in the system. But let us first concentrate on one particle. Hence, we can drop the index i to simplify the notation. Inserting the fluid-type ansatz (5.43) into the Boltzmann equation (5.41) leads to

$$v_{g,z}\left[\left((\partial_z E)_{p_z} - \mu'\right)\tilde{f} + \partial_z \delta f\right] + F_z\left[\left((\partial_{p_z} E)_z + v_\mathrm{w}\right)\tilde{f} + \partial_{p_z}\delta f\right] = \mathcal{C}[f], \tag{5.47}$$

where

$$\tilde{f} = -\frac{\beta e^{\beta[\gamma_\mathrm{w}(E+v_\mathrm{w}p_z)-\mu]}}{\left(e^{\beta[\gamma_\mathrm{w}(E+v_\mathrm{w}p_z)-\mu]} \pm 1\right)^2}, \tag{5.48}$$

and $E = E_0 + \Delta E$ denotes the full energy of the particle under consideration (cf. equation (5.32) of the previous section). Note that everything is formulated in terms of the kinetic momentum. Therefore, we cannot use the canonical equations of motion to reduce equation (5.47), i.e. $(\partial_{p_z} E)_z \neq v_{g,z}$ and $-(\partial_z E)_{p_z} \neq F_z$. Nevertheless, some terms cancel due to the conversation of energy in the wall frame

$$d_t E = \dot{z}(\partial_z E)_{p_z} + \dot{p}_z(\partial_{p_z} E)_z = v_{g,z}(\partial_z E)_{p_z} + F_z(\partial_{p_z} E)_z = 0, \tag{5.49}$$

where

$$(\partial_{p_z} E)_z = \frac{p_z}{E_0} - cs\frac{\theta' m^2 p_z (E_0^2 + E_{0z}^2)}{2E_{0z}^3 E_0^3}, \tag{5.50}$$
$$(\partial_z E)_{p_z} = \frac{(m^2)'}{2E_0} + cs\frac{(\theta' m^2)'}{2E_{0z}E_0} - cs\frac{\theta'(m^2)' m^2 (E_0^2 + E_{0z}^2)}{4E_{0z}^3 E_0^3}. \tag{5.51}$$

The group velocity $v_{g,z}$ and the semiclassical force F_z are given by equations (5.33) and (5.39). We finally end up with

$$v_{g,z}\left[-\mu'\tilde{f} + \partial_z \delta f\right] + F_z\left[v_\mathrm{w}\tilde{f} + \partial_{p_z}\delta f\right] = \mathcal{C}[f]. \tag{5.52}$$

We expand $\tilde{f}$ around E_0 to second order in derivatives and to first order in the wall velocity as

$$\tilde{f} = \tilde{f}^0 + \tilde{g}^0 \left(\Delta E - \mu + v_\mathrm{w} p_z\right) + \tilde{h}^0 \left(\Delta E - \mu + v_\mathrm{w} p_z\right)^2 , \tag{5.53}$$

where

$$\begin{aligned} \tilde{f}^0 &= -\frac{\beta e^{\beta E_0}}{\left(e^{\beta E_0} \pm 1\right)^2}, \\ \tilde{g}^0 &= \frac{d\tilde{f}^0}{dE_0} = -\frac{\beta^2 \left(-e^{2\beta E_0} \pm e^{\beta E_0}\right)}{\left(e^{\beta E_0} \pm 1\right)^3}, \\ \tilde{h}^0 &= \frac{d^2\tilde{f}^0}{d^2 E_0} = -\frac{\beta^3 \left(e^{3\beta E_0} \mp 4e^{2\beta E_0} \pm e^{\beta E_0}\right)}{\left(e^{\beta E_0} \pm 1\right)^4}. \end{aligned} \tag{5.54}$$

Now we have derived all necessary ingredients for the l.h.s. of the Boltzmann equation (5.52). We weight the terms in this equation with 1 and p_z/E_0, respectively, and subtract the results for particles and anti-particles. After momentum averaging we obtain the following two independent equations

$$\begin{aligned} &-v_\mathrm{w} \left\langle \frac{p_z^2}{E_0} \tilde{g}^0 \right\rangle \mu_2' + v_\mathrm{w} \left\langle \frac{1}{2E_0} \tilde{g}^0 \right\rangle (m^2)' \mu_2 + \left\langle \frac{p_z}{E_0} \partial_z \delta f_2 \right\rangle \\ &\quad - \left\langle \frac{(m^2)'}{2E_0} \partial_{p_z} \delta f_2 \right\rangle + \left\langle \frac{|p_z|}{2E_{0z} E_0^2} \left(\frac{\tilde{f}^0}{E_0} - \tilde{g}^0 \right) \right\rangle m^2 \theta' \mu_1' &= \langle \mathcal{C}[f] \rangle , \\ &\quad - \left\langle \frac{p_z^2}{E_0^2} \tilde{f}^0 \right\rangle \mu_2' + \left\langle \frac{p_z^2}{E_0^2} \partial_z \delta f_2 \right\rangle - \left\langle \frac{(m^2)' p_z}{2E_0^2} \partial_{p_z} \delta f_2 \right\rangle \\ &\qquad + v_\mathrm{w} \left\langle \frac{|p_z|}{4E_{0z} E_0^3} \left(\frac{\tilde{f}^0}{E_0} - \tilde{g}^0 \right) \right\rangle m^2 (m^2)' \theta' \\ &-v_\mathrm{w} \left\langle \frac{|p_z|}{2E_{0z} E_0^2} \tilde{f}^0 \right\rangle (m^2 \theta')' - \left\langle \frac{\mathrm{sign}(p_z) p_z^2 m^2 \theta'}{2E_{0z} E_0^4} \partial_z \delta f_1 \right\rangle \\ &\quad - \left\langle \frac{|p_z| (m^2\theta')'}{2E_{0z} E_0^2} \partial_{p_z} \delta f_1 \right\rangle + \left\langle \frac{|p_z| m^2 \theta' (m^2)'}{4E_{0z} E_0^4} \partial_{p_z} \delta f_1 \right\rangle &= \left\langle \frac{p_z}{E_0} \mathcal{C}[f] \right\rangle , \end{aligned} \tag{5.55, 5.56}$$

which are exact to third order in gradients. We do not take into account higher orders, so all terms proportional to $\tilde{h}^0$ no longer occur. Here the second order perturbations label the difference between particles and anti-particles, i.e. $\mu_2 = \mu_{2\mathrm{o}} - \bar{\mu}_{2\mathrm{o}}$ and $\delta f_2 = \delta f_{2\mathrm{o}} - \delta \bar{f}_{2\mathrm{o}}$. The CP-even parts drop out. For the first order perturbation we have $\mu_1 = \mu_{1\mathrm{e}} + \bar{\mu}_{1\mathrm{e}}$ and $\delta f_1 = \delta f_{1\mathrm{e}} + \delta \bar{f}_{1\mathrm{e}}$. In addition, we have utilized that some terms integrate to zero. As shortcut notation we have introduced

$$\langle X \rangle = \frac{\int d^3p \; X(p, p_z)}{\int d^3p \; \tilde{f}_+^0(m=0)} \tag{5.57}$$

as a momentum average of an operator, normalized relative to the massless Fermi-Dirac case. We use this normalization also for bosons to keep the interaction rates for fermions and bosons equal.
In order to obtain a closed system of equations we have to make assumptions on the moments of δf. We define the plasma velocity

$$u = \left\langle \frac{p_z}{E_0} \delta f \right\rangle . \tag{5.58}$$

Furthermore, we introdude some symbols K_i as a shorter notation for the momentum averages,

$$\begin{aligned}
K_1 &= -\left\langle \frac{p_z^2}{E_0} \tilde{g}^0 \right\rangle , & \tilde{K}_6 &= \left[\frac{E_0^2 - p_z^2}{2E_0^3} \tilde{f}^0 \right] , \\
K_2 &= \left\langle \frac{1}{2E_0} \tilde{g}^0 \right\rangle , & K_7 &= \left\langle \frac{|p_z|}{2E_0^2 E_{0z}} \left(\frac{\tilde{f}^0}{E_0} - \tilde{g}^0 \right) \right\rangle , \\
K_3 &= \left\langle \frac{1}{2E_0} \tilde{f}^0 \right\rangle , & K_8 &= \left\langle \frac{|p_z|}{2E_0^2 E_{0z}} \tilde{f}^0 \right\rangle , \\
K_4 &= \left\langle \frac{p_z^2}{E_0^2} \tilde{f}^0 \right\rangle , & K_9 &= \left\langle \frac{|p_z|}{4E_0^3 E_{0z}} \left(\frac{\tilde{f}^0}{E_0} - \tilde{g}^0 \right) \right\rangle , \\
\tilde{K}_5 &= \left[\frac{p_z^2}{E} \tilde{f}^0 \right] , & \tilde{K}_{10} &= \left[\frac{|p_z|}{2E_0^3 E_{0z}} f_0 \right] .
\end{aligned} \tag{5.59}$$

The averages $\tilde{K}_5$, $\tilde{K}_6$ and $\tilde{K}_{10}$ are related to averages involving the kinetic perturbations δf. Unfortunately, we do not know the momentum dependence of δf, so that we have to make further assumptions. Presuming that these averages factorize, we can use equation (5.58) such that for example $\langle p_z^3 \delta f \rangle \approx [p_z^2 E_0 f_\pm^{(\mathrm{eq})}] u$. Since it is not clear which distribution function should be used for the factorization, we decided to use the equilibrium distribution function in the rest frame of the wall $f_\pm^{(\mathrm{eq})}$ to put only a minimal amount of new information into the resulting averages. Thus we define

$$[X] = \frac{\int d^3p \; X}{\int d^3p \; f_\pm^{(\mathrm{eq})}}, \tag{5.60}$$

where we normalize these averages by the massive distribution of the boson or fermion under consideration, respectively. Obviously, the normalization of these averages differ from those defined by equation (5.57). Since there is some arbitrariness in this procedure, we will test the impact of these averages, which fortunately turns out to be small. All details about the precise definition of the thermal averages K_i and $\tilde{K}_j$ can be found in the appendix C.

Now the equations (5.55) and (5.56) can be written in a more managable form. After organizing some terms one obtains

$$v_{\rm w}K_1\mu_2' + v_{\rm w}K_2(m^2)'\mu_2 + u_2' - \langle\mathcal{C}[f]\rangle = S_{\mu'}, \tag{5.61}$$

$$-K_4\mu_2' + v_{\rm w}\tilde{K}_5 u_2' + v_{\rm w}\tilde{K}_6(m^2)'u_2 - \left\langle\frac{p_z}{E_0}\mathcal{C}[f]\right\rangle = S_{\theta'} + S_{u'}, \tag{5.62}$$

with the source terms on the r.h.s.

$$S_{\mu'} = -K_7 m^2\theta'\mu_1', \tag{5.63}$$
$$S_{\theta'} = v_{\rm w}K_8(m^2\theta')' - v_{\rm w}K_9 m^2(m^2)'\theta', \tag{5.64}$$
$$S_{u'} = \tilde{K}_{10}m^2\theta' u_1'. \tag{5.65}$$

All source terms are induced by the change in the particle mass along the wall. Bear in mind that in the limit of a wall at rest, meaning $v_{\rm w} = 0$, the trivial unperturbed Fermi-Dirac or Bose-Einstein distribution becomes a solution as it should. Only a moving wall distorts the plasma away from the equilibrium distributions. The sources $S_{\mu'}$ and $S_{u'}$ are related to the first order perturbations. For this reason also μ_1 and u_1 have to be determined by means of an extra set of equations which will be introduced below. The analysis of the relevance of $S_{\mu'}$ and $S_{u'}$ for the generation of the baryon asymmetry will be a main issue of this work. Formally, these sources are one order higher in gradients than $S_{\theta'}$, since the first order perturbations are first order in v_w. Indeed, it will turn out that they contribute only a small fraction to the total source term.
Of course, the transport equations of the first order perturbations μ_1 and u_1 resemble those of the second order perturbations. But at first order in derivatives there is no difference between particles and anti-particles. Unlike (5.61) and (5.62) the source term is now CP-even and only first order in derivatives, i.e.

$$v_{\rm w}K_1\mu_1' + v_{\rm w}K_2(m^2)'\mu_1 + u_1' - \langle\mathcal{C}[f]\rangle = v_{\rm w}K_3(m^2)', \tag{5.66}$$

$$-K_4\mu_1' + v_{\rm w}\tilde{K}_5 u_1' + v_{\rm w}\tilde{K}_6(m^2)'u_1 - \left\langle\frac{p_z}{E_0}\mathcal{C}[f]\right\rangle = 0. \tag{5.67}$$

A nice result is that our source terms (5.63) - (5.65) agree with those obtained from the Schwinger-Keldysh formalism. The authors of ref. [36] find an additional source term, which is related to the renormalization of the Wigner function. In the Dirac equation approach this extra term seems to be missing. However, it is of order m^4 like the second part of the source $S_{\theta'}$ (cf. the term proportional to K_9 in equation (5.64)). Terms of this form are subleading, as we will demonstrate in chapter 6.
Note that there can also arise source terms S_u of the form $m^2(m^2)'\theta' u_1$ and $(m^2\theta')'u_1$ depending on how we treat the averages involving δf. We do not discuss them here since the sources related to the first order perturbations are small anyway. But a detailed discussion can be found in appendix D.

5.4.1 The Collision Term

Let us now focus on the r.h.s. of the Boltzmann equation (5.41). The collision integral generates damping terms for the perturbations from equilibrium. In general, $\mathcal{C}_i$ takes the form

$$\mathcal{C}_i[f] = -\frac{1}{2E_i}\sum_P \int \prod_{j=2}^{n} \frac{d\mathbf{p}_j}{(2\pi)^3 2E_j} |\mathcal{M}_P|^2 (2\pi)^4 \delta^{(4)}\left(p_i^\mu + p_2^\mu \ldots - p_{n-1}^\mu - p_n^\mu\right) \mathcal{P}_i[f], \tag{5.68}$$

where we have to sum over each process P the particle of type i is involved in. $\mathcal{M}_P$ is the corresponding matrix element and the four-dimensional delta-function arranges the energy-momentum conservation in these interactions. The statistical factor $\mathcal{P}_i$ reads

$$\mathcal{P}_i[f] = f_i f_2 \ldots (1 \pm f_{n-1})(1 \pm f_n) - f_n f_{n-1} \ldots (1 \pm f_2)(1 \pm f_i), \tag{5.69}$$

where "+" applies to bosons while "−" applies to fermions. For equilibrium distributions the collision term vanishes by means of energy conservation. But taking the fluid ansatz (5.43) to linear order in perturbations we finally end up with [106]

$$\langle \mathcal{C}_i[f] \rangle = \sum_P \Gamma_P^{\text{inel}} \sum_k \mu_k, \tag{5.70}$$

$$\left\langle \frac{p_z}{E_0} \mathcal{C}_i[f] \right\rangle = -\Gamma_i^{\text{tot}} u_i. \tag{5.71}$$

Here Γ_P^{inel} denotes the rate of the inelastic interactions in a process P, and Γ^{tot} is the total interaction rate. In equation (5.70) the chemical potentials of the incoming particles enter the sum with a positive sign, while the ones of the out-going particles enter with a negative sign. Here we only have to take the inelastic interactions into account because the elastic interactions do not contribute to $\langle \mathcal{C}_i[f] \rangle$ since the elastic scatterings do not change the number of particles, i.e. $\langle \mathcal{C}_i^{\text{el}}[f] \rangle = 0$. The negative sign in front of Γ^{tot} in equation (5.71) is related to our sign convention for the plasma velocity (5.58).[3]

In previous works the transport equations were usually formulated in the plasma frame while the dispersion relations were derived in the wall frame. In that case one has to take into account that in equation (5.68) energy conservation is spoiled. The transition from the wall to the plasma frame yields $\theta(z) \to \theta(z - v_{\text{w}} t)$ which to leading order in derivatives can be written as $\theta(z) - v_{\text{w}}\theta'(z)$ leading to $\delta(E_i + E_2 \ldots - E_{n-1} - E_n) \to \delta(E_i - v_{\text{w}}\theta' + E_2 \ldots - E_{n-1} - E_n)$. Accordingly, an additional CP-violating contribution to the collision integral arises such that

$$\langle \mathcal{C}_i[f] \rangle = \sum_P \Gamma_P^{\text{inel}} \left(\sum_k \mu_k + \Delta E_{sp,P} \right). \tag{5.72}$$

[3]The authors of ref. [106] work in the plasma frame. We end up with the same result in the wall frame since Γ is invariant under Lorentz transformations.

Here $\Delta E_{sp,P} \sim v_{\rm w} m^2 \theta'$ denotes the deviation from energy conservation in the corresponding process [104]. This additional source term coming from the collision integral is associated to the so called "spontaneous" baryogenesis [100, 116, 117]. We do not have to take this effect into account since we have formulated the whole system in the rest frame of the bubble wall. However, compared to the direct CP-violation in interactions of the particles with the wall this effect should be small anyway [36].
Now all ingredients for the transport equations are complete. We have

$$v_{\rm w} K_{1,i} \mu'_{i,1} + v_{\rm w} K_{2,i} (m_i^2)' \mu_{i,1} + u'_{i,1} - \sum_P \Gamma_P^{\rm inel} \sum_k \mu_{k,1} = v_{\rm w} K_{3,i} (m_i^2)', \tag{5.73}$$

$$-K_{4,i} \mu'_{i,1} + v_{\rm w} \tilde{K}_{5,i} u'_{i,1} + v_{\rm w} \tilde{K}_{6,i} (m_i^2)' u_{i,1} + \Gamma_i^{\rm tot} u_{i,1} = 0, \tag{5.74}$$

to first order in derivatives and

$$v_{\rm w} K_{1,i} \mu'_{i,2} + v_{\rm w} K_{2,i} (m_i^2)' \mu_{i,2} + u'_{i,2} - \sum_P \Gamma_P^{\rm inel} \sum_k \mu_{k,2} = -K_{7,i} m_i^2 \theta'_i \mu'_{i,1}, \tag{5.75}$$

$$\begin{aligned} -K_{4,i} \mu'_{i,2} + v_{\rm w} \tilde{K}_{5,i} u'_{i,2} + v_{\rm w} \tilde{K}_{6,i} (m_i^2)' u_{i,2} + \Gamma_i^{\rm tot} u_{i,2} &= \\ v_{\rm w} K_{8,i} (m_i^2 \theta'_i)' - v_{\rm w} K_{9,i} m_i^2 (m_i^2)' \theta'_i + \tilde{K}_{10,i} m_i^2 \theta'_i u'_{i,1}, \end{aligned} \tag{5.76}$$

to second order in derivatives. Note that in equation (5.73) also the quite large annihilation rates enter in $\sum \Gamma_P^{\rm inel}$. In this whole set of equations we can approximately eliminate the plasma velocities to receive diffusion equations for the chemical potential perturbations. From the coefficient of the μ'' term we obtain the diffusion constants [106]

$$D_i = \frac{K_{4,i}}{K_{1,i} \Gamma_i^{\rm tot}}. \tag{5.77}$$

In our computation we will use this relation to express the total interaction rate in terms of the diffusion constant.
In order to compute the asymmetry in the left-handed quark density we have to solve the coupled set of differential equations (5.73) - (5.76) for every relevant particle of type i. Before we discuss these systems of equations for both models under consideration in detail, we will briefly comment on the validity of the ansatz which we use for f_i.

5.4.2 Validity of the Fluid Approximation

In principle, the Boltzmann equation (5.41) can be solved numerically. However, in order to have an analytically tractable expression we use the fluid-type approximation for the phase space densities (5.43). Let us now summarize the discussion in

ref. [101] concerning the conditions under which this truncation is valid.
We do not know whether the velocity perturbations we have introduced model the perturbations in the fluid properly. However, we simply use them to describe the particle movement in response to the semiclassical force. It is important that the velocity perturbations are anisotropic in momentum space. They cannot be ignored because otherwise the transport equations cannot be solved self-consistenly. Nevertheless, their precise form is not terribly important, and in the end we are mostly intersted in the chemical potential perturbations.
The chemical potential perturbations are only damped by inelastic reactions, as already mentioned. In our calculation we distinguish between particles and anti-particles in order to produce a difference in the perturbations of these. So we have to treat each species as a fluid, which makes the self-interaction collision terms vanish. On this system we superimpose the interaction of the different fluids leading to a damping of all perturbations to the local thermal equilibrium for the whole fluid. This is a good approximation if the interactions are fast enough, meaning the system keeps in the approximate form (5.43) although the bubble wall moves. Therefore, we require $L_\mathrm{w}/v_\mathrm{w} > \tau$, where τ is the time scale for the system to damp fluctuations away from this form. τ is proportional to the diffusion constant D. In addition, to be able to treat the particles as "free particles", the mean free time for interactions should be long compared to the particle energies. This condition is well satisfied, since the "width" of an eigenstate of the particles under consideration is much smaller than its energy.
The authors of ref. [101] kept temperature fluctuations δT to describe the perturbations beyond the ansatz (5.43). They found that the relaxation time for chemical potential perturbations is large compared to the one for δT provides that

$$\frac{L_\mathrm{w}}{3D} > v_\mathrm{w} \tag{5.78}$$

holds. Accordingly, thermalization is more efficient for small perturbations, i.e. a slow and thick wall, and frequently scattering particles, i.e. small D. Simultaneously, this condition is the same as that of the validity of our initial ansatz itself.
Moreover, we assume that the wall velocity is smaller than the speed of sound in the plasma ($v_s = 1/\sqrt{3}$), because there is no possibility for the perturbations to move into the region in front of the wall if the wall propagates faster than this.

5.5 Top Transport in Both Models

As already mentioned, we want to solve the coupled set of differential equations (5.73) - (5.76) for every relevant particle type i. This is possible numerically if we know the rates of the interactions between the different particle species in the

plasma. Furthermore, we can simplify the situation by using conservation laws and disregarding "slow" interactions. This means that an interaction rate Γ can be neglected if the typical interaction time $\tau_{int} \sim \Gamma^{-1}$ is much larger than the average time τ_d a particle spends diffusing in front of before being caught by the bubble wall. The time τ_d is approximately given by $v_w \tau_d = \sqrt{D\tau_d}$, where $v_w \tau_d$ is obviously the distance the wall moves, and $\sqrt{D\tau_d}$ represents the distance the diffusing particle moves. Accordingly, an interaction is irrelevant if the criterion

$$\Gamma \ll \frac{v_w^2}{D} \tag{5.79}$$

is satisfied [101]. The weak sphaleron rate Γ_{ws} fulfills this criterion as long as the wall does not move too slowly. Consequently, we can neglect the baryon and lepton number violating processes in the computation of the asymmetry in the left-handed quark density. We only have to include the weak sphalerons in a second step at the end, where they convert the left-handed quark number into a baryon asymmetry. But at this stage baryon and lepton number are conserved.
In addition, the leptons are only produced by small Yukawa couplings and therefore irrelevant in our transport equations. Hence, we only have to concentrate on quarks and Higgs densities. Of course, the most important quarks are the top quarks due to their huge Yukawa coupling compared to all other flavors. In the transport equations we include a finite rate for the inelastic processes $bW \leftrightarrow tX$ where X denotes a gauge boson. In the following, we denote the corresponding rate by the "W-scattering rate" Γ_W. In previous investigations scatterings with W bosons were set to equilibrium, i.e. $\Gamma_W \to \infty$. But with a finite rate we can study the perturbations of the bottom and top quarks seperately because the top quark source is no longer locked to the bottom degrees of freedom [74]. This improvement is another important issue of this work. So we will end up with the coupled set of transport equations for the chemical potentials of the left-handed $SU(2)$ doublet tops μ_t, the left-handed $SU(2)$ bottoms μ_b, the left-handed $SU(2)$ singlet tops μ_{t^c}, the Higgs bosons μ_h and the corresponding plasma velocities u_t, u_b, u_{t^c} and u_h. Besides the W scatterings we also take into account the top Yukawa interaction, the strong sphalerons, the top helicity flips and the Higgs number violating processes with the rates Γ_y, Γ_{ss}, Γ_m and Γ_h. The latter two are caused by the interactions with the bubble wall and only present in the broken phase.
We use baryon number conservation to express the strong sphaleron interactions in terms of μ_t, μ_b and μ_{t^c}. It is convenient to define the chemical potentials $\mu_{q_k} = (\mu(u_k) + \mu(d_k))/2$ for the three generations ($k = 1, 2, 3$). In general, the interaction term for the strong sphalerons takes the form

$$\Gamma_{ss}(2\mu_{q_3} + 2\mu_{q_2} + 2\mu_{q_1} + \mu_{t^c} + \mu_{b^c} + \mu_{c^c} + \mu_{s^c} + \mu_{u^c} + \mu_{d^c}). \tag{5.80}$$

The first and second family of quarks are only approximately produced by the strong sphalerons due to their small Yukawa couplings. Furthermore, all quarks have nearly

the same diffusion constant. Using the baryon number conservation

$$n_{q_3} + n_{q_2} + n_{q_1} - n_{t^c} - n_{b^c} - n_{c^c} - n_{s^c} - n_{u^c} - n_{d^c} = 0, \tag{5.81}$$

where $n_{q_k} = n_{u_k} + n_{d_k}$, we can specify the various number densities by [118]

$$n_{q_2} = n_{q_1} = 2n_{b^c} = 2n_{c^c} = 2n_{s^c} = 2n_{u^c} = 2n_{d^c} = 2(n_{q_3} - n_{t^c}). \tag{5.82}$$

Each number density is related to the chemical potentials by

$$n_i = \frac{1}{2}\kappa_i \mu_i T^2 \quad (i = t, ..., d, t^c, ..., d^c) \tag{5.83}$$

if the system is close to thermal equilibrium, as we assume. The statistical factors κ_i are defined as $\kappa_i = \langle 1 \rangle$ via equation (5.57).[4] With equations (5.82) and (5.83) the interaction term (5.80) becomes

$$\Gamma_{ss}\left[2\mu_{q_3} + \mu_{t^c} + 9\frac{2(n_{q_3} - n_{t^c})}{T^2}\right] = \Gamma_{ss}\left[(1+9\kappa_t)\mu_t + (1+9\kappa_b)\mu_b + (1-9\kappa_t)\mu_{t^c}\right], \tag{5.84}$$

where the quarks of the first and second family are taken to be massless ($\kappa_j = 1$ for $j = u, d, c, s, u^c, d^c, c^c, s^c$).
Altogether, the set of transport equations become

$$\begin{aligned} 3v_w K_{1,t}\mu'_{t,2} + 3v_w K_{2,t}(m_t^2)'\mu_{t,2} + 3u'_{t,2} & \\ -3\Gamma_y(\mu_{t,2} + \mu_{t^c,2} + \mu_{h,2}) - 6\Gamma_m(\mu_{t,2} + \mu_{t^c,2}) - 3\Gamma_W(\mu_{t,2} - \mu_{b,2}) & \\ -3\Gamma_{ss}[(1+9K_{1,t})\mu_{t,2} + (1+9K_{1,b})\mu_{b,2} + (1-9K_{1,t})\mu_{t^c,2}] &= 3S_{\mu'_t}, \end{aligned} \tag{5.85}$$

$$\begin{aligned} 3v_w K_{1,b}\mu'_{b,2} + 3u'_{b,2} & \\ -3\Gamma_y(\mu_{b,2} + \mu_{t^c,2} + \mu_{h,2}) - 3\Gamma_W(\mu_{b,2} - \mu_{t,2}) & \\ -3\Gamma_{ss}[(1+9K_{1,t})\mu_{t,2} + (1+9K_{1,b})\mu_{b,2} + (1-9K_{1,t})\mu_{t^c,2}] &= 0, \end{aligned} \tag{5.86}$$

$$\begin{aligned} 3v_w K_{1,t}\mu'_{t^c,2} + 3v_w K_{2,t}(m_t^2)'\mu_{t^c,2} + 3u'_{t^c,2} & \\ -3\Gamma_y(\mu_{t,2} + \mu_{b,2} + 2\mu_{t^c,2} + 2\mu_{h,2}) - 6\Gamma_m(\mu_{t,2} + \mu_{t^c,2}) & \\ -3\Gamma_{ss}[(1+9K_{1,t})\mu_{t,2} + (1+9K_{1,b})\mu_{b,2} + (1-9K_{1,t})\mu_{t^c,2}] &= 3S_{\mu'_t}, \end{aligned} \tag{5.87}$$

$$\begin{aligned} 2dv_w K_{1,h}\mu'_{h,2} + 2du'_{h,2} & \\ -3\Gamma_y(\mu_{t,2} + \mu_{b,2} + 2\mu_{t^c,2} + 2\mu_{h,2}) - 2d\Gamma_h\mu_{h,2} &= 0, \end{aligned} \tag{5.88}$$

[4] The averages κ_i and $K_{1,i}$ are identical.

$$\begin{aligned} -3K_{4,t}\mu'_{t,2} + 3v_w\tilde{K}_{5,t}u'_{t,2} + 3v_w\tilde{K}_{6,t}(m_t^2)'u_{t,2} & \\ +3\Gamma_W(u_{t,2}-u_{b,2}) + 3\Gamma_t^{\rm tot}u_{t,2} &= 3S_{\theta'_t} + 3S_{u'_t}, \quad (5.89) \end{aligned}$$

$$-3K_{4,b}\mu'_{b,2} + 3v_w\tilde{K}_{5,b}u'_{b,2} + 3\Gamma_W(u_{b,2}-u_{t,2}) + 3\Gamma_b^{\rm tot}u_{b,2} = 0, \quad (5.90)$$

$$-3K_{4,t}\mu'_{t^c,2} + 3v_w\tilde{K}_{5,t}u'_{t^c,2} + 3v_w\tilde{K}_{6,t}(m_t^2)'u_{t^c,2} + 3\Gamma_t^{\rm tot}u_{t^c,2} = 3S_{\theta'_t} + 3S_{u'_t}, \quad (5.91)$$

$$-2dK_{4,h}\mu'_{h,2} + 2dv_w\tilde{K}_{5,h}u'_{h,2} + 2d\Gamma_h^{\rm tot}u_{h,2} = 0. \quad (5.92)$$

Note that in principle Γ_W can be neglected in equations (5.89) and (5.90) since the plasma velocities of t and b are damped by the much faster gluon scatterings. However, in our numerical evaluation we have additionally included the finite rate Γ_W in these equations for the sake of completeness. This affects the final results only at the few percent level.
The terms on the r.h.s. denote the source terms of the top quark,

$$\begin{aligned} S_{\mu'_t} &= -K_{7,t}m_t^2\theta'_t\mu'_{t,1}, & (5.93)\\ S_{\theta'_t} &= v_{\rm w}K_{8,t}(m_t^2\theta'_t)' - v_{\rm w}K_{9,t}m_t^2(m_t^2)'\theta'_t, & (5.94)\\ S_{u'_t} &= \tilde{K}_{10,t}m_t^2\theta'_tu'_{t,1}. & (5.95) \end{aligned}$$

A possible source term for the bottom quark has been neglected because it is suppressed by the factor $m_b^2/m_t^2 \sim 10^{-3}$. The Higgs bosons do not have a source term to second order in gradients. For the quarks we have taken the sum over the three colors, and the Higgses we count as two complex degrees of freedom. The factor d in equations (5.88) and (5.92) counts the number of Higgs doublets which occur in each model. Remember, that the complex top mass is given by equation (3.13) in case of the ϕ^6 model and by equation (4.27) in the 2HDM.
We obtain the first order perturbations $\mu_{t,1}$ and $u_{t,1}$ from

$$3v_wK_{1,t}\mu'_{t,1} + 3v_wK_{2,t}(m_t^2)'\mu_{t,1} + 3u'_{t,1} - 3\Gamma_t^{\rm tot}\mu_{t,1} = 3v_wK_{3,t}(m_t^2)', \quad (5.96)$$

$$-3K_{4,t}\mu'_{t,1} + 3v_w\tilde{K}_{5,t}u'_{t,1} + 3v_w\tilde{K}_{6,t}(m_t^2)'u_{t,1} + 3\Gamma_t^{\rm tot}u_{t,1} = 0. \quad (5.97)$$

We assume that the damping of $\mu_{t,1}$ is dominated by gluon annihilation, the rate of which we have approximated by $\Gamma_t^{\rm tot}$. Therefore, we can neglect all other scatterings. To this approximation the first order chemical potential perturbations of t and t^c are identical. This avoids a direct source for baryon number which can be generated if $\mu_{t,1} \neq \mu_{t^c,1}$. This source would lead to spurious effects in the baryon asymmetry.

5.6 The Baryon Asymmetry

With the solution of the coupled set of transport equations we are able to compute the chemical potential of the left-handed quarks, μ_{B_L}, which plays the role as the source for baryon production. Using again the baryon number conservation (5.81) and the equations (5.82) and (5.83), μ_{B_L} is obtained as

$$\mu_{B_L} = \mu_{q_1,2} + \mu_{q_2,2} + \mu_{q_3,2} = \frac{1}{2}(1+4\kappa_t)\mu_{t,2} + \frac{1}{2}(1+4\kappa_b)\mu_{b,2} - 2\kappa_{t^c}\mu_{t^c,2}. \tag{5.98}$$

Up to this point we have neglected the weak sphaleron processes in our calculation. But now these processes generate a baryon number in front of the moving wall. In the symmetric phase the baryon violation rate reads [106]

$$\dot{n}_B = \frac{3}{2}\Gamma_{ws}\left(3\mu_{B_L}T^2 - An_B\right), \tag{5.99}$$

where $\Gamma_{ws} = \hat{\Gamma}_{ws}/T^3$ denotes the weak sphaleron rate. ($\hat{\Gamma}_{ws}$ is given by equation (2.11).) The first term in equation (5.99) simply acts as a source term. This source is approximately constant, since the interactions leading to the asymmetry in the left-handed quark density are fast compared to the sphaleron processes. The second term in equation (5.99) describes the relaxation of n_B if the sphaleron processes have time to equilibrate in the symmetric phase in the case of a slow moving wall. Here the flavour-changing interactions are faster than the sphaleron processes yielding left-handed quark and lepton asymmetries. Hence, n_B is related to these by

$$An_B = \mu_{CS}T^2 = 9\mu_{quark}T^2 + \sum_{lepton}\mu_{lepton}T^2, \tag{5.100}$$

because each weak sphaleron creates nine quarks and three leptons. μ_{CS} denotes the chemical potential for the Chern-Simons number. For the leptons we assume that each flavour asymmetry is separately conserved due to their weak mixing. But the quarks all have the same chemical potential μ_{quark} because of the strong mixing in the quark sector. Using the relation between the number densities and the chemical potentials (5.83) as well as the equality $\sum \mu_{lepton} = 3n_B/T^2$, we obtain $A = 9/2+3 = 15/2$.

Assuming again a stationary situation where the wall moves with constant velocity ($\partial_t \to -v_\mathrm{w}\partial_z$) the baryon violation rate (5.99) becomes

$$n_B' = -\frac{3\Gamma_{ws}}{2v_\mathrm{w}}\left(3\mu_{B_L}T^2 - \frac{15n_B}{2}\right), \tag{5.101}$$

which is easy to integrate analytically by variation of constants. We obtain the general result

$$n_B(z) = e^{\nu(z-z_0)}\left(n_B(z_0) - \frac{9\Gamma_{ws}T^2}{2v_\mathrm{w}}\int_{z_0}^{z} d\tilde{z}\ \mu_{B_L}(\tilde{z})e^{-\nu(\tilde{z}-z_0)}\right) \tag{5.102}$$

with $\nu = 45\Gamma_{ws}/(4v_{\mathrm{w}})$. We know that the baryon number density remains constant inside the bubble ($z < 0$) where the sphalerons are inactive and vanishes far in front of the wall ($z \to \infty$). Thus, we have to fix the boundary condition such that $n_B(z_0 \to \infty) = 0$, and the total baryon number after the phase transition is finally given by [105, 106]

$$n_B \equiv n_B(0) = \frac{9\Gamma_{ws}T^2}{2v_{\mathrm{w}}} \int_0^\infty d\tilde{z}\ \mu_{B_L}(\tilde{z}) e^{-\nu\tilde{z}}. \tag{5.103}$$

The factor ν in the exponent accounts for the aforementioned relaxation of the baryon number. In the following we will use the baryon to entropy ratio η_B. With the entropy density

$$s = \frac{2\pi^2}{45} g_* T^3, \tag{5.104}$$

where $g_* = 106.75$ is the effective number of degrees of freedom in the hot plasma, the baryon asymmetry reads

$$\eta_B = \frac{n_B}{s} = \frac{405\Gamma_{ws}}{4\pi^2 v_{\mathrm{w}} g_* T} \int_0^\infty d\tilde{z} \mu_{B_L}(\tilde{z}) e^{-\nu\tilde{z}}. \tag{5.105}$$

6 Numerical Evaluation and Discussion

In this chapter the results of our computation of the baryon asymmetry are presented. Let us first introduce the values for the relevant interaction rates appearing in the set of transport equations (5.85) - (5.92). We use the following values for the strong sphaleron rate [119], the top Yukawa rate, the top helicity flip rate and the Higgs number violating rate [118],

$$\begin{aligned} \Gamma_{ss} &= 4.9 \times 10^{-4} T, & \Gamma_y &= 4.2 \times 10^{-3} T, \\ \Gamma_m &= \frac{m_t^2(z,T)}{63T}, & \Gamma_h &= \frac{m_W^2(z,T)}{50T}. \end{aligned} \tag{6.1}$$

With equation (5.77), the total interaction rates can be inferred from the diffusion constants. The quark diffusion constant [102] and the Higgs diffusion constant [106] are given by

$$D_q = \frac{6}{T} \quad \text{and} \quad D_h = \frac{20}{T}. \tag{6.2}$$

We assume that the rates Γ_i^{tot} are position-independent. Therefore, we evaluate the thermal averages at $z = 0$ in this procedure, i.e. in the center of the bubble wall. The finite W-scattering rate we approximate as $\Gamma_W = \Gamma_h^{\text{tot}}$. For the weak sphaleron rate we use

$$\Gamma_{ws} = 1.0 \times 10^{-6} T. \tag{6.3}$$

Note that all rates have been computed in the plasma frame. We assume that, to leading order in v_w, they can also be used in the wall frame.
In our numerical evaluation only the top quarks are massive, the bottom quarks and the Higgs bosons are taken as massless. To solve the set of differential equations one has to fix boundary conditions. We have chosen the boundary conditions such that the chemical potential perturbations vanish at the endpoints of the space-interval in which the equations are solved numerically. In the majority of cases the interval runs from $z = -100/T$ to $z = 100/T$. The bubble wall is always located at $z = 0$.

6.1 Solutions of the Transport Equations

Before we discuss the baryon asymmetry generated in detail, let us illustrate the numerical solutions of the transport equations. In general, the shapes of the various solutions look similar for all relevant parameter combinations in both models under consideration. Only the absolute values differ for different parameter sets. For a qualitative discussion we choose one particular parameter set in the ϕ^6 model as a representative example.

In the ϕ^6 model the complex top quark mass is given by equation (3.13). We take maximal CP-violation, i.e. $\sin(\varphi_t) = 1$, and $|x_t| = 1$. At this stage we do not yet relate the bubble properties to the model introduced in chapter 3. We rather choose the parameters for the strength of the transition, the cut-off scale, the wall width and the wall velocity as $\xi = 1.5$, $\Lambda = 6T$, $L_\mathrm{w} = 8/T$ and $v_\mathrm{w} = 0.01$. These values correspond to a setting where we find a baryon asymmetry close to the observed one.

The distribution of the perturbations corresponding to the quarks should be smaller than the one of the Higgs due to the difference between the respective diffusion constants D_q and D_h [112]. Since there is no source term for the Higgs bosons, also the amplitude of $\mu_{h,2}$ should be small compared to the chemical potential perturbations corresponding to the top quarks. In figure 6.1 the resulting chemical potential perturbations $\mu_{t,2}$, $\mu_{b,2}$, $\mu_{t^c,2}$ and $\mu_{h,2}$ are shown as a function of the space coordinate z. The maximal change of the various perturbations is located in the center of the bubble wall ($z = 0$), as expected. In general, the shapes of the curves corresponding to the quarks are quite similar, i.e. $\mu_{t,2}$, $\mu_{b,2}$ and $\mu_{t^c,2}$ are peaked in the vicinity of the bubble wall, and they approach zero rather fast for distances $|z| \gtrsim 5L_\mathrm{w}$. However, the amplitudes of the perturbations corresponding to t and t^c are much larger than the one of b. In contrast, the shape of $\mu_{h,2}$ is flatter. So the influence of the Higgs bosons on the baryon asymmetry should be rather small.

The velocity perturbations show a similar behavior. In figure 6.2 we display the z-dependence of the solutions $u_{t,2}$, $u_{b,2}$, $u_{t^c,2}$ and $u_{h,2}$. The peaks are located around the bubble wall, and for the quarks an equilibrium situation is restored for distances larger than about $5L_\mathrm{w}$ away from it. The damping of the Higgs bosons is much weaker, and so $u_{h,2}$ does not vanish at the endpoints of the shown area. However, if we choose a larger integration interval, also the Higgs plasma velocity goes to zero for $z \to \infty$ as it should.

Since we are interested in the contributions of the source terms generated by the CP-conserving perturbations, we have to determine $\mu_{t,1}$ and $u_{t,1}$ via the equations (5.96) and (5.97). The solutions for the first order perturbations are presented in figure 6.3. Their amplitudes are approximately three orders of magnitude larger than the amplitudes of the second order perturbations.

Once we know the solutions of the coupled set of transport equations we can compute the chemical potential of the left-handed quarks with equation (5.98). The resulting

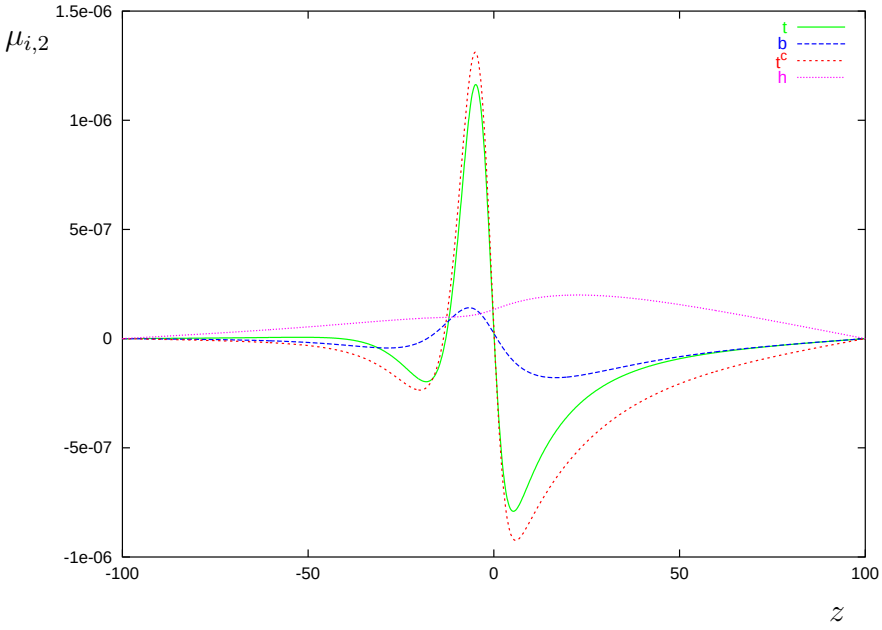

Figure 6.1: The chemical potential perturbations $\mu_{t,2}$, $\mu_{b,2}$, $\mu_{t^c,2}$ and $\mu_{h,2}$ as functions of z for one representative parameter combination. The space coordinate z is given in units of T^{-1}.

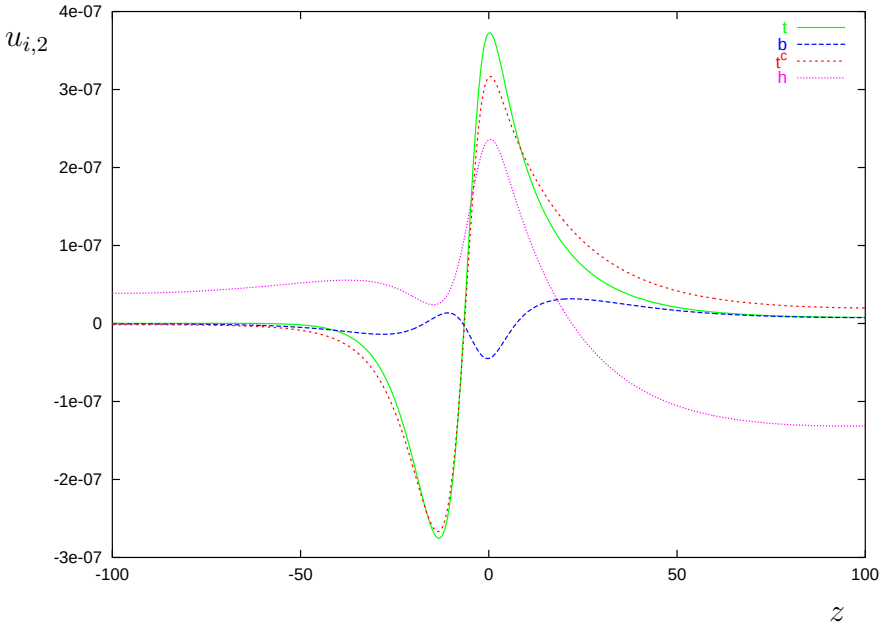

Figure 6.2: The plasma velocities $u_{t,2}$, $u_{b,2}$, $u_{t^c,2}$ and $u_{h,2}$ as functions of z.

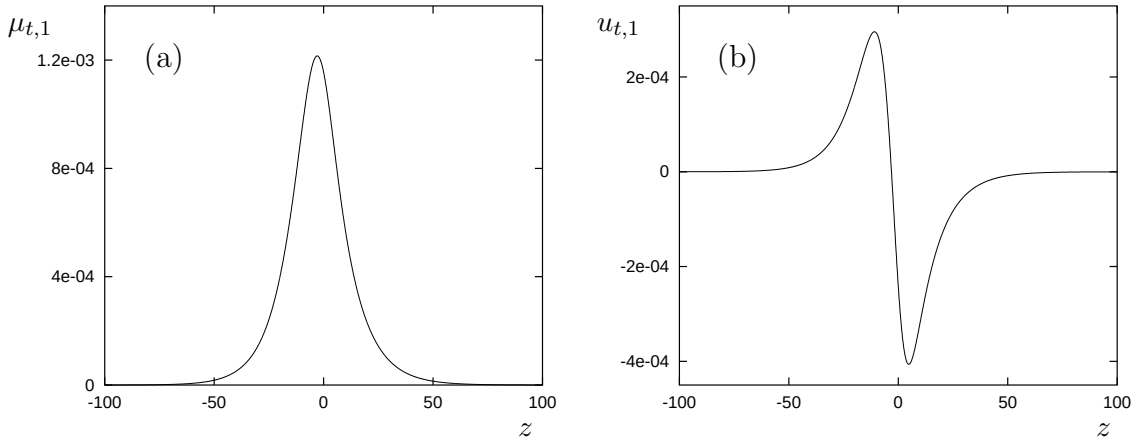

Figure 6.3: The z-dependence of the CP-even perturbations $\mu_{t,1}$ (a) and $u_{t,1}$ (b).

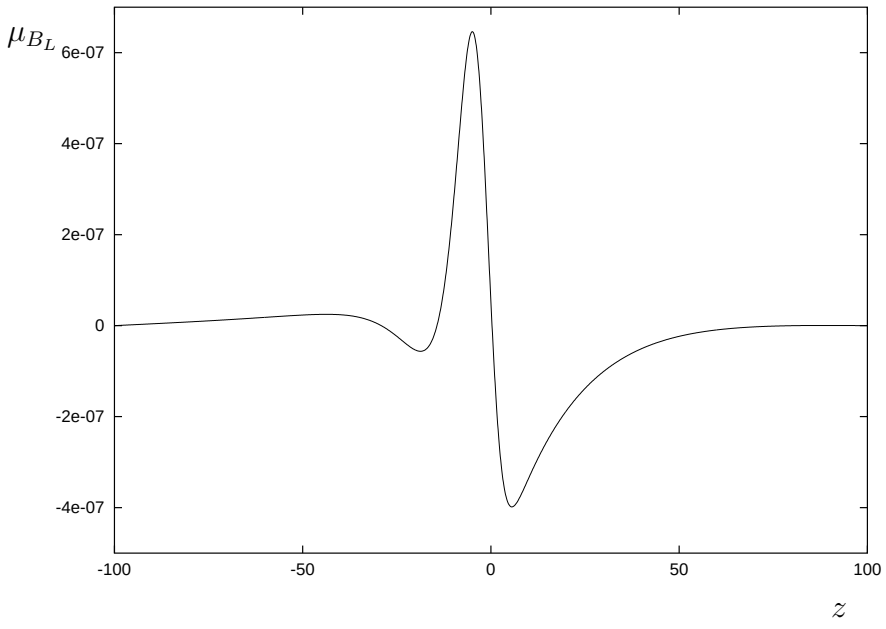

Figure 6.4: The chemical potential of the left-handed quark density μ_{B_L} as a function of z.

shape of μ_{B_L} in the vicinity of the bubble wall is shown in figure 6.4. For the generation of the baryon asymmetry the deviation of μ_{B_L} from zero in front of the wall ($z \geq 0$) is important. In the symmetric phase the weak sphalerons partly transform the asymmetry in the left-handed quark density into a baryon asymmetry, while in the broken phase the sphaleron processes are switched off.

6.2 The Baryon Asymmetry in the ϕ^6 Model

Because the ϕ^6 model is pretty simple, it is particular suitable to study the universal dependence of η_B on some of the parameters. Let us first discuss the influence of the wall width on the baryon asymmetry. For this analysis we neglect the sources $S_{\mu_t'}$ and $S_{u_t'}$ in the transport equations. From section 3.1 we know that $2 \lesssim L_{\rm w}T \lesssim 16$. We again take $\xi = 1.5$ and $\Lambda = 6T$ fixed, but now $v_{\rm w}$ varies between 0.001 and 0.4. Figure 6.5 indicates η_B as a function of the wall velocity for $L_{\rm w}T = 4$, 8, 12 and 16. We find that the baryon asymmetry increases for decreasing bubble wall widths as approximately $\eta_B \sim L_{\rm w}^{-1}$. This behavior is not surprising, since the source terms involve derivatives of the background Higgs field ϕ which are proportional to $L_{\rm w}^{-1}$. Another general result is that the total baryon asymmetry depends only slightly on

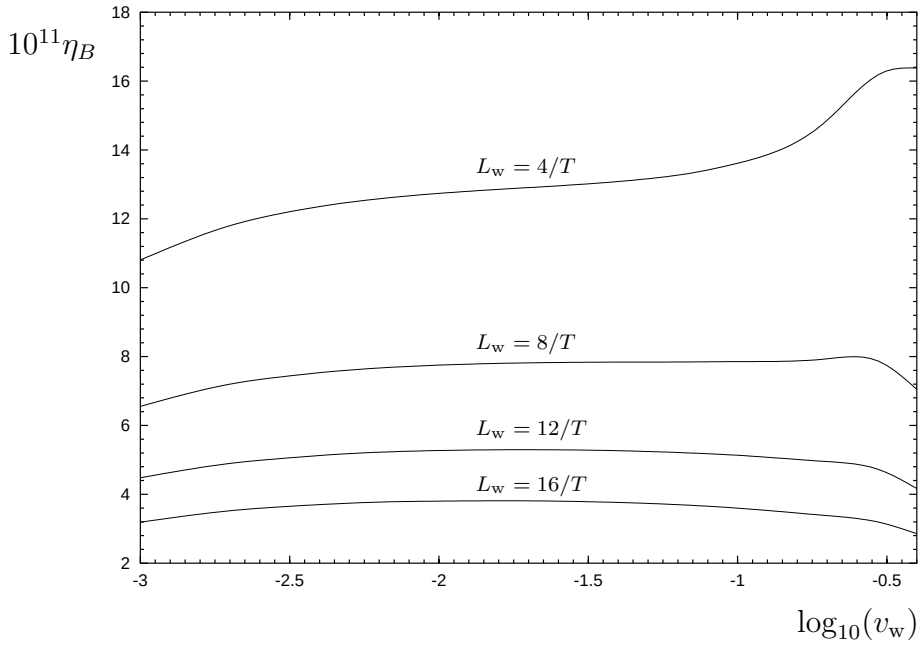

Figure 6.5: The baryon asymmetry as a function of the wall velocity for four different values of $L_{\rm w}$. The other parameters are taken as $\xi = 1.5$ and $\Lambda = 6T$.

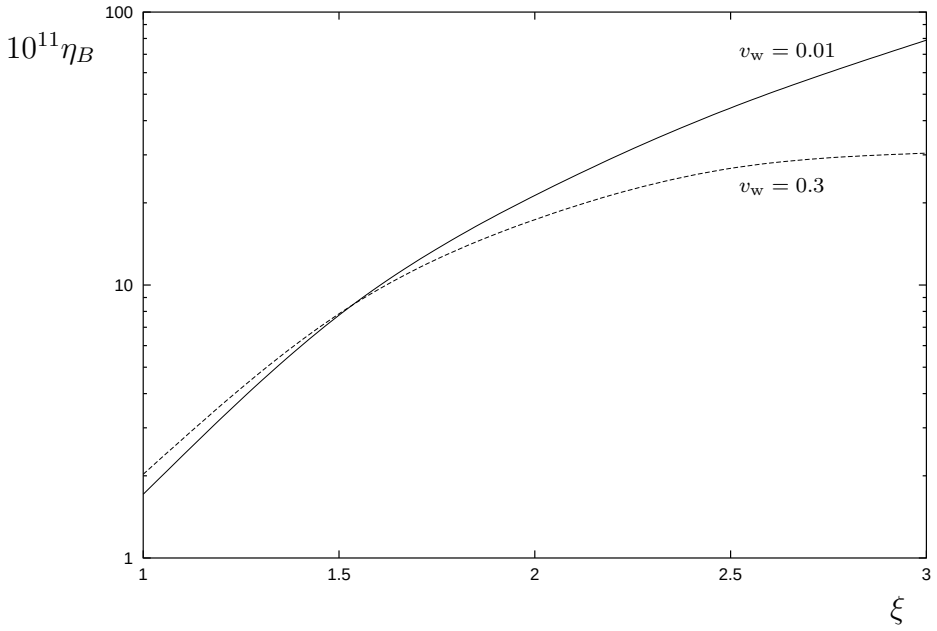

Figure 6.6: The baryon asymmetry as a function of the strength of the phase transition for two different values of v_w. The other parameters are taken as $L_w = 8/T$ and $\Lambda = 6T$.

v_w, especially for thicker walls. This is quite positive considering our poor understanding of this parameter.
Figure 6.6 demonstrates that the baryon asymmetry increases rapidly the stronger the phase transition becomes. We fixed again $L_w = 8/T$, $\Lambda = 6T$ and two different wall velocities, $v_w = 0.01$ and $v_w = 0.3$. The behavior shown is quite obvious. For increasing ξ the top quark mass raises in the broken phase. The source terms involve powers of m_t^2 and the derivative of the CP-violating phase θ_t from equation (3.14), which also becomes stronger. Clearly, an increasing source generates an increasing baryon asymmetry.
Next we analyze the influence of the various rates on the final result. Therefore, we compare η_B computed with our rates from equations (6.1) - (6.3) with the result when one of the rates is doubled or halved, respectively. In table 6.1 the arising values of η_B in each case are listed for three different wall velocities. The other parameters are chosen again as $\xi = 1.5$, $\Lambda = 6T$ and $L_w = 8/T$. η_B depends significantly on the value of Γ_{ss}. In the case of massless quarks, i.e. $\kappa_i = 1$, equation (5.84) is proportional to μ_{B_L} (cf. equation (5.98)). Therefore, doubling the value of Γ_{ss} reduces the baryon asymmetry because the strong sphalerons "wash out" the asymmetry in the left-handed quark density [120]. Of course, for Γ_{ss} reduced by a factor of two the baryon asymmetry changes the other way round. The dependence of η_B on Γ_y is quite similar. The Yukawa interactions change the chirality of the particles. Therefore, a larger value of Γ_y leads to a decrease of μ_{B_L} (and finally η_B).

$10^{11}\eta_B$	$v_w = 0.003$	$v_w = 0.03$	$v_w = 0.3$
our rates	7.416	7.834	7.846
$\Gamma_{ss} \cdot 2$	5.822	6.088	6.438
Γ_{ss} / 2	9.169	9.782	9.057
$\Gamma_y \cdot 2$	6.213	6.569	7.024
Γ_y / 2	8.697	9.201	8.620
$\Gamma_m \cdot 2$	7.821	8.181	7.489
Γ_m / 2	7.026	7.478	7.861
$\Gamma_h \cdot 2$	7.397	7.810	7.818
Γ_h / 2	7.428	7.847	7.864
$\Gamma_W \cdot 2$	7.818	8.199	7.290
Γ_W / 2	7.065	7.515	8.330
$\Gamma_i^{\text{tot}} \cdot 2$	5.075	5.242	5.023
Γ_i^{tot} / 2	10.281	11.270	11.615
$\Gamma_{ws} \cdot 2$	13.939	15.570	15.687
Γ_{ws} / 2	3.829	3.929	3.924

Table 6.1: The amount of the baryon asymmetry for various combinations of the rates. The first column indicates the change of a particular rate (doubled or halved) while the other rates keep unchanged.

The top helicity flip rate is non-zero only in the broken phase. Thus, its effect on the baryon asymmetry is rather small. Also the Higgs number violation rate has a minor impact on η_B. A variation of Γ_h basically affects the chemical potential perturbation of the Higgs bosons. However, $\mu_{h,2}$ only couples via the Yukawa interaction with $\mu_{t,2}$, $\mu_{b,2}$ and $\mu_{t^c,2}$, while the rest of the transport equations corresponding to the quarks remains unchanged. Accordingly, the asymmetry in the left-handed quark density is comparatively independent of Γ_h. Enhancing the W-scattering rate reduces the difference between the perturbations corresponding to t and b. Whether η_B increases or decreases for a larger (lower) value of finite rate Γ_W depends on the wall velocity. However, the baryon asymmetry changes only slightly when Γ_W is doubled or halved. Later on, we will demonstrate how the baryon asymmetry is affected if the W-scatterings were in equilibrium. This can have a much stronger effect. The variation of the total interaction rate is in fact a variation of the diffusion constants, more precisely $\Gamma_i^{\text{tot}} \sim D_i^{-1}$. η_B rises significantly with increasing diffusion constants because of more efficient diffusion, while it is lowered when the D_i are small. This behavior is expected, since the sources are proportional to the diffusion constants if one reduces two coupled transport equations to a single one by eliminating u_i in favor of μ_i [106, 112]. Finally, the baryon asymmetry depends strongest on the weak sphaleron rate. In the computation of the asymmetry in the left-handed

quark density the weak sphaleron transitions are neglected. Thus, in contrast to the other rates, Γ_{ws} does not affect the size of μ_{B_L}. However, if one neglects the relaxation of the baryon number, η_B is proportional to Γ_{ws} (cf. equation (5.105)). Hence, the baryon asymmetry is nearly doubled (halved) if the weak sphaleron rate is multiplied (divided) by two.
We now compare the baryon asymmetry computed in different approximations to demonstrate the relevance of various contributions to the full transport equations. Therefore, we choose two typical parameter settings. In figure 6.7 η_B is shown as function of v_w for the parameter combination $\xi = 1.5$, $\Lambda = 6T$ and $L_\mathrm{w} = 8/T$. Figure 6.8 indicates the same for a very strong phase transition with a small wall width, i.e. $\xi = 2.5$, $\Lambda = 6T$, $L_\mathrm{w} = 3/T$.
In both plots the bold solid line (a) displays the baryon asymmetry generated only by the source $S_{\theta_t'}$; the sources $S_{\mu_t'}$ and $S_{u_t'}$ are neglected. Furthermore, we kept the full space-dependence of the various thermal averages from equation (5.59).
This z-dependence of the averages is dropped in (b). Here they are fixed to their values at the center of the bubble wall, meaning $K_{i,t}(z) \to K_{i,t}(z=0)$. Generally, one would imagine that the space-dependence of the averages should be dispensable, since this is formally a higher order effect in gradients. However, taking the averages as constants considerably underestimates η_B, especially for thin walls and small wall velocities. The full space-dependence reduces the impact of v_w on the baryon asymmetry.
The line (c) shows the same as (a) but with the substitution $E_{0z} \to E_0$ in the dispersion relation (5.27), the group velocity (5.33) and the semiclassical force (5.39), meaning we go back to these quantities as determined in ref. [106]. The resulting baryon asymmetry is substantially reduced compared to η_B computed using the correct factors E_{0z} in the relevant quantities, in particular for weaker phase transitions. This confirms that performing the boost back to a general Lorentz frame has a sizeable effect and should not be neglected.
Neglecting the Higgs bosons in the transport equations (5.85) - (5.92) diminishes η_B by roughly 10% (d). This effect seems to be almost independent of the wall velocity and the strength of the transition.
Setting the W-scatterings to equilibrium (e) affects the resulting η_B considerably, especially for strong phase transitions. In figure 6.8 there is an overestimation of the baryon asymmetry by a factor of almost two for $v_\mathrm{w} \lesssim 0.1$, while for very large wall velocities ($v_\mathrm{w} \approx 0.4$) it underestimates η_B by a similar size. So keeping the W-scatterings at a finite rate leads to a much milder v_w-dependence of η_B.
Line (f) indicates the case when one adds the contributions of the source terms proportional to the first order perturbations to line (a). $S_{\mu_t'}$ and $S_{u_t'}$ enhance the baryon asymmetry only by a few percent in the whole v_w-range. Since these source terms are of higher order in gradients, this behavior is expected. For completeness, the effect of the source term S_{u_t} on η_B is discussed in appendix D.
Finally, (g) represents the result when switching off the terms proportional to $\tilde{K}_{5,i}$ and $\tilde{K}_{6,i}$. If these terms are neglected, the final result is reduced by a contribution

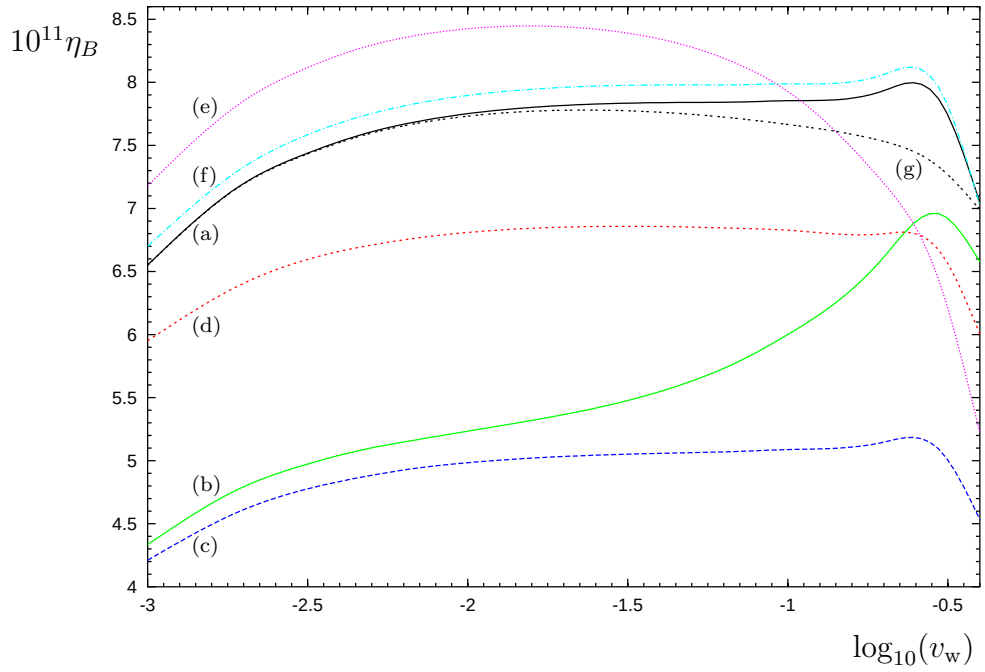

Figure 6.7: The baryon asymmetry as a function of v_w for $\xi = 1.5$, $\Lambda = 6T$ and $L_w = 8/T$. The labeling is explained in the text.

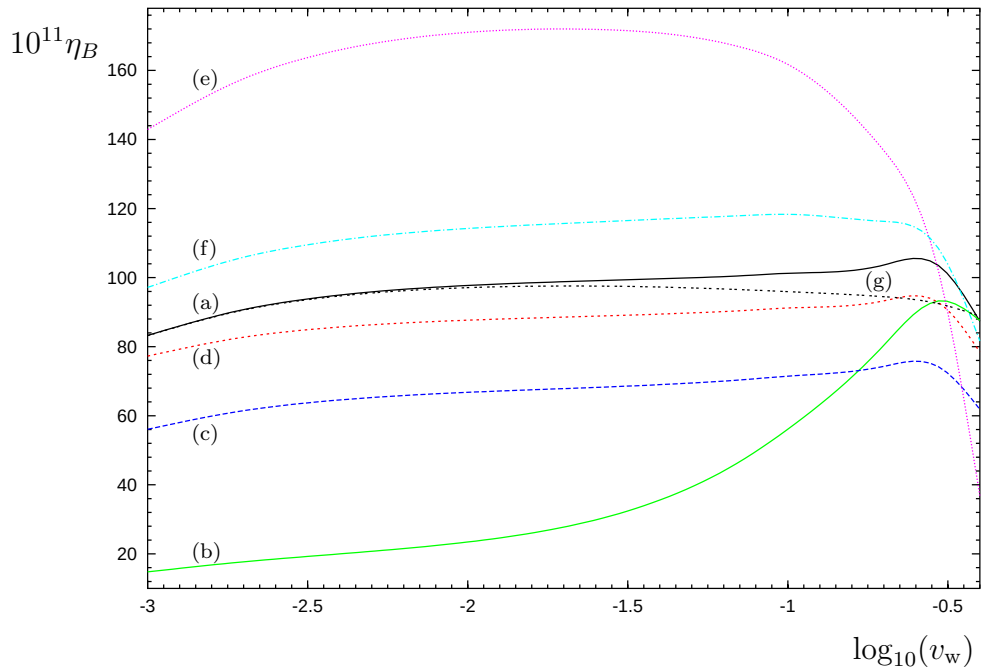

Figure 6.8: The baryon asymmetry as a function of v_w for $\xi = 2.5$, $\Lambda = 6T$ and $L_w = 3/T$.

proportional to the wall velocity. Thus, fortunately, the precise procedure how we factorize the thermal averages involving the perturbation δf (cf. equation (5.60)) has only a minor impact on η_B.
Note that in this thesis we use δf to allow for a particle movement in response to the force acting on it while it passes through the wall. It is also possible to include the plasma velocities directly in the fluid ansatz, as we did for instance in ref. [72]. Then, for example, the u_2' term in equation (5.61) obtains an additional coefficient ~ 1.1. Numerically there is not much difference between these two prescriptions.
Altogether, the examples demonstrate that the leading contribution to the baryon asymmetry comes from the source $S_{\theta_t'}$. Using the correct factors E_{0z} in the dispersion relation, group velocity and semiclassical force and keeping the full space-dependence of the thermal averages, enhances the baryon asymmetry significantly. Furthermore, keeping the W-scatterings at a finite rate has a sizeable effect, the direction of which is v_w-dependent. In general, for each approximation, η_B grows slowly with an increasing wall velocity and reaches a maximum at $v_\mathrm{w} \simeq 0.2 - 0.3$. However, the v_w-dependence of the baryon asymmetry is rather mild. Whether one takes the Higgs bosons and the sources $S_{\mu_t'}$ and $S_{u_t'}$ into account or not is less important. Their effect is of the same order of magnitude as typical uncertainties from higher order terms in the gradient expansion.
Next let us comment on the source $S_{\theta_t'}$. It consists of two parts, one proportional to $K_{8,t}$ and the other to $K_{9,t}$. Since the latter one has an additional factor of m_t^2, the $K_{9,t}$-part of the source is subleading. This extra factor of m_t^2 causes a suppression compared to the $K_{8,t}$-part, in particular for weak phase transitions. In fact, for the parameter setting $\xi = 1.5$, $\Lambda = 6T$, $L_\mathrm{w} = 8/T$ and $v_\mathrm{w} = 0.1$, the $K_{9,t}$-part contributes only about 15% to the total baryon asymmetry. As already mentioned in section 5.4, an additional source term arises in the Schwinger-Keldysh formalism due to the gradient renormalization of the Wigner function [36]. This extra term also has an extra factor of m_t^2 and should be subleading in our case too.
Let us finally relate the bubble wall parameters to the ϕ^6 model. Figure 6.9 displays the baryon asymmetry as a function of the cut-off scale Λ for two different Higgs masses $m_h = 115$ GeV and $m_h = 150$ GeV. We consider two wall velocities $v_\mathrm{w} = 0.01$ and $v_\mathrm{w} = 0.3$. For every value of Λ we compute the strength of the transition and the wall width as described in chapter 3. The baryon asymmetry grows rapidly as we lower Λ. Again the minor dependence of η_B on the wall velocity is apparent. At the very lowest values of Λ the WKB approach ceases to be reliable because L_w becomes of order $1/T$ (cf. figure 3.2). Furthermore, the bubble walls may become relativistic in this regime, and diffusion of charges into the symmetric phase may no longer be efficient.
Nevertheless, we can easily generate the observed baryon asymmetry for reasonably small values of the cut-off scale Λ, independent of the Higgs mass we have chosen.

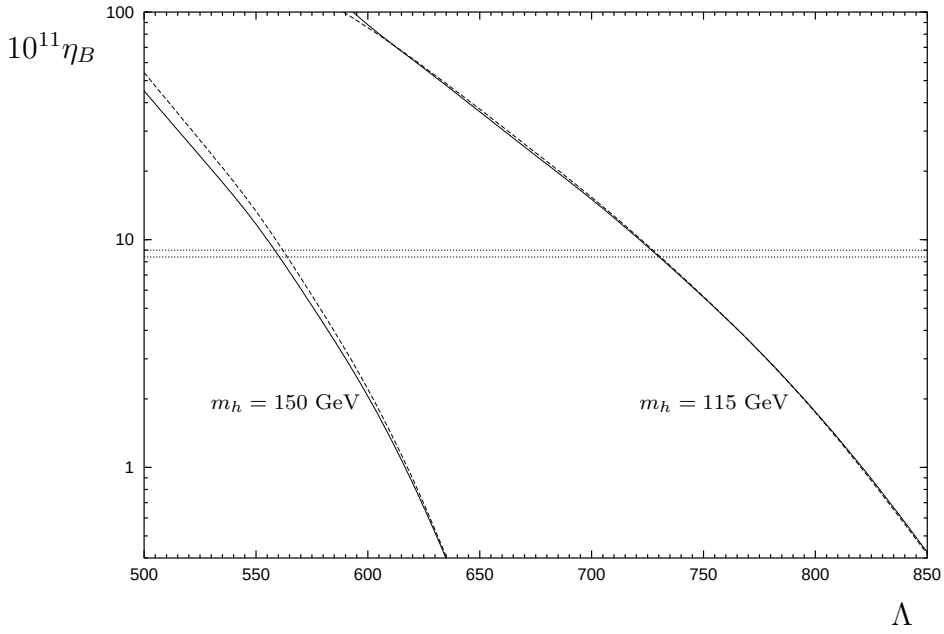

Figure 6.9: The baryon asymmetry in the ϕ^6 model for two different Higgs masses as a function of Λ (in units of GeV) for $v_{\rm w} = 0.01$ (solid) and $v_{\rm w} = 0.3$ (dashed). The horizontal lines indicate the error band of the observed value.

6.3 The Baryon Asymmetry in the 2HDM

In the 2HDM the complex top quark mass is given by equation (4.27), and the number of Higgs degrees of freedom is twice as large as in the ϕ^6 model discussed in the previous section. As already mentioned, in the 2HDM the distributions of the various solutions of the transport equations look similar to those described in section 6.1. Furthermore, the dependence of the baryon asymmetry on the wall width, the strength of the phase transition and the various interaction rates is analogous to the behavior of η_B in the model discussed above. To reduce repetition, we do not go into detail concerning this analysis. We rather resume briefly the main results.
Also in the 2HDM the baryon asymmetry is approximately proportional to $L_{\rm w}^{-1}$. Moreover, η_B increases rapidly with growing ξ for the reasons discussed above. A variation of the rates Γ_m, Γ_h and Γ_W has only a minor impact on the resulting asymmetry. But reducing the strong sphaleron rate, or the Yukawa interaction rate or making the diffusion more efficient leads to an increase of μ_{B_L} and therefore of η_B. Of course, the baryon asymmetry is again nearly proportional to the weak sphaleron rate.
Next we demonstrate that the relevance of the different contributions to the transport equations is similar as well. Figure 6.10 indicates the behavior of the baryon asymmetry in the approximations (a) - (g) for one typical parameter set. We

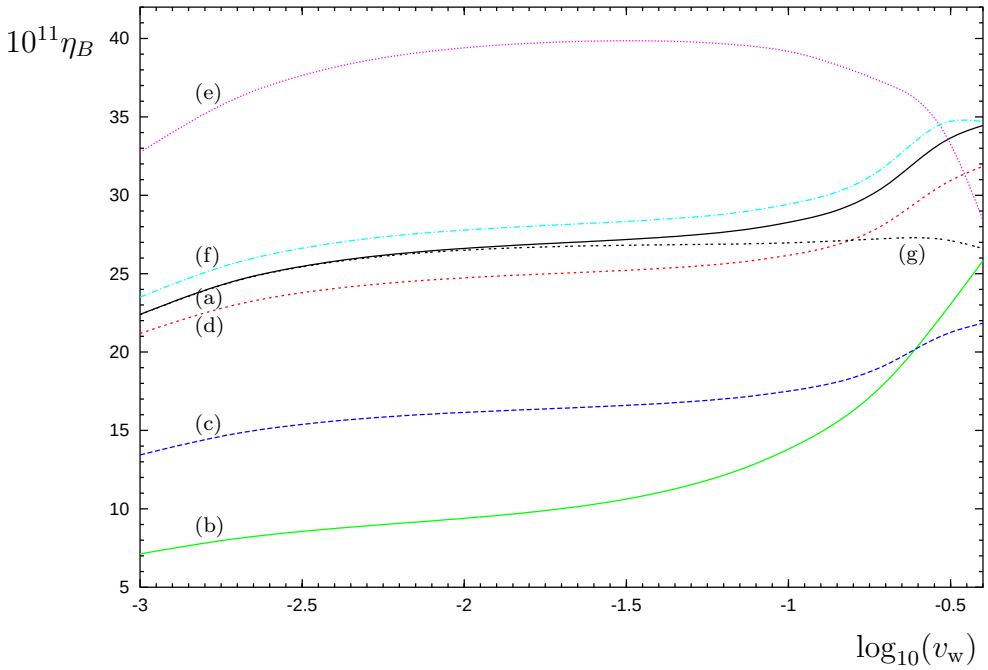

Figure 6.10: The baryon asymmetry as a function of v_w for $m_h = 125$ GeV, $m_H = 350$ GeV, $\mu_3^2 = 10000$ GeV^2 and $\alpha = 0.2$. The labeling is as in figures 6.7 and 6.8.

have chosen the Higgs masses $m_h = 125$ GeV and $m_H = 350$ GeV and fixed $\mu_3^2 = 10000$ GeV^2 and $\alpha = 0.2$. This parameter setting determines $\xi = 1.6$, $L_w = 4.5/T$ (cf. figure 4.2) and $\Delta\theta = 0.19$.
Line (a) represents η_B generated by the source $S_{\theta_t'}$ and keeping the full z-dependence of the thermal averages. Taking constant averages, i.e. $K_{i,t}(z) \to K_{i,t}(z=0)$, underestimates the resulting baryon asymmetry, in particular for small wall velocities (b). If we substitude $E_{0z} \to E_0$ in the dispersion relation, the group velocity and the semiclassical force, η_B is considerably reduced in the whole v_w-range (c). The Higgs bosons and the source terms proportional to the first order perturbations $\mu_{t,1}$ and $u_{t,1}$ play no significant role. Taking them into account affects the final result by an amount less than 10%. Neglecting the Higgs bosons reduces η_B slightly (d) and the contributions of $S_{\mu_t'}$ and $S_{u_t'}$ enhance η_B with the same order of magnitude (f). Additionally, this example demonstrates that the improvement of the transport equations by keeping scatterings with W bosons at a finite rate affects the resulting baryon asymmetry significantly. Putting the W-scatterings to equilibrium, as was done in the literature so far, causes a much stronger v_w-dependence of η_B (e). The result is then considerably overestimated for small wall velocities, i.e. $v_w \lesssim 0.1$, and underestimated for larger wall velocities. The precise treatment of the velocity perturbations is less important. As line (g) demonstrates, η_B is reduced by a contribution approximately proportional to v_w if the $\tilde{K}_{5,i}$- and $\tilde{K}_{6,i}$-terms are neglected

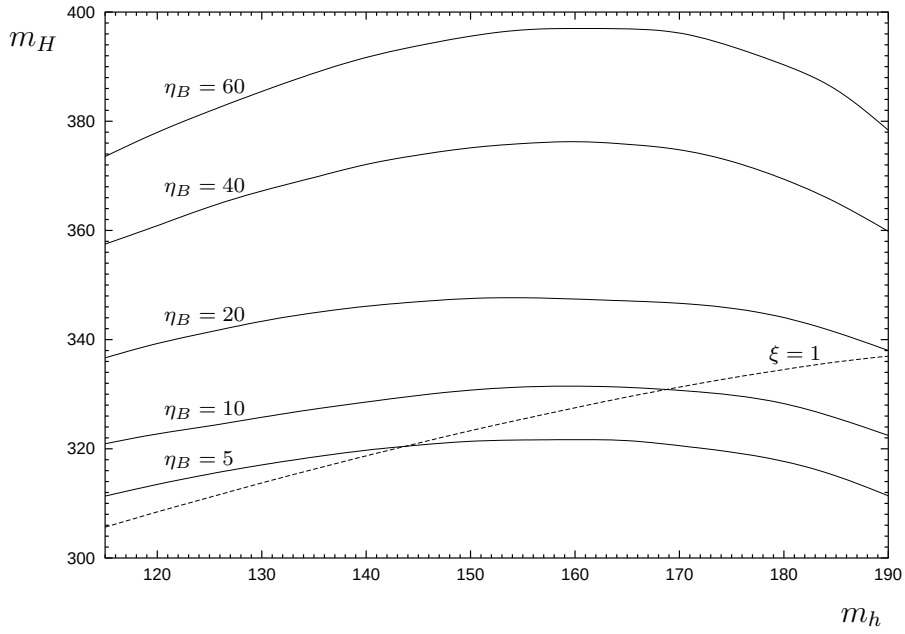

Figure 6.11: Contours of constant η_B in the m_h-m_H-plane for $\mu_3^2 = 10000$ GeV^2, $\alpha = 0.2$ and $v_\mathrm{w} = 0.1$. The Higgs masses are given in units of GeV and η_B in units of 10^{-11}.

in the full set of transport equations.
Figure 6.10 looks similar for other parameter combinations in the model under consideration. Altogether, the behavior of the baryon asymmetry in the 2HDM is in good agreement with the one discussed in the ϕ^6 model.
Next we discuss the dependence of η_B on the Higgs masses. We again fix $\mu_3^2 = 10000$ GeV^2 and $\alpha = 0.2$. We determine for each mass combination all relevant quantities for the transport equations, i.e. ξ, L_w, θ_brk, θ_sym and $\tan(\beta_T)$. Since there is only a mild v_w-dependence of the result as shown in figure 6.10, we can restrict ourselves to considering only one wall velocity, which we have chosen as $v_\mathrm{w} = 0.1$. Figure 6.11 displays contours of constant η_B in the m_h-m_H-plane. Additionally, the (ξ=1)-contour of figure 4.2 is plotted for orientation. Leaving the light Higgs mass fixed, the baryon asymmetry becomes larger with a growing heavy Higgs mass. This behavior is expected since the top source term is proportional to ξ^2. Hence, η_B increases the stronger the phase transition becomes. For fixed m_H and increasing m_h the asymmetry decreases slightly and reaches a minimum at a light Higgs mass between 150 and 160 GeV, similar to the behavior of L_w (cf. figure 4.2). However, in general there is only a minor dependence on m_h. In this particular example the observed baryon asymmetry can be generated for heavy Higgs masses between 320 and 330 GeV and a light Higgs mass up to 160 GeV.
However, it is also possible to generate the measured value for many other parameter settings. Since the baryon asymmetry is more or less proportional to the

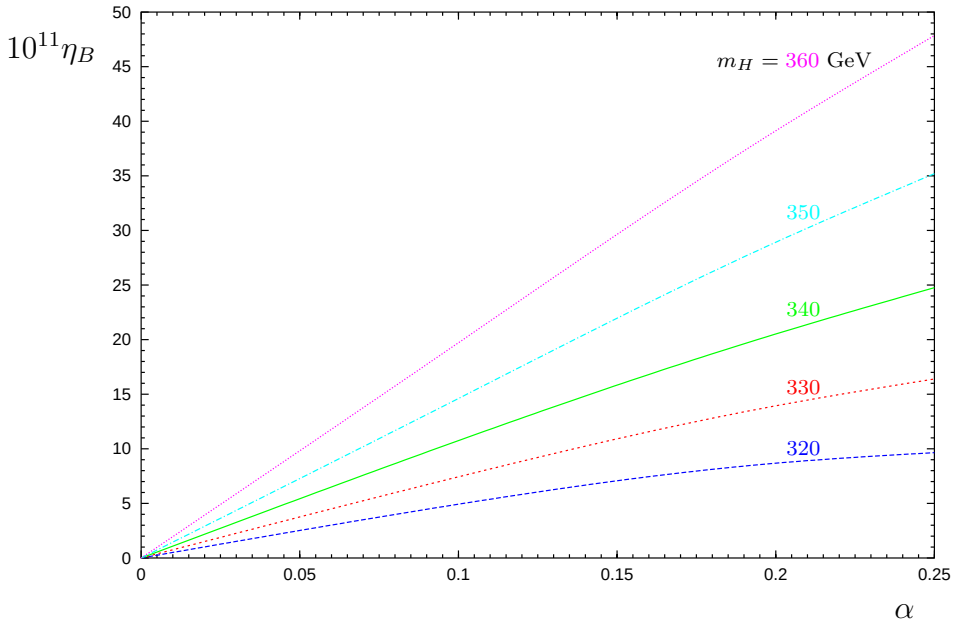

Figure 6.12: The baryon asymmetry as a function of the CP-violating phase α for different values of m_H. The light Higgs mass we have chosen as $m_h = 120$ GeV.

CP-violating phase α, the appropriate heavy Higgs mass interval is somewhat shifted if we adjust α. Figure 6.12 demonstrates this behavior for one representative fixed value of $m_h = 120$ GeV. For instance, in the particular case when $\alpha = 0.05$ the measured value can be achieved for a heavy Higgs mass around 350 GeV.
In principle, the baryon asymmetry can be used to predict the EDMs of the electron and the neutron in terms of the Higgs masses and the parameters μ_3^2 and α. As briefly demonstrated in section 4.3, one can compute $|d_e|$ and $|d_n|$ in each parameter setting. Comparing, for instance, figure 6.11 with figure 5 of ref. [83] we find that the experimental bound on the neutron EDM starts to cut into the parameter space of the 2HDM, while the electron EDM is one to two orders of magnitude below the current bound. We do not go into the details of this analysis here. A discussion of the EDMs in the 2HDM can be found in ref. [64].
Altogether, we find a wide range of realistic model parameters yielding the observed baryon asymmetry, where the computation of η_B is well under control.

7 Summary and Conclusions

We investigated the EWPT and baryogenesis in two non-supersymmetric extensions of the SM. We focused on top transport and tested the relevance of various contributions to the generated baryon asymmetry.
For successful baryogenesis the three Sakharov conditions have to be satisfied. Baryon number violation can be provided by the sphaleron transitions. In addition, a C- and CP-violating mechanism has to be available for each model under consideration. Furthermore, for a baryogenesis scenario operating at the electroweak scale, as we considered, the required deviation from thermal equilibrium can only be achieved by a first order phase transition, which guarantees the coexistence of two different phases at the critical temperature. To prevent baryon number washout after the transition is completed, a further condition has to be satisfied: the sphaleron transitions have to be sufficiently suppressed in the broken phase which happens if the Higgs expectation value is larger than about the critical temperature. Then the phase transition is called strong first order. In practice, the most important tool to study the behavior of the system close to the critical temperature is the effective potential. Many relevant properties like the strength of the transition and the bubble wall width can be computed from it.
The SM does not fulfill the necessary requirements to produce a sufficiently large baryon number. For a Higgs boson mass larger than the current experimental lower bound the phase transition is not of first order. Moreover, the CP-violation in the CKM matrix is too small to fuel baryogenesis. Thus, extensions are required which induce a strong first order phase transition and provide additional CP-violation.
The first model considered in this thesis is the SM extended by dimension-6 Higgs interactions. In this case, non-renormalizable operators parameterize new physics beyond some cut-off scale Λ. The model contains a single Higgs doublet, whose potential is stabilized by a ϕ^6 interaction. The suppression scale Λ and the Higgs mass are the two free parameters of this model. Using the one-loop thermal potential, we found a large part of the parameter space where the phase transition is strong enough to avoid baryon number washout even for Higgs masses up to 180 GeV. In this parameter region the wall thickness varies between $2/T$ and $16/T$. In addition, this model provides a new source of CP-violation. A dimension-six operator involving the Higgs field and the top quark induces a complex phase in the top mass which varies along the bubble wall during the phase transition. Demanding $\Lambda \gtrsim 500$ GeV, the model satisfies the requirements of electroweak baryogenesis for a wide range of

parameters, without being in conflict with the precision measurements.
The second model we investigated is the 2HDM, in which the SM Higgs sector is augmented by an additional Higgs doublet leading to extra Higgs states. The most general potential can be parameterized by the Higgs masses, $\tan(\beta)$, μ_3^2 and a single CP-violating phase α. We focused on degenerate extra Higgs states and $\tan(\beta) = 1$. Analyzing the thermal one-loop potential, we found a strong first order phase transition for a large region of the parameter space. In case of $\mu_3^2 = 10000\ \text{GeV}^2$ this is possible for one light (SM-like) Higgs mass up to about 200 GeV and a heavy Higgs mass larger than about 305 GeV. The wall thickness varies between $2/T$ and $15/T$ depending on the Higgs masses. The introduction of the phase α directly in the tree-level potential leads to a relative phase between the two Higgs expectation values and accordingly to a complex top quark mass. Since this phase differs in both coexisting phases during the transition, this arranges the necessary source of CP-violation. Therefore, also in this model the ingredients of electroweak baryogenesis are met in a wide parameter range. If α is not too large, no constraints on these parameters arise due to the EDMs.
In both models we computed the baryon asymmetry in the semiclassical approximation, where the baryogenesis mechanism is described by a set of transport equations. In general, that means that the plasma is treated as consisting of quasiclassical particles, and the evolution of the particle distributions is described by classical Boltzmann equations. Using the fluid-type ansatz for the phase-space densities results in a coupled set of differential equations for chemical potentials and velocity perturbations. The CP-violating interactions of particles with the bubble wall cause different dispersion relations for particles with different helicities, which we determined in the WKB approximation. Thus, different particles experience different forces as they pass through the phase boundary leading to CP-violating source terms in the transport equations. As a result, an excess of left-handed quarks is created in front of the bubble. Finally, the weak sphalerons partly convert this left-handed quark density into a baryon asymmetry.
In non-supersymmetric models of electroweak baryogenesis the top quark plays a crucial role, so that we concentrated on top transport. We computed the dispersion relation by solving the one-particle Dirac equation to first order in gradients of the bubble profile in a special Lorentz frame. Before carrying out further manipulations we boosted the result to a general frame, which has not been done in the literature so far. The resulting expressions for the dispersion relation, the group velocity and the semiclassical force are in agreement with these quantities derived in the full Schwinger-Keldysh formalism. Thus, we demonstrated how to obtain the same result in a much simpler way. We showed that performing the boost back to a general Lorentz frame has a sizeable effect on the baryon asymmetry generated. This improvement alone can enhance η_B by a factor up to about two.
We also improved on the transport equations by keeping the inelastic scattering processes $bW \leftrightarrow tX$ at a finite rate. This procedure allowed us to determine the perturbations of the top and bottom quarks separately. Setting the scatterings with

the W bosons to equilibrium can enhance or reduce the baryon asymmetry by a large amount, depending on the wall width and wall velocity.
In addition, we investigated the relevance of novel source terms related to CP-conserving perturbations in the plasma. It turned out that their contribution to the baryon asymmetry generated is rather small, since these sources are one order higher in gradients than the other sources.
Furthermore, we demonstrated that the influence of the Higgs bosons on the final result is negligible. But surprisingly, the position dependence of the thermal averages appearing in the transport equations has a considerable impact on the baryon asymmetry, even though it is formally a higher order effect in the gradient expansion.
We found a baryon asymmetry in the range of the measured value for natural parameter values in both models. Since also the electron and neutron EDM can be computed for each parameter setting, η_B can be used to predict $|d_e|$ and $|d_n|$ in terms of the Higgs masses and the remaining parameters of the respective model.

To conclude, both models under consideration provide ingredients for electroweak baryogenesis that are missing in the SM, i.e. a strong first order phase transition and additional CP-violation. Using the semiclassical approximation one obtains a baryon to entropy ratio in the right order of magnitude for typical parameter values, respectively. However, the substantial impact of the precise treatment of the W-scattering rate as well as the space-dependence of the thermal averages probably indicate that there is still some uncertainty related to transport.

Appendix A

Thermal Potential

At finite temperature the one-loop contribution to the effective potential is given by

$$\begin{aligned} V_1^T = & \sum_B \frac{n_B T^4}{2\pi^2} \int_0^\infty dx\, x^2 \ln\left[1 - \exp\left(-\sqrt{x^2 + \frac{m_B^2}{T^2}}\right)\right] \\ & - \sum_F \frac{n_F T^4}{2\pi^2} \int_0^\infty dx\, x^2 \ln\left[1 + \exp\left(-\sqrt{x^2 + \frac{m_F^2}{T^2}}\right)\right] \\ \equiv & \; T^4 \sum_B n_B\, f_B\left(\frac{m_B}{T}\right) + T^4 \sum_F n_F\, f_F\left(\frac{m_F}{T}\right) \end{aligned} \tag{A.1}$$

These integrals can be evaluated in the high temperature limit, $m/T \ll 1$, yielding [58]

$$f_B^{\mathrm{HT}}\left(\frac{m}{T}\right) \approx \frac{-\pi^2}{90} + \frac{m^2}{24T^2} - \frac{m^3}{12\pi T^3} - \frac{m^4}{64\pi^2 T^4} \ln\left(\frac{m^2}{c_B T^2}\right) \tag{A.2}$$

$$f_F^{\mathrm{HT}}\left(\frac{m}{T}\right) \approx \frac{-7\pi^2}{720} + \frac{m^2}{48T^2} + \frac{m^4}{64\pi^2 T^4} \ln\left(\frac{m^2}{c_F T^2}\right) \tag{A.3}$$

with $c_F = \pi^2 \exp(3/2 - 2\gamma_e) \approx 13.94$ and $c_B = 16 c_F$, and in the low temperature limit, $m/T \gg 1$, yielding [59]

$$\begin{aligned} f^{\mathrm{LT}}\left(\frac{m}{T}\right) &= f_B^{\mathrm{LT}}\left(\frac{m}{T}\right) = f_F^{\mathrm{LT}}\left(\frac{m}{T}\right) \\ &\approx -\left(\frac{m}{2\pi T}\right)^{3/2} \exp\left(-\frac{m}{T}\right)\left(1 + \frac{15m}{8T}\right). \end{aligned} \tag{A.4}$$

In the low temperature limit the contributions from bosons and fermions have the same asymptotic behavior.
We use these analytic approximations instead of the exact expression (A.1) since it

is much more convenient to handle analytic expressions. In order to deal with an expression valid in the whole temperature range we have to connect both temperature regions. It appears appropriate to use a smooth interpolation like

$$f_B^{\rm int}(x) = \begin{cases} f_B^{\rm HT}(x) & x < 1.8 \\ \frac{-0.39+0.05069x}{5.2186-1.8874x+x^2} & 1.8 < x < 4.5 \\ f^{\rm LT}(x) & x > 4.5 \end{cases} \tag{A.5}$$

$$f_F^{\rm int}(x) = \begin{cases} f_F^{\rm HT}(x) & x < 1.1 \\ \frac{-0.6087+0.0856x}{6.321-0.725x+x^2} & 1.1 < x < 3.4 \\ f^{\rm LT}(x) & x > 3.4 \end{cases} . \tag{A.6}$$

These interpolations between the low and high temperature limits are done such that the functions as well as their derivatives match at the connecting points. The deviation between $f_{B(F)}^{\rm int}$ and the corresponding exact integral is less than 4%.

Appendix B

Generalization of the Transformation Matrix D

In the computation of the dispersion relations for fermions we made a useful simplification. To solve the free Dirac equation (5.6) we diagonalized the matrix $Q(z)$ (5.7) by $Q = DQ_D D^{-1}$ and switched to the local helicity basis. Then the Dirac equation is in diagonal form to leading order. But the choice of the transformation matrix to the local helicity basis D (5.8) is not unique. Its generalization is given by [112]

$$\hat{D}(z) = \begin{pmatrix} e^{i\alpha}\cosh X & e^{-i\beta}\sinh X \\ e^{i\beta}\sinh X & e^{-i\alpha}\cosh X \end{pmatrix}, \tag{B.1}$$

where again X is defined by $\tanh X = (E - \sqrt{E^2 - m^2})/m$. This matrix diagonalizes $Q(z)$ (5.7) if the two conditions

$$\begin{aligned} \sqrt{E^2 - m^2}\left(\sinh^2 X + \cosh^2 X\right) &= E, \\ 2e^{i(\beta-\alpha)}\sqrt{E^2 - m^2}\sinh X \cosh X &= me^{i\theta} \end{aligned} \tag{B.2}$$

are fulfilled. In section 5.2.2 we considered the special case $\alpha = 0$ and $\beta = \theta$. To order $\hbar$ the dispersion relations of the canonical momentum in the most general form are obtained from the eigenvalues of the matrix $\pm Q_D - \hat{D}^{-1} i\hbar\partial_z \hat{D}$, where

$$\hat{D}^{-1} i\hbar\partial_z \hat{D} = \tag{B.3}$$

$$\begin{pmatrix} -\hbar\alpha'\cosh^2 X + \hbar\beta'\sinh^2 X & \hbar e^{-i(\alpha+\beta)}[iX' + \frac{1}{2}(\beta' - \alpha')\sinh 2X] \\ \hbar e^{i(\alpha+\beta)}[iX' + \frac{1}{2}(\alpha' - \beta')\sinh 2X] & \hbar\alpha'\cosh^2 X - \hbar\beta'\sinh^2 X \end{pmatrix}.$$

As a result, the CP-violating part of the dispersion relations contains not only a β'- but also a α'-contribution, i.e. $\Delta p_z = \hbar\beta'\sinh^2 X - \hbar\alpha'\cosh^2 X$. This Δp_z is difficult to handle, since the α'-term does not vanish in the limit $m \to 0$. Hence, it cannot be directly associated to CP-violation but to an artificial position dependent redefinition of the chirality eigenstates. However, we can avoid this problem since

we use the kinetic variables, where this difficulty does not appear [106]. Using the special choice made in section 5.2.2, the dispersion relations for the canonical quantities are also well-defined.

Appendix C

Thermal Averages

In section 5.4 we have introduced the symbols K_i to work with more manageable equations. Denoting the momentum integral of the massless Fermi-Dirac case by the normalization constant N, i.e.

$$N = \int d^3p \; \tilde{f}^0_+(m=0) = -\int d^3p \; \frac{\beta e^{\beta p}}{(e^{\beta p}+1)^2}, \tag{C.1}$$

we directly obtain

$$\begin{aligned}
K_1(m) &= -\left\langle \frac{p_z^2}{E_0}\tilde{g}^0 \right\rangle = -\frac{4\pi}{3N}\int dp \; \frac{p^4}{\sqrt{p^2+m^2}}\tilde{g}^0(p,m), && \text{(C.2)}\\
K_2(m) &= \left\langle \frac{1}{2E_0}\tilde{g}^0 \right\rangle = \frac{2\pi}{N}\int dp \; \frac{p^2}{\sqrt{p^2+m^2}}\tilde{g}^0(p,m), && \text{(C.3)}\\
K_3(m) &= \left\langle \frac{1}{2E_0}\tilde{f}^0 \right\rangle = \frac{2\pi}{N}\int dp \; \frac{p^2}{\sqrt{p^2+m^2}}\tilde{f}^0(p,m), && \text{(C.4)}\\
K_4(m) &= \left\langle \frac{p_z^2}{E_0^2}\tilde{f}^0 \right\rangle = \frac{4\pi}{3N}\int dp \; \frac{p^4}{p^2+m^2}\tilde{f}^0(p,m), && \text{(C.5)}\\
K_7(m) &= \left\langle \frac{|p_z|}{2E_0^2E_{0z}}\left(\frac{\tilde{f}^0}{E_0}-\tilde{g}^0\right)\right\rangle \\
&= \frac{2\pi}{N}\int dp \; \frac{p(\sqrt{p^2+m^2}-m)}{p^2+m^2}\left(\frac{\tilde{f}^0(p,m)}{\sqrt{p^2+m^2}}-\tilde{g}^0(p,m)\right), && \text{(C.6)}\\
K_8(m) &= \left\langle \frac{|p_z|}{2E_0^2E_{0z}}\tilde{f}^0 \right\rangle = \frac{2\pi}{N}\int dp \; \frac{p(\sqrt{p^2+m^2}-m)}{p^2+m^2}\tilde{f}^0(p,m), && \text{(C.7)}\\
K_9(m) &= \left\langle \frac{|p_z|}{4E_0^3E_{0z}}\left(\frac{\tilde{f}^0}{E_0}-\tilde{g}^0\right)\right\rangle \\
&= \frac{\pi}{N}\int dp \; \frac{p(\sqrt{p^2+m^2}-m)}{\sqrt{p^2+m^2}^3}\left(\frac{\tilde{f}^0(p,m)}{\sqrt{p^2+m^2}}-\tilde{g}^0(p,m)\right) && \text{(C.8)}
\end{aligned}$$

for the thermal averages as a function of the particle mass m. In the special case $E_{0z} \to E_0$ the latter two are given by

$$\bar{K}_8(m) = \left\langle \frac{|p_z|}{2E_0^3} \tilde{f}^0 \right\rangle = \frac{\pi}{N} \int dp \, \frac{p^3}{\sqrt{p^2+m^2}^3} \tilde{f}^0(p,m), \tag{C.9}$$

$$\begin{aligned} \bar{K}_9(m) &= \left\langle \frac{|p_z|}{4E_0^4} \left(\frac{\tilde{f}^0}{E_0} - \tilde{g}^0 \right) \right\rangle \\ &= \frac{\pi}{2N} \int dp \, \frac{p^3}{(p^2+m^2)^2} \left(\frac{\tilde{f}^0(p,m)}{\sqrt{p^2+m^2}} - \tilde{g}^0(p,m) \right). \end{aligned} \tag{C.10}$$

In addition, there are averages involving the kinetic perturbations δf which have to be treated in a different way. We assume that these averages factorize such that we can separate u. Introducing the equilibrium distribution function in the rest frame of the wall

$$f_\pm^{(\mathrm{eq})} = \frac{1}{e^{\beta\gamma_\mathrm{w}(E_0 + v_\mathrm{w} p_z)} \pm 1}, \tag{C.11}$$

an arbitrary momentum average can be splitted in the following way

$$\langle A\delta f \rangle = \left[A \frac{E_0}{p_z} f_\pm^{(\mathrm{eq})} \right] \left\langle \frac{p_z}{E_0} \delta f \right\rangle = \left[A \frac{E_0}{p_z} f_\pm^{(\mathrm{eq})} \right] u, \tag{C.12}$$

where the brackets are defined as in equation (5.60). Since we are only interested in results to first order in the wall velocity we use

$$f_\pm^{(\mathrm{eq})} \simeq f^0 + v_\mathrm{w} p_z \tilde{f}^0, \tag{C.13}$$

with

$$f^0 = \frac{1}{e^{\beta E_0} \pm 1} \quad \text{and} \quad \tilde{f}^0 = \frac{\partial f^0}{\partial E_0} = -\frac{\beta e^{\beta E_0}}{(e^{\beta E_0} \pm 1)^2}. \tag{C.14}$$

There are seven different averages involving δf in the equations (5.55) and (5.56). Let us demonstrate for two representative examples how the "factorization" precisely works:

$$\begin{aligned} \left\langle \frac{p_z}{E_0} \partial_z \delta f \right\rangle &= \left(\left\langle \frac{p_z}{E_0} \delta f \right\rangle \right)' - \left\langle \left(\frac{p_z}{E_0} \right)' \delta f \right\rangle \\ &= u' - \left[\left(\frac{p_z}{E_0} \right)' \frac{E_0}{p_z} f_\pm^{(\mathrm{eq})} \right] \left\langle \frac{p_z}{E_0} \delta f \right\rangle \\ &= u' + \left[\frac{E_0'}{E_0} f_\pm^{(\mathrm{eq})} \right] u \\ &= u' + \left[\frac{(m^2)'}{2E_0^2} f_\pm^{(\mathrm{eq})} \right] u \\ &= u' + \left[\frac{1}{2E_0^2} f^0 \right] (m^2)' u, \end{aligned} \tag{C.15}$$

$$\begin{aligned}
\left\langle \frac{(m^2)'}{2E_0}\partial_{p_z}\delta f \right\rangle &= -\left\langle \partial_{p_z}\left(\frac{(m^2)'}{2E_0}\right)\delta f \right\rangle \\
&= \left\langle \frac{p_z}{2E_0^3}\delta f \right\rangle (m^2)' \\
&= \left[\frac{1}{2E_0^2} f_{\pm}^{(\mathrm{eq})}\right](m^2)'u \\
&= \left[\frac{1}{2E_0^2} f^0\right](m^2)'u. \qquad \text{(C.16)}
\end{aligned}$$

Similarly, we obtain

$$\left\langle \frac{p_z^2}{E_0^2}\partial_z\delta f \right\rangle = v_{\mathrm{w}}\left[\frac{p_z^2}{E_0}\tilde{f}^0\right]u' + v_{\mathrm{w}}\left[\frac{p_z^2}{2E_0^3}\tilde{f}^0\right](m_i^2)'u, \qquad \text{(C.17)}$$

$$\left\langle \frac{(m^2)'p_z}{2E_0^2}\partial_{p_z}\delta f \right\rangle = v_{\mathrm{w}}\left[\frac{2p_z^2 - E_0^2}{2E_0^3}\tilde{f}^0\right](m^2)'u, \qquad \text{(C.18)}$$

$$\begin{aligned}
\left\langle \frac{\mathrm{sign}(p_z)p_z^2 m^2\theta'}{2E_0^4 E_{0z}}\partial_z\delta f \right\rangle &= \left[\frac{|p_z|}{2E_0^3E_{0z}}f^0\right]m^2\theta'u' \\
&\quad + \left[\frac{|p_z|}{4E_0^5E_{0z}}f^0\right]m^2(m^2)'\theta'u. \qquad \text{(C.19)}
\end{aligned}$$

Since we do not know the the momentum dependence of δf, we additionally define

$$x = \langle \mathrm{sign}(p_z)\,\delta f\rangle\,. \qquad \text{(C.20)}$$

This quantity x can also be expressed in terms of the plasma velocity u, i.e.

$$\begin{aligned}
u &= \left\langle \frac{p_z}{E_0}\delta f \right\rangle = \left\langle \frac{|p_z|}{E_0}\mathrm{sign}(p_z)\,\delta f \right\rangle = \left[\frac{|p_z|}{E_0}f^0\right]x \\
\Rightarrow\quad x &= \left[\frac{|p_z|}{E_0}f^0\right]^{-1}u. \qquad \text{(C.21)}
\end{aligned}$$

Hereby, the last two remaining averages appearing in the equations (5.55) and (5.56) can also be determined:

$$\begin{aligned}
\left\langle \frac{|p_z|(m^2\theta')'}{2E_0^2E_{0z}}\partial_{p_z}\delta f \right\rangle &= -\left[\frac{1}{2E_0^2E_{0z}^3}f^0\right]\left[\frac{|p_z|}{E_0}f^0\right]^{-1}m^2(m^2\theta')'u \\
&\quad + \left[\frac{|p_z|}{E_0^3E_{0z}}f^0\right](m^2\theta')'u, \qquad \text{(C.22)}
\end{aligned}$$

$$\begin{aligned}
\left\langle \frac{|p_z|m^2\theta'(m^2)'}{4E_0^4E_{0z}}\partial_{p_z}\delta f \right\rangle &= -\left[\frac{1}{4E_0^4E_{0z}^3}f^0\right]\left[\frac{|p_z|}{E_0}f^0\right]^{-1}m^4\theta'(m^2)'u \\
&\quad + \left[\frac{|p_z|}{E_0^5E_{0z}}f^0\right]m^2\theta'(m^2)'u. \qquad \text{(C.23)}
\end{aligned}$$

With the m-dependent normalization functions

$$N_1(m) = 4\pi \int dp\; p^2 f^0(p,m) \tag{C.24}$$

and

$$N_2(m) = 2\pi \int dp\; \frac{p^3}{\sqrt{p^2+m^2}^3} f^0(p,m) \tag{C.25}$$

the averages $\tilde{K}_j$ are given by

$$\tilde{K}_5(m) = \left[\frac{p_z^2}{E}\tilde{f}^0\right] = \frac{4\pi}{3N_1(m)} \int dp\; \frac{p^4}{\sqrt{p^2+m^2}} \tilde{f}^0(p,m) = -1, \tag{C.26}$$

$$\tilde{K}_6(m) = \left[\frac{E_0^2 - p_z^2}{2E_0^3}\tilde{f}^0\right] = \frac{2\pi}{3n_1(m)} \int dp\; \frac{p^2(3m^2+2p^2)}{\sqrt{p^2+m^2}^3} \tilde{f}^0(p,m), \tag{C.27}$$

$$\tilde{K}_{10}(m) = \left[\frac{|p_z|}{2E_0^3 E_{0z}} f^0\right] = \frac{2\pi}{N_1(m)} \int dp\; \frac{p(\sqrt{p^2+m^2}-m)}{\sqrt{p^2+m^2}^3} f^0(p,m), \tag{C.28}$$

$$\tilde{K}_{11}(m) = \left[\frac{3|p_z|}{4E_0^5 E_{0z}} f^0\right] = \frac{3\pi}{N_1(m)} \int dp\; \frac{p(\sqrt{p^2+m^2}-m)}{\sqrt{p^2+m^2}^5} f^0(p,m), \tag{C.29}$$

$$\tilde{K}_{12}(m) = \frac{\left[\frac{m^2}{4E_0^4 E_{0z}^3} f^0\right]}{\left[\frac{|p_z|}{E_0} f^0\right]} = \frac{\pi}{N_2(m)} \int dp\; \frac{p^2}{\sqrt{p^2+m^2}^5} f^0(p,m), \tag{C.30}$$

$$\tilde{K}_{13}(m) = \frac{\left[\frac{m^2}{2E_0^2 E_{0z}^3} f^0\right]}{\left[\frac{|p_z|}{E_0} f^0\right]} = \frac{2\pi}{N_2(m)} \int dp\; \frac{p^2}{\sqrt{p^2+m^2}^3} f^0(p,m). \tag{C.31}$$

$\tilde{K}_5$ is a constant. In the latter two averages an extra power of m^2 is included in the numerator to compensate the factor m^2 induced by the angular integration in the denominator, i.e. in $N_2(m) \sim m^2$. The averages $\tilde{K}_{11}$, $\tilde{K}_{12}$ and $\tilde{K}_{13}$ do not appear in chapter 5. They are the coefficients of additional source terms S_u which are discussed in appendix D.

In figures C.1 and C.2 all thermal averages are shown as functions of the fermion mass for $0 \leq m/T \leq 2.5$. Some of them (K_7, K_9, $\tilde{K}_{10}$, $\tilde{K}_{11}$, $\tilde{K}_{12}$, $\tilde{K}_{13}$) are divergent for small m. However, this is unproblematic in the computation of the baryon asymmetry since these averages only appear in combination with m^2 in the different source terms which vanish in the limit $m \to 0$.

If we replace $m \to m(z)$, the averages are z-dependent as needed for the transport equations. The bottom quarks and the Higgs bosons are taken as massless. Therefore, the corresponding averages are z-independent, and we get $K_{1,b} = 1$, $K_{4,b} = 1/3$, $K_{1,h} = 2$ and $K_{4,h} = 2/3$.

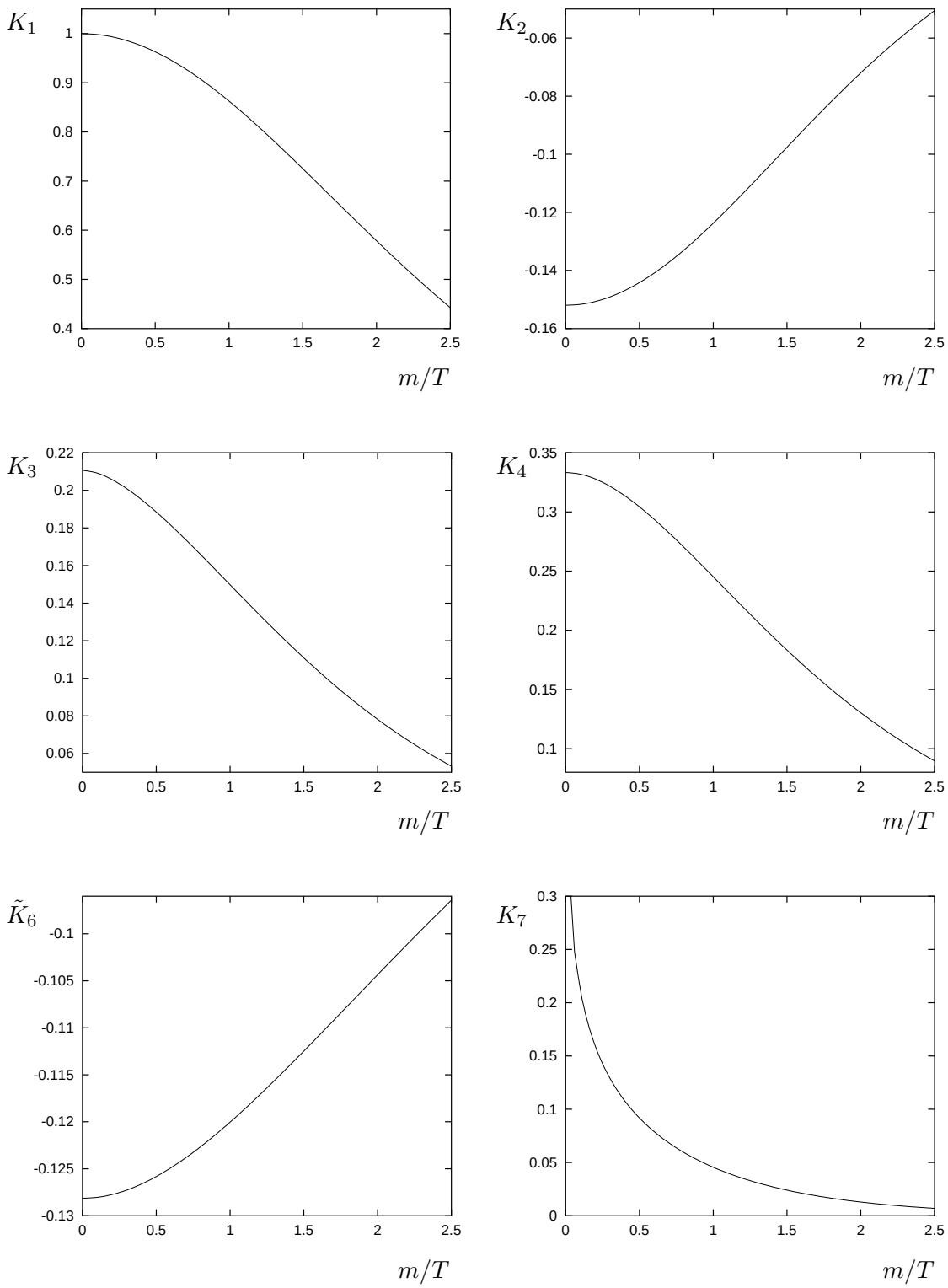

Figure C.1: The thermal averages K_1, K_2, K_3, K_4, $\tilde{K}_6$ and K_7 as a function of the fermion mass.

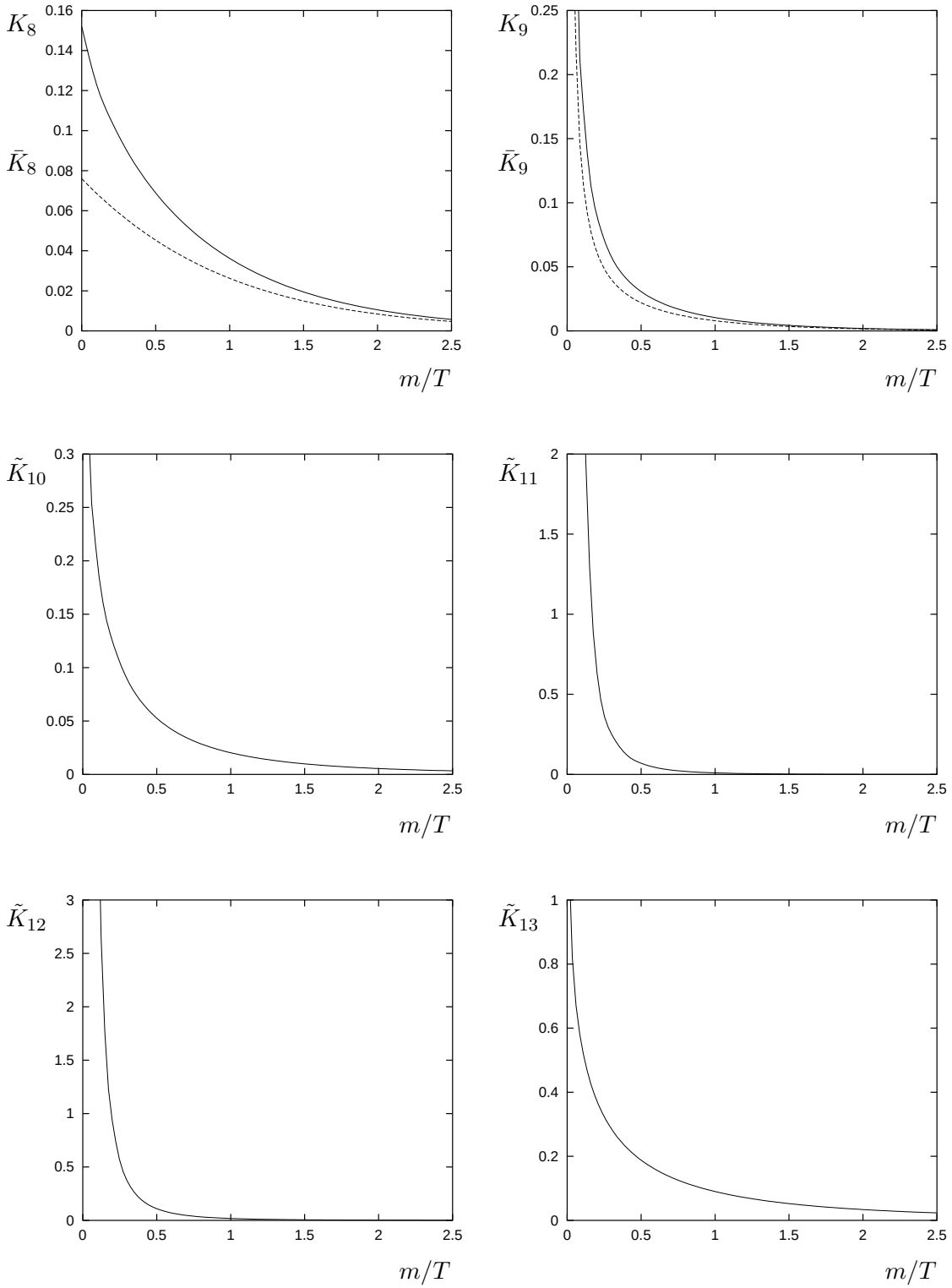

Figure C.2: The thermal averages K_8, K_9, $\tilde{K}_{10}$, $\tilde{K}_{11}$, $\tilde{K}_{12}$ and $\tilde{K}_{13}$ as a function of the fermion mass. In addition $\bar{K}_8$ and $\bar{K}_9$ are shown in the upper plots (dashed lines).

Appendix D

The Additional Source Term S_u

As pointed out in chapter 5, some extra source terms related to the first order perturbations appear in the transport equations. Since we do not know the exact momentum dependence of the velocity perturbations δf, we have made some assumptions. In principle, additional source terms would arise, if we treat the averages involving δf as described in appendix C. We have neglected these sources in our numerical evaluations of the baryon asymmetry. Here we want to investigate whether this is a good approximation or not.
On one hand we assume that the averages factorize, which is necessary to separate the plasma velocity u. On the other hand we introduced the quantity x, defined by equation (C.20), to handle the averages involving $\mathrm{sign}(p_z)\,\delta f$. Of course, this is only one possibility to treat these averages. Using this particular prescription we obtain an additional source of the form

$$S_u = (2\tilde{K}_{10} - \tilde{K}_{13})(m^2\theta')'u_1 + (\tilde{K}_{12} - \tilde{K}_{11})m^2(m^2)'\theta' u_1 \tag{D.1}$$

on the r.h.s. of equation (5.62). Accordingly, we have to add $3S_{u_t}$ on the r.h.s. of the equations (5.89) and (5.91) in the full set of transport equations, since we are only dealing with source terms for the top quarks.
The resulting baryon asymmetry for the same two parameter settings as discussed in section 6.2 is presented in figures D.1 and D.2. In addition, the lines (a) and (f) are plotted for orientation. (a) corresponds to η_B generated only by the source $S_{\theta'_t}$, and (f) represents the case when the sources $S_{\mu'_t}$ and $S_{u'_t}$ are added. Considering also the source S_{u_t} enhances the baryon asymmetry substantially in the whole v_w-range (h), especially for strong phase transitions. The contribution of the extra source is of the same order of magnitude as the contribution coming from the sources $S_{\mu'_t}$ and $S_{u'_t}$. However, we do not know if we treat the averages involving $\mathrm{sign}(p_z)\,\delta f$ in a consistent way. Therefore, also the the final result is plotted, if one neglects the $\tilde{K}_{12}$- and $\tilde{K}_{13}$-parts of the new source (i) (cf. D.1)). Surprisingly, η_B is then reduced even below the result generated without any sources proportional to the first order perturbations. This demonstrates that there exist large uncertainties

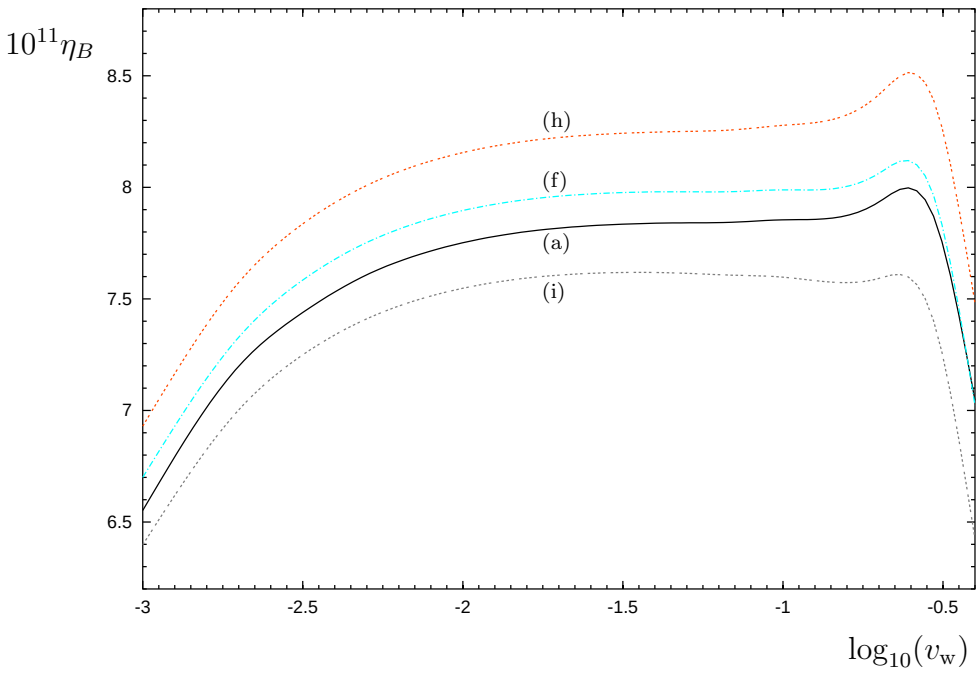

Figure D.1: The baryon asymmetry as a function of v_w for the same parameter set as in figure 6.7. The labeling is explained in the text.

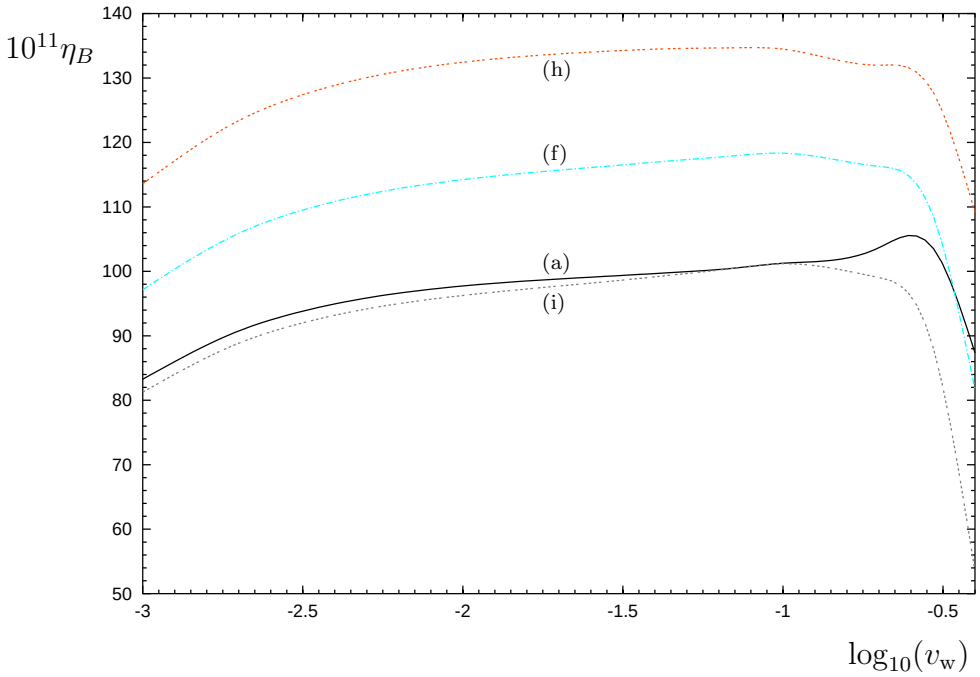

Figure D.2: The baryon asymmetry as a function of v_w for the same parameter set as in figure 6.8.

concerning the precise treatment of the averages. S_{u_t} is obviously dominated by the $\tilde{K}_{12}$- and $\tilde{K}_{13}$-parts, which presumably can be explained by the E_{0z}^3-dependence of their denominators. Another reason could be that the proposed transformation of the averages involving $\mathrm{sign}(p_z)\,\delta f$ via the quantity x may overestimate these terms. It would be interesting to test the influence of these terms if one uses other approximations. However, this example gives us an idea about the error band surrounding the final result of our numerical evaluation.
Because of the mentioned uncertainties we decided to neglect all source terms proportional to the plasma velocity $u_{t,1}$. Nevertheless, independent of the respective approximation we use, the sources proportional to the first order perturbations effect η_B only by an amount of the order $1/L_{\mathrm{w}}$, which is in the same order of magnitude as the intrinsic uncertainty of the computation.

Bibliography

[1] A. G. Cohen, A. De Rujula and S. L. Glashow, *A matter-antimatter universe?*, Astrophys. J. **495** (1998) 539 [astro-ph/9707087].

[2] E. W. Kolb and M. S. Turner, *The early universe*, Frontiers in Physics **Vol. 69** (1990).

[3] WMAP Collaboration, D. N. Spergel *et al.*, *Wilkinson Microwave Anisotropy Probe (WMAP) three year results: Implications for cosmology*, astro-ph/0603449.

[4] SDSS Collaboration, M. Tegmark *et al.*, *Cosmological parameters from SDSS and WMAP*, Phys. Rev. **D 69** (2004) 103501 [astro-ph/0310723].

[5] Particle Data Group Collaboration, S. Eidelman *et al.*, *Review of Particle Physics*, Physical Letters **B 592** (2004) 1.

[6] A. D. Sakharov, *Violation of CP invariance, C asymmetry, and baryon asymmetry of the universe*, Pisma Zh. Eksp. Teor. Fiz. **5** (1967) 32 [JETP Lett. **5** (1967) 24].

[7] W. Bernreuther, *CP violation and baryogenesis*, Lect. Notes Phys. **591** (2002) 237 [hep-ph/0205279].

[8] A. Riotto and M. Trodden, *Recent progress in baryogenesis*, Ann. Rev. Nucl. Part. Sci. **49** (1999) 35 [hep-ph/9901362].

[9] A. D. Dolgov, *Baryogenesis, 30 years after*, hep-ph/9707419.

[10] W. Buchmüller, P. Di Bari and M. Plümacher, *Leptogenesis for pedestrians*, Annals Phys. **315** (2005) 305 [hep-ph/0401240].

[11] W. Buchmüller, *Recent progress in leptogenesis*, hep-ph/0107153.

[12] M. Trodden, *Electroweak baryogenesis*, Rev. Mod. Phys. **71** (1999) 1463 [hep-ph/9803479].

[13] V. A. Rubakov and M. E. Shaposhnikov, *Electroweak baryon number non-conservation in the early universe and in high-energy collisions*, Usp. Fiz. Nauk **166** (1996) 493 [Phys. Usp. **39** (1996) 461] [hep-ph/9603208].

[14] C. Zwaneveld, *Baryogenesis and leptogenesis*, Masters thesis, University of Amsterdam, 2002.

[15] G. 't Hooft, *Symmetry breaking through Bell-Jackiw anomalies*, Phys. Rev. Lett. **37** (1976) 8.

[16] G. 't Hooft, *Computation of the quantum effects due to a four-dimensional pseudoparticle*, Phys. Rev. **D 14** (1976) 3432, Erratum-ibid. **D 18** (1978) 2199.

[17] M. E. Shaposhnikov, *Possible appearance of the baryon asymmetry of the universe in an electroweak theory*, JETP Lett. **44** (1986) 465.

[18] G. D. Moore, *Measuring the broken phase sphaleron rate nonperturbatively*, Phys. Rev. **D 59** (1999) 014503 [hep-ph/9805264].

[19] V. A. Kuzmin, V. A. Rubakov and M. E. Shaposhnikov, *On the anomalous electroweak baryon number nonconservation in the early universe*, Phys. Lett. **B 155** (1985) 36.

[20] M. B. Gavela, P. Hernandez, J. Orloff, O. Pene and C. Quimbay, *Standard model CP-violation and baryon asymmetry, part 2. Finite temperature*, Nucl. Phys. **B 430** (1994) 382 [hep-ph/9406289].

[21] P. Huet and E. Sather, *Electroweak baryogenesis and standard model CP-violation*, Phys. Rev. **D 51** (1995) 379 [hep-ph/9404302].

[22] T. Konstandin, T. Prokopec and M. G. Schmidt, *Axial currents from CKM matrix CP-violation and electroweak baryogenesis*, Nucl. Phys. **B 679** (2004) 246 [hep-ph/0309291].

[23] K. Kajantie, M. Laine, K. Rummukainen and M. E. Shaposhnikov, *Is there a hot electroweak phase transition at $m_H \gtrsim m_W$?*, Phys. Rev. Lett. **77** (1996) 2887 [hep-ph/9605288].

[24] K. Kajantie, M. Laine, K. Rummukainen and M. E. Shaposhnikov, *A non-perturbative analysis of the finite t phase transition in $SU(2)\times U(1)$ electroweak theory*, Nucl. Phys. **B 493** (1997) 413 [hep-lat/9612006].

[25] F. Csikor, Z. Fodor and J. Heitger, *Endpoint of the hot electroweak phase transition*, Phys. Rev. Lett. **82** (1999) 21 [hep-ph/9809291].

[26] LEP collaboration, *A combination of preliminary electroweak measurements and constraints on the standard model*, hep-ex/0312023.

[27] M. Carena, M. Quiros and C. E. M. Wagner, *Opening the window for electroweak baryogenesis*, Phys. Lett. **B 380** (1996) 81 [hep-ph/9603420].

[28] D. Bödeker, P. John, M. Laine and M. G. Schmidt, *The 2-loop MSSM finite temperature effective potential with stop condensation*, Nucl. Phys. **B 497** (1997) 387 [hep-ph/9612364].

[29] B. de Carlos and J. R. Espinosa, *The baryogenesis window in the MSSM*, Nucl. Phys. **B 503** (1997) 24 [hep-ph/9703212].

[30] M. Laine and K. Rummukainen, *The MSSM electroweak phase transition on the lattice*, Nucl. Phys. **B 535** (1998) 423 [hep-lat/9804019].

[31] M. Pietroni, *The electroweak phase transition in a nonminimal supersymmetric model*, Nucl. Phys. **B 402** (1993) 27 [hep-ph/9207227].

[32] A. T. Davies, C. D. Froggatt and R. G. Moorhouse, *Electroweak baryogenesis in the next to minimal supersymmetric model*, Phys. Lett. **B 372** (1996) 88 [hep-ph/9603388].

[33] S. J. Huber and M. G. Schmidt, *SUSY variants of the electrweak phase transition*, Eur. Phys. J. **C 10** (1999) 473 [hep-ph/9809506].

[34] M. Bastero-Gil, C. Hugonie, S. F. King, D. P. Roy and S. Vempati, *Does lep prefer the NMSSM?*, Phys. Lett. **B 489** (2000) 359 [hep-ph/0006198].

[35] T. Prokopec, M. G. Schmidt and S. Weinstock, *Transport equations for chiral fermions to order h-bar and electroweak baryogenesis*, Annals Phys. **314** (2004) 208 [hep-ph/0312110].

[36] T. Prokopec, M. G. Schmidt and S. Weinstock, *Transport equations for chiral fermions to order h-bar and electroweak baryogenesis. II*, Annals Phys. **314** (2004) 267 [hep-ph/0406140].

[37] S. L. Adler, *Axial vector vertex in spinor electrodynamics*, Phys. Rev. **177** (1969) 2426.

[38] J. S. Bell and R. Jackiw, *A Pcac puzzle: Pi0 → Gamma Gamma in the Sigma Model*, Nuovo Cim. **A 60** (1969) 47.

[39] N. S. Manton, *Topology in the Weinberg-Salam theory*, Phys. Rev. **D 28** (1983) 2019.

[40] F. R. Klinkhamer and N. S. Manton, *A saddle point solution in the Weinberg-Salam theory*, Phys. Rev. **D 30** (1984) 2212.

[41] P. Arnold and L. D. McLerran, *Sphalerons, small fluctuations and baryon number violation in electroweak theory*, Phys. Rev. **D 36** (1987) 581.

[42] P. Arnold, D. Son and L. G. Yaffe, *The hot baryon violation rate is O(alpha(w)**5 T**4)*, Phys. Rev. **D 55** (1997) 6264 [hep-ph/9609481].

[43] D. Bödeker, *On the effective dynamics of soft non-abelian gauge fields at finite temperature*, Phys. Lett. **B 426** (1998) 351 [hep-ph/9801430].

[44] D. Bödeker, *Effective theories for hot non-Abelian dynamics*, hep-ph/9909375.

[45] D. Bödeker, G. D. Moore and K. Rummukainen, *Chern-Simons number diffusion and hard thermal loops on the lattice*, Phys. Rev. **D 61** (2000) 056003 [hep-ph/9907545].

[46] G. D. Moore, *Sphaleron rate in the symmetric electroweak phase*, Phys. Rev. **D 62** (2000) 085011 [hep-ph/0001216].

[47] G. D. Moore, *Do we understand the sphaleron rate?*, hep-ph/0009161.

[48] G. D. Moore, *The sphaleron rate: Boedeker's leading log*, Nucl. Phys. **B 568** (2000) 367 [hep-ph/9810313].

[49] P. Arnold and L. G. Yaffe, *High temperature color conductivity at next-to-leading log order*, Phys. Rev. **D 62** (2000) 125014 [hep-ph/9912306].

[50] J. J. Binney, N. J. Dowrick, A. J. Fisher and M. E. J. Newman, *The theory of critical phenomena: An introduction to the renormalization group*, Oxford University Press (1992).

[51] H. Römer and T. Filk, *Statistische Mechanik*, VCH (1994).

[52] K. Enqvist, J. Ignatius, K. Kajantie and K. Rummukainen, *Nucleation and bubble growth in a first order cosmological electroweak phase transition*, Phys. Rev. **D 45** (1992) 3415.

[53] R. Jackiw, *Functional evaluation of the effective potential*, Phys. Rev. **D 9** (1974) 1686.

[54] M. E. Peskin and D. V. Schroeder, *An introduction to quantum field theory*, Westview Press (1995).

[55] P. Ramond, *Field theory: a modern primer*, Frontiers in Physics **Vol. 74** (1992).

[56] M. Quiros, *Finite temperature field theory and phase transitions*, hep-ph/9901312.

[57] S. R. Coleman and E. Weinberg, *Radiative corrections as the origin of spontaneous symmetry breaking*, Phys. Rev. **D 7** (1973) 1888.

[58] L. Dolan and R. Jackiw, *Symmetry behavior at finite temperature*, Phys. Rev. **D 9** (1974) 3320.

[59] G. W. Anderson and L. J. Hall, *The electroweak phase transition and baryogenesis*, Phys. Rev. **D 45** (1992) 2685.

[60] A. D. Linde, *On the vacuum instability and the Higgs meson mass*, Phys. Lett. **B 70** (1977) 306.

[61] A. D. Linde, *Fate of the false vacuum at finite temperature: theory and applications*, Phys. Lett. **B 100** (1981) 37.

[62] A. D. Linde, *Decay of the false vacuum at finite temperature*, Nucl. Phys. **B 216** (1983) 421, Erratum-ibid. **B 223** (1983) 544.

[63] G. D. Moore and K. Rummukainen, *Electroweak bubble nucleation, nonperturbatively*, Phys. Rev. **D 63** (2001) 045002 [hep-ph/0009132].

[64] M. Seniuch, *Analysis of the phase structure in extended Higgs models*, PhD-Thesis, University of Bielefeld, 2006.

[65] G. D. Moore, *Electroweak bubble wall friction: analytic results*, J. High Energy Phys. **03** (2000) 006 [hep-ph/0001274].

[66] G. D. Moore and T. Prokopec, *How fast can the wall move? A study of electroweak phase transition dynamics*, Phys. Rev. **D 52** (1995) 7182 [hep-ph/9506475].

[67] B. C. Regan, E. D. Commins, C. J. Schmidt and D. DeMille, *New limit on the electron electric dipole moment*, Phys. Rev. Lett. **88** (2002) 071805.

[68] C. A. Baker *et al.*, *An improved experimental limit on the electric dipole moment of the neutron*, hep-ex/0602020.

[69] X. Zhang, *Operators analysis for Higgs potential and cosmological bound on Higgs mass*, Phys. Rev. **D 47** (1993) 3065 [hep-ph/9301277].

[70] C. Grojean, G. Servant and J. D. Wells, *First-order electroweak phase transition in the standard model with a low cutoff*, Phys. Rev. **D 71** (2005) 036001 [hep-ph/0407019].

[71] S. W. Ham and S. K. Oh, *Electroweak phase transition in the standard model with a dimension-six Higgs operator at one-loop level*, Phys. Rev. **D 70** (2004) 093007 [hep-ph/0408324].

[72] D. Bödeker, L. Fromme, S. J. Huber and M. Seniuch, *The baryon asymmetry in the standard model with a low cut-off*, J. High Energy Phys. **02** (2005) 026 [hep-ph/0412366].

[73] L. Fromme, *Electroweak baryogenesis with dimension-6 Higgs interactions*, Surveys High Energ. Phys. **19** (2004) 193 [hep-ph/0504222].

[74] L. Fromme and S. J. Huber, *Top transport in electroweak baryogenesis*, hep-ph/0604159.

[75] M. Dine, P. Huet, R. Singleton and L. Susskind, *Creating the baryon asymmetry at the electroweak phase transition*, Phys. Lett. **B 257** (1991) 351.

[76] X. Zhang, S. K. Lee, K. Whisnant and B. L. Young, *Phenomenology of a nonstandard top quark Yukawa coupling*, Phys. Rev. **D 50** (1994) 7042 [hep-ph/9407259].

[77] V. Barger, T. Han, P. Langacker, B. McElrath and P. Zerwas, *Effects of genuine dimension-six Higgs operators*, Phys. Rev. **D 67** (2003) 115001 [hep-ph/0301097].

[78] C. D. Froggatt and H. B. Nielsen, *Hierarchy of quark masses, Cabibbo angles and CP-violation*, Nucl. Phys. **B 147** (1979) 277.

[79] A. I. Bochkarev, S. V. Kuzmin and M. E. Shaposhnikov, *Electroweak baryogenesis and the Higgs boson mass problem*, Phys. Lett. **B 244** (1990) 275.

[80] N. Turok and J. Zadrozny, *Phase transitions in the two doublet model*, Nucl. Phys. **B 369** (1992) 729.

[81] A. T. Davies, C. D. Froggatt, G. Jenkins and R. G. Moorhouse, *Baryogenesis constraints on two Higgs doublet models*, Phys. Lett. **B 336** (1994) 464.

[82] J. M. Cline and P. A. Lemieux, *Electroweak phase transition in two Higgs doublet models*, Phys. Rev. **D 55** (1997) 3873 [hep-ph/9609240].

[83] L. Fromme, S. J. Huber and M. Seniuch, *Baryogenesis in the two Higgs doublet model*, hep-ph/0605242.

[84] M. Sher, *Electroweak Higgs potentials and vacuum stability*, Phys. Rept. **179** (1989) 273.

[85] J. F. Gunion, H. E. Haber, G. Kane, S. Dawson, *The Higgs hunter's guide*, Frontiers in Physics **Vol. 80** (2000).

[86] G. C. Branco and M. N. Rebelo, *The Higgs mass in a model with two scalar doublets and spontaneous CP violation*, Phys. Lett. **B 160** (1985) 117.

[87] P. M. Ferreira, R. Santos and A. Barroso, *Stability of the tree-level vacuum in two Higgs doublet models against charge or CP spontaneous violation*, Phys. Lett. **B 603** (2004) 219, Erratum-ibid. **B 629** (2005) 114 [hep-ph/0406231].

[88] C. D. Froggatt, R. G. Moorhouse and I. G. Knowles, *Leading radiative corrections in two scalar doublet models*, Phys. Rev. **D 45** (1992) 2471.

[89] M. Neubert, *Renormalization-group improved calculation of the $B \to X/s+$ gamma branching ratio*, Eur. Phys. J. **C 40** (2005) 165 [hep-ph/0408179].

[90] K. Cheung and O. C. W. Kong, *Can the two-Higgs-doublet model survive the constraint from the muon anomalous magnetic moment as suggested?*, Phys. Rev. **D 68** (2003) 053003 [hep-ph/0302111].

[91] M. Krawczyk and D. Temes, *2HDM(II) radiative corrections in leptonic tau decays*, Eur. Phys. J. **C 44** (2005) 435 [hep-ph/0410248].

[92] T. Konstandin and S. J. Huber, *Numerical approach to multi dimensional phase transitions*, hep-ph/0603081.

[93] S. J. Huber, P. John, M. Laine and M. G. Schmidt, *CP violating bubble wall profiles*, Phys. Lett. **B 475** (2000) 104 [hep-ph/9912278].

[94] S. Weinberg, *Larger Higgs exchange terms in the neutron electric dipole moment*, Phys. Rev. Lett. **63** (1989) 2333.

[95] S. M. Barr and A. Zee, *Electric dipole moment of the electron and of the neutron*, Phys. Rev. Lett. **65** (1990) 21, Erratum-ibid. **65** (1990) 2920].

[96] D. Chang, W. Y. Keung and T. C. Yuan, *Two loop bosonic contribution to the electron electric dipole moment*, Phys. Rev. **D 43** (1991) 14.

[97] J. F. Gunion and D. Wyler, *Inducing a large neutron electric dipole moment via a quark chromoelectric dipole moment*, Phys. Lett. **B 248** (1990) 170.

[98] M. Pospelov and A. Ritz, *Electric dipole moments as probes of new physics*, Annals Phys. **318**, 119 (2005) [hep-ph/0504231].

[99] A. G. Cohen, D. B. Kaplan and A. E. Nelson, *Progress in electroweak baryogenesis*, Ann. Rev. Nucl. Part. Sci. **43** (1993) 27 [hep-ph/9302210].

[100] A. G. Cohen, D. B. Kaplan and A. E. Nelson, *Diffusion enhances spontaneous electroweak baryogenesis*, Phys. Lett. **B 336** (1994) 41 [hep-ph/9406345].

[101] M. Joyce, T. Prokopec and N. Turok, *Electroweak baryogenesis from a classical force*, Phys. Rev. Lett. **75** (1995) 1695, Erratum-ibid. **75** (1995) 3375 [hep-ph/9408339].

[102] M. Joyce, T. Prokopec and N. Turok, *Nonlocal electroweak baryogenesis. Part 1. Thin wall regime*, Phys. Rev. **D 53** (1996) 2930 [hep-ph/9410281].

[103] M. Joyce, T. Prokopec and N. Turok, *Nonlocal electroweak baryogenesis, part 2. The classical regime*, Phys. Rev. **D 53** (1996) 2958 [hep-ph/9410282].

[104] J. M. Cline, M. Joyce and K. Kainulainen, *Supersymmetric electroweak baryogenesis in the WKB approximation*, Phys. Lett. **B 417** (1998) 79, Erratum-ibid. **B 448** (1999) 321 [hep-ph/9708393].

[105] J. M. Cline and K. Kainulainen, *A new source for electroweak baryogenesis in the MSSM*, Phys. Rev. Lett. **85** (2000) 5519 [hep-ph/0002272].

[106] J. M. Cline, M. Joyce and K. Kainulainen, *Supersymmetric electroweak baryogenesis*, J. High Energy Phys. **07** (2000) 018 [hep-ph/0006119], *Erratum* hep-ph/0110031.

[107] A. E. Nelson, D. B. Kaplan and A. G. Cohen, *Why there is something rather than nothing: Matter from weak interactions*, Nucl. Phys. **B 373** (1992) 453.

[108] M. Carena, M. Quiros, A. Riotto, I. Vilja and C. E. M. Wagner, *Electroweak baryogenesis and low energy supersymmetry*, Nucl. Phys. **B 503** (1997) 387 [hep-ph/9702409].

[109] M. Carena, J. M. Moreno, M. Quiros, M. Seco and C. E. M. Wagner, *Supersymmetric CP-violating currents and electroweak baryogenesis*, Nucl. Phys. **B 599** (2001) 158 [hep-ph/0011055].

[110] M. Carena, M. Quiros, M. Seco and C. E. M. Wagner, *Improved results in supersymmetric electroweal baryogenesis*, Nucl. Phys. **B 650** (2003) 24 [hep-ph/0208043].

[111] T. Konstandin, *CP-Violation and baryogenesis on electroweak scales: Cosmological predictions for the Standard Model and beyond*, PhD-Thesis, Rupertus-Carola University of Heidelberg, 2005.

[112] S. J. Huber, *Electroweak baryogenesis in the supersymmetric Standard Model with a gauge singlet*, PhD-Thesis, Rupertus-Carola University of Heidelberg, 1999.

[113] S. J. Huber and M. G. Schmidt, *Electroweak baryogenesis: concrete in a SUSY model with a gauge singlet*, Nucl. Phys. **B 606** (2001) 183 [hep-ph/0003122].

[114] K. Kainulainen, T. Prokopec, M. G. Schmidt and S. Weinstock, *First principle derivation of semiclassical force for electroweak baryogenesis*, J. High Energy Phys. **06** (2001) 031 [hep-ph/0105295].

[115] K. Kainulainen, T. Prokopec, M. G. Schmidt and S. Weinstock, *Semiclassical force for electroweak baryogenesis: three-dimensional derivation*, Phys. Rev. **D 66** (2002) 043502 [hep-ph/0202177].

[116] A. G. Cohen and D. B. Kaplan, *Spontaneous Baryogenesis*, Nucl. Phys. **B 308** (1988) 913.

[117] A. G. Cohen, D. B. Kaplan and A. E. Nelson, *Spontaneous baryogenesis at the weak phase transition*, Phys. Lett. **B 263** (1991) 86.

[118] P. Huet and A. E. Nelson, *Electroweak baryogenesis in supersymmetric models*, Phys. Rev. **D 53** (1996) 4578 [hep-ph/9506477].

[119] G. D. Moore, *Computing the strong sphaleron rate*, Phys. Lett. **B 412** (1997) 359 [hep-ph/9705248].

[120] G. F. Giudice and M. E. Shaposhnikov, *Strong sphalerons and electroweak baryogenesis*, Phys. Lett. **B 326** (1994) 118 [hep-ph/9311367].

Acknowledgements

In a couple of sentences I would like to express my gratitude to everyone who helped and supported me while doing the research which eventually lead to the present doctoral thesis.
First of all, with great pleasure I would like to thank my supervisor Prof. Dr. Dietrich Bödeker for his guidance and collaboration. Beside providing a very attractive subject for this thesis, he gave me the opportunity to participate in several national and international conferences and workshops, where I gained very instructive experiences.
I am much obliged to the second referee of this work, Prof. Dr. Mikko Laine, who was always open for questions and helpful discussions.
Most of the work presented here resulted from a close, fruitful and enjoyable collaboration with Dr. Stephan J. Huber. I am particularly indebted to him. Stephan never hesitated to continue our illuminating discussions until the convergence of opinions. He had a substantial part in bringing this thesis to a successful conclusion.
As a companion I am thankful to Michael Seniuch for our friendship and the excellent and enjoyable collaboration. I benefited immensely from our teamwork not only during the last few years but during our whole studies.
I really appreciate Jörg Erdmann, Dr. Hendrik van Hees and Dr. Steffen Weinstock for many enlightening and valuable discussions. I also gratefully acknowledge Dr. Jan van der Heide for reading carefully the manuscript.
In addition, I would like to express my gratefulness to all members of the Theoretical High Energy Physics group at the Bielefeld University, especially Prof. Dr. Jürgen Engels and the secretaries Gudrun Eickmeyer and Susi von Reeder, for all the help and support I received in all circumstances. I benefited enormously from several interesting discussions (not only about physics) and the pleasant atmosphere in our group.
Schließlich gilt mein ganz besonderer Dank meiner Frau Corinna für ihre Liebe, Geduld und Unterstützung sowie meinen Eltern, die mir das Studium und die anschließende Promotion erst ermöglicht haben.

Lars Fromme, Bielefeld, July 2006